THE SYNTHESIS OF TITANIUM DIOXIDE PHOTOCATALYSTS BY
SOL-GEL METHOD: THE EFFECT OF HYDROTHERMAL TREATMENT
CONDITIONS AND USE OF CARBON NANOTUBE TEMPLATE

A THESIS SUBMITTED TO
THE GRADUATE SCHOOL OF NATURAL AND APPLIED SCIENCES
OF
MIDDLE EAST TECHNICAL UNIVERSITY

BY

ALP YÜRÜM

IN PARTIAL FULFILLMENT OF THE REQUIRMENTS
FOR
THE DEGREE OF DOCTOR OF PHILOSOPHY
IN
CHEMICAL ENGINEERING

AUGUST 2009

Approval of the thesis:

THE SYNTHESIS OF TITANIUM DIOXIDE PHOTOCATALYSTS BY SOL-GEL METHOD: THE EFFECT OF HYDROTHERMAL TREATMENT CONDITIONS AND USE OF CARBON NANOTUBE TEMPLATE

submitted by **ALP YÜRÜM** in partial fulfillment of the requirements for the degree of **Doctor of Philosophy in Chemical Engineering Department, Middle East Technical University** by,

Prof. Dr. Canan Özgen   _____
Dean, Graduate School of **Natural and Applied Sciences**

Prof. Dr. Gürkan Karakaş   _____
Head of Department, **Chemical Engineering**

Prof. Dr. Gürkan Karakaş   _____
Supervisor, **Chemical Engineering Dept., METU**

Examining Committee Members:

Prof. Dr. Timur Doğu   _____
Chemical Engineering Dept., METU

Prof. Dr. Gürkan Karakaş   _____
Chemical Engineering Dept., METU

Prof. Dr. Suna Balcı   _____
Chemical Engineering Dept., Gazi University

Prof. Dr. Deniz Üner   _____
Chemical Engineering Dept., METU

Prof. Dr. H. Önder Özbelge   _____
Chemical Engineering Dept., METU

Date: _____

I hereby declare that all information in this document has been obtained and presented in accordance with academic rules and ethical conduct. I also declare that, as required by these rules and conduct, I have fully cited and referenced all material and results that are not original to this work.

Name, Last Name: ALP YÜRÜM

Signature   :

ABSTRACT

THE SYNTHESIS OF TITANIUM DIOXIDE PHOTOCATALYSTS BY SOL-GEL METHOD: THE EFFECT OF HYDROTHERMAL TREATMENT CONDITIONS AND USE OF CARBON NANOTUBE TEMPLATE

Yürüm, Alp

Ph. D., Department of Chemical Engineering

Supervisor: Prof. Dr. Gürkan Karakaş

August 2009, 150 pages

Titanium dioxide (TiO_2), a semiconductor, has been used in many areas like heterogeneous photocatalysis. In the present study, the effect of hydrothermal treatment conditions and the use of carbon nanotubes on the photocatalytic activity of sol-gel synthesized titanium dioxide were examined.

The anatase particles were transformed into layered trititanate particles with either nanotube or nanoplate structure by hydrothermal treatment under the alkaline conditions. Post hydrothermal treatment under neutral conditions was also applied and mesoporous particles were transformed into nanostructured, highly crystalline and ordered anatase particles. Photocatalytic activities of hydrothermally treated samples were determined against *Escherichia coli* under solar irradiation. Results showed that hydrothermal treatment under alkaline conditions improved the photocatalytic activity. However, although being highly crystalline, after post treatment, a limited activity was obtained because of dehydration of active (101) face of anatase. Nevertheless, TiO_2's initial inactivation constant rose

from 0.6 to 2.9 hr^{-1} after regeneration of active sites in aqueous medium under solar irradiation.

In order to enhance the surface area and improve activity, multi-walled carbon nanotubes were utilized during the synthesis of TiO_2. The effect of calcination conditions and presence of sodium, iron and cobalt on the photocatalytic activity were also studied. For these samples, photocatalytic activities were tested with methylene blue solution under UV irradiation. It was observed that the utilization of CNTs enhanced both the surface area and the activity. Compositions with highest CNT content had better activities for their ability to delay charge recombination. While pure TiO_2's initial decomposition constant was 0.8 hr^{-1}, with sodium doping the best value of 1.9 hr^{-1} was achieved.

ÖZ

TİTANYUM DİOKSİT FOTOKATALİZÖRLERİN SOL-JEL YÖNTEMİ İLE SENTEZİ: HİDTROTERMAL İŞLEM KOŞULLARININ VE KARBON NANOTÜP KALIP KULLANIMININ ETKİSİ

Yürüm, Alp

Doktora, Kimya Mühendisliği Bölümü

Tez Yöneticisi: Prof. Dr. Gürkan Karakaş

Ağustos 2009, 150 sayfa

Bir yarı iletken olan titanyum dioksit (TiO_2) heterojen fotokataliz gibi bir çok alanda kullanılmaktadır. Bu çalışmada hidrotermal işlem koşullarının ve karbon nanotüp kullanımının, sol-jel yöntemi ile sentezlenmiş titanyum dioksitin aktivitesi üzerine etkisi araştırılmıştır.

Anataz parçacıkları, alkali koşullar altında hidrotermal işlem ile nanotüp ya da nanoplaka yapılı, katmanlı trititanat parçacıklarına dönüştürülmüştür. Nötr koşullar altında ardıl hidrotermal işlem de uygulanmış ve mezogözenekli parçacıklar, nanoyapılı, büyük ölçüde kristalize ve düzenli antaz parçacıklarına dönüştürülmüştür. Hidrotermal işleme tabi tutulmuş örneklerin fotokatalitik aktiviteleri güneş ışıldaması altında *Escherichia coli* üzerinde denenmiştir. Sonuçlar, alkali koşullar altında hidrotermal işlemin fotokatalitik aktiviteyi geliştirdiğini göstermiştir. Ancak, büyük ölçüde kristalize olmasına rağmen ardıl işlemden sonra, anatazın aktif (101) yüzeyinin dehidrasyonu sebebiyle kısıtlı aktivite elde edilmiştir. Yine de, TiO_2'nin başlangıç inaktivasyon sabiti, güneş ışıldaması altındaki sulu ortamda, aktif sitelerin rejenerasyonundan sonra 0.6'dan 2.9 s^{-1}'e yükselmiştir.

Yüzey alanını ve aktiviteyi geliştirmek için, TiO_2'nin sentezi sırasında çoklu duvarlı karbon nanotüplerden faydalanılmıştır. Kalsinasyon koşullarının ve sodyum, demir ve kobalt varlığının fotokatalitik aktivite üzerindeki etkisi de incelenmiştir. Bu örnekler için fotokatalitik aktiviteler, UV ışıldaması altında metilen mavisi çözeltisi ile test edilmiştir. KNT'nin kullanımının hem yüzey alanını hem de aktiviteyi geliştirdiği gözlemlenmiştir. KNT içeriği en yüksek olan bileşimler, yük geri birleşimini geciktirme özelliği sebebiyle daha iyi aktiviteye sahip olmuştur. Saf TiO_2'nin başlangıç bozunma sabiti $0.8 \ s^{-1}$ iken, sodyum katısı ile en iyi değer olan $1.9 \ s^{-1}$'e ulaşılmıştır.

Anahtar Sözcükler: sol-jel titanyum dioksit, anataz, trititanat, karbon nanotüp, hidrotermal

To My Family

ACKNOWLEDGEMENTS

TABLE OF CONTENTS

LIST OF TABLES

TABLES

LIST OF FIGURES

CHAPTER 1

INTRODUCTION

Titanium dioxide is one of the most studied metal oxide in the literature for its wide range of applications. These areas can be listed as paint industry, biomaterials, ceramics, electronic devices, gas sensors, solar cell applications, heterogeneous catalysis, some specialized coatings and photocatalysis [1].

TiO_2 (titania) is widely used as pigment virtually in every kind of paint for its high refractive index [2]. For being non-toxic it is also used food products, pharmaceuticals and cosmetics [2-4]. This non toxicity is also very important for the biomaterials area. Body accepts titanium implants easily and the oxide layer has sufficient corrosion resistance [5].

Semiconductor metal oxides may change their conductivity when they adsorb gases; thus this change in the material can be utilized in sensors. Although TiO_2 is not used as much as SnO_2 and ZnO_2, it can be used in some O_2 sensors [6, 7].

Titania as a solar cell can be used for decomposition of water into H_2 & O_2 and also for electric production [8-11], but unfortunately titania has a low quantum yield for the photochemical conversion of solar energy. On the other hand, addition of some dyes to those cells has been shown to improve the wavelength range [12].

Most heterogeneous catalysts consist of small metal clusters on an oxide support and many growth studies of catalysts on titania were investigated. Traditionally, titania is a component in mixed vanadia/titania catalysts used for selective oxidation reactions [13-17]. Also it was found out that finely dispersed Au particles supported on titania oxidize CO at low temperatures [18]. But the most studied research area on titania is its use for photo-assisted degradation of organic molecules. Titania is a semiconductor and its photocatalytic activity is

1

accomplished by low energy (UV-A) irradiation (320-400nm/3.9-3.1eV) which exists in natural sunlight and artificial illumination.

TiO_2 photocatalysts with anatase structure generate strong oxidizing power under UV irradiation which corresponds to lower wavelength than its edge energy (385 nm, 3.4 eV) as a result of charge separation. The hole (h+) and electron (e-) pairs formed reacts with H_2O and O_2 over the surface and hydroxyl radicals ($\bullet OH^-$) and super oxide ions (O_2^-) are generated, which are very active on the decomposition and mineralization of organic compounds [19]. These species may also lead to complete decomposition of hydrocarbons into CO_2 and H_2O. This property can be used in applications like wastewater purification, antimicrobial surfaces and self-cleaning surfaces [20-23].

The photocatalytic efficiency of many synthetically produced TiO_2 samples depends on many factors such as band gap, surface area, particle size, crystallinity, etc. and during the last decade, much effort has been devoted to increase the photocatalytic efficiency of TiO_2 materials [24-33]. The most important reason of low photocatalytic efficiency of TiO_2 materials is the competition of hole/electron charge recombination reaction with charge separation and free radical production reactions. The photocatalytic performance of TiO_2 materials can be improved by reducing the particle size to the mean charge carrier path which is reported as 100 nm for TiO_2 [34]. Thus TiO_2 with nanostructures like nanotubes and nanofibers may perform much better catalytic, optical and electronic properties.

The first examples of nanotubes were carbon nanotubes and they played a central role in leading the overall progress of nanoscience and nanotechnology in both academic research and industry applications. Carbon nanotubes have great potential as materials with unique properties that are not found in typical graphite or carbon fullerene [35-37]. Their applications benefit to a wide range of engineering, applied physics and biomaterials areas, because of their superior mechanical and electrical properties. In the nanotechnology area, extensive works including the synthesis of different types of nanotubes, manufacturing process of nanotube-related materials, electrical and mechanical characterizations of these materials, have been conducted in the past few years [38].

The discovery of carbon nanotubes has brought the question of the possibility of nanotubes that could be made from materials other than carbon.

There are lots of researches on developing different kind of nanotubes. Some of these are nanotubes made from BN, $B_xC_yN_z$, WS_2, MoS_2, $W_xMo_yC_zS_2$ [39], also from the oxides SiO_2, Al_2O_3, V_2O_5, MoO_3, and TiO_2 as expected [40].

The nanostructured TiO_2 materials other than anatase structure having layered structure are alkali titanates ($A_2Ti_nO_{2n+1}$) and protonic titanate ($H_2Ti_4O_9$). The unique mesoporous, high surface area properties of these materials offer promising results as semiconductors, catalytic materials and sensing behaviors. The synthesis of alkali titanates (e.g. $Na_2Ti_nO_{2n+1}$) with wet methods is possible with both solid state reaction by treating TiO_2 with alkali carbonate-peroxide mixtures [41] and hydrothermal treatment with strong basic solutions [42]. The hydrothermal synthesis of $Na_2Ti_nO_{2n+1}$ yield crystalline structure above 7 N NaOH concentrations within the 80-125 ºC range and higher concentrations lead to the formation of amorphous titania phase [42]. The alkali titanate structure can be transformed to the protonic-titanate by alkali-proton exchange [43] as a result of hydrothermal treatment under acidic conditions [39]. Although, considerable effort have been devoted to the synthesis and the characterization, a few number of studies reported the photocatalytic activities of these mesoporous nanostructured TiO_2 materials [44, 45]. It is stated that nanotubes synthesized with this technique is not photocatalytically active, since the obtained material is protonic titanate having a different phase structure than TiO_2 [33]. Also it is mentioned that mesoporous anatase TiO_2 nanofibers with highly photocatalytic activity were prepared by a simple hydrothermal post-treatment of titanate nanotubes. Hydrothermal post-treatment at 200 ºC resulted in the destruction of nanotube structures and the formation of anatase TiO_2 nanofibers [33].

As mentioned above, titania has been widely used and investigated as a photocatalytic material for its nontoxic, chemical, and optoelectronic properties. However, it is difficult to separate suspended TiO_2 after the completion of each reaction cycle and some processes can not benefit from powder TiO_2. TiO_2 can be immobilized as thin films on substrates. One of the most common and easy technique to immobilize it, is the sol-gel process route. Synthesizing TiO_2 photocatalysts with sol–gel technique has been the subject of many application fields. Especially, it has been stated in literature that the sol–gel process is a flexible technique for the preparation of optical quality photocatalytic TiO_2 thin films. Recently, nanostructured or nanocrystalline titania films have attracted the attention due to its better overall performance over the traditional coarse-

grained films [46]. Many recent studies report on improved photocatalytic properties of sol–gel nanocrystalline TiO_2 films deposited on glass or silica. However, photocatalytic activities of such films are limited by the fact that efficient photo-induced charges (electrons and holes) are preferably generated in films composed of a well crystallized anatase phase. During calcination of these thin films, it can be hard to synthesize that perfect crystals. Also since thins films have relatively smaller surface areas, the utilization of the charges will drop.

For increasing the effectiveness and strengthening the bonds between the substrate and the titania coating, different methods have been attempted [21, 47-61]. Either the substrate surface has been chemically or physically modified or some composite titania with better adhesion properties have been formulated. As a substrate, soda lime glass is the most common item, but in addition to that silicone wafers [47, 48] and aluminum [49] substrates were also used. Soda lime glass can also be modified with hydrothermal processes to achieve more effective adhesion [50]. Also some cellulose based fillers or spacer can be utilized as a binder [51, 52] which is not suitable for high temperature processes and applications. Doping of titania film with silver [53], palladium [21] and some rare earth metals [54] was also reported to be effective. In addition to that a composite film consisting zirconia/titania proved to be effective [55], but the most common composite is silica/titania [56-61]; which is stated to have an improved hydrophilicity and adsorption of materials, thus a better photocatalytic properties.

In this study, titania were synthesized with sol-gel technique and modified with two methods: hydrothermal synthesis and carbon nanotube (CNT) templating. With hydrothermal synthesis, anatase crystals were modified to obtain nanoparticles like nanotubes and nanoplates. While with CNT template method, CNT's were used as a support for CNT/TiO_2 matrix which enhances the photocatalytic activity and as a template to increase the specific surface area of titania. Various characterizations were made. For all of the samples XRD, SEM and surface area analysis were made. Also TGA analyses were utilized for CNT samples. Photocatalytic activities of hydrothermally treated catalysts were made against *Escherichia coli* and for CNT samples; methylene blue was used to characterize their photocatalytic activity.

CHAPTER 2

LITERATURE SURVEY

2.1. Titanium Dioxide (TiO$_2$)

The major use of TiO$_2$ is as white pigment in the paint, plastic, and paper industries. The annual raw mineralite consumption is approximately one billion metric tons. Ninety-seven percent is used in the pigment industry [62]. It is also used in sunscreen as a UV absorber. But increasingly, TiO$_2$ is used more and more as a photocatalyst for pollution reduction. It is non-toxic, chemically stable, and has a low cost [63]. It is found in the electronics industry in certain MOSFET (metal oxide semiconductor field-effect transistor) applications. Additionally it is useful as a gas sensor at high temperature for the determination of oxygen, carbon monoxide, and methane. TiO$_2$ has a high index of refraction (3.87 and 2.5-3 for rutile and anatase respectively [64]).

TiO$_2$ also functions as an excellent model catalyst for oxide materials [1, 65]. Titanium cations are present in a variety of different coordination environments and oxidation states [66]. The numerous surface valance states are capable of interacting with adsorbed species in unique ways facilitating many different chemical reactions. It is mentioned that surface oxygen plays an important role in the state of the titanium surface atoms [65]. Fully oxidized surfaces show traits similar to transition metal complexes. Moreover, the fully oxidized surface has insulator properties with very low electrical conductivity. The removal of surface oxygen causes electron transfer into the 3d orbital. Therefore at non-zero temperatures, electrons can be thermally excited to conduction band creating a more conductive surface. Surface oxygen can be removed creating vacancies via several methods: annealing in hydrogen, annealing in vacuum [1, 66-68], and argon sputtering under ultrahigh vacuum conditions [1, 66, 69, 70]. This creates a useful material for catalytic [1, 21, 65,

71-85] and gas sensing applications [86-91]. For example the trimerization of acetylene to benzene and other C2 through C6 alkynes requires Ti^{+2} cations [66, 80, 81]. The Ti^{+2} (and lower oxidation) sites are capable of undergoing a two electron oxidation in a manner completely described using organometallic homogeneous catalysis. The catalytic reactions on TiO_2 surfaces occur at oxygen vacancies and other surface defects. Gas molecules adsorbing at oxygen vacancies create measurable changes in the surface conductivity of a TiO_2 film [87, 89-91].

The general properties of the most common phases of TiO_2 are described in section 2 of this chapter. There are three common polymorphs: rutile, anatase, and brookite. Rutile is the thermodynamically most stable polymorph. Majority of the surface science studies on single crystals have been conducted on rutile crystals. Rutile is also used in all pigments and sunscreens for its poor photoactivity which would be harmful to product performance. Anatase is the more photoactive phase and is subject to most photocatalysis studies. Brookite is the least common of the three phases. Both anatase and brookite are metastable phases.

2.2 Crystal Structures of Titania

Titania has three polymorphs; rutile, anatase, and brookite. They are all composed of octahedral groups of oxygen atoms around titanium, exhibiting the characteristic six-coordination of this element. However the position in which the groups are linked together is different for each mineral [92].

The Rutile Group: The a dimension of rutile is 4.58 Å, while the c dimension is 2.95 Å. The structure of rutile is shown in Fig. 2.2-1&2. The structure is of 6:3 coordination. Every titanium atom is surrounded by oxygen atoms approximately at the corners of a regular octahedron, and every oxygen atom by three titanium atoms approximately at the corners of an equilateral triangle. This atomic arrangement is one of the standard types for AB_2 compounds in which the atom is in six-coordination and it is also characteristic of a very large number of crystals.

6
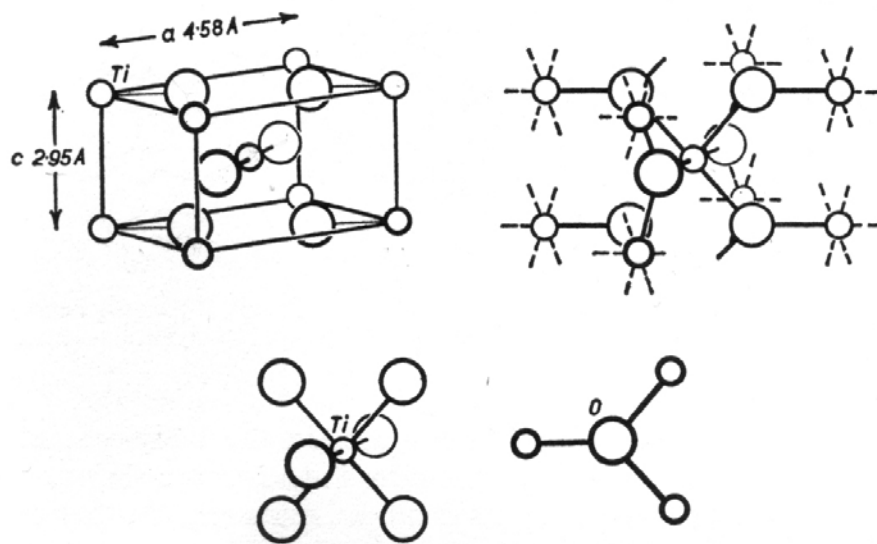
Fig. 2.2-1 The structure of rutile, TiO$_2$. Above (left) unit cell and (right) bonds between Ti and O. Below, environment of Ti and O atoms.
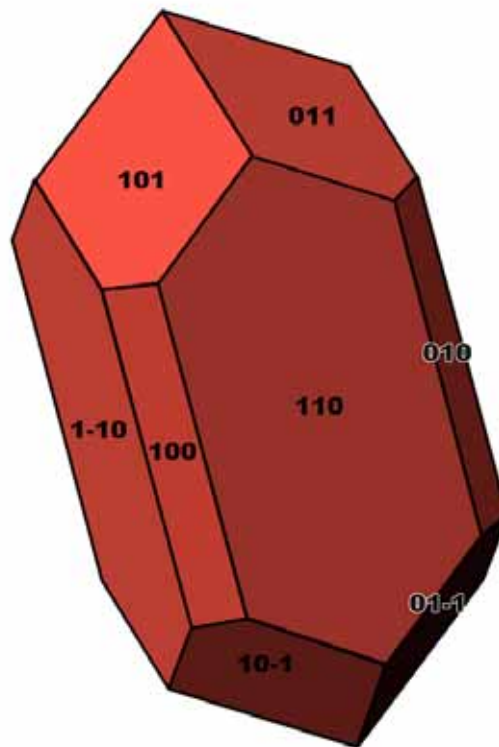
Figure 2.2-2 Crystal form structure of rutile

Anatase: It's a dimension is 3.78 Å and c dimension is 9.50 Å. Fig. 2.2-3(a) shows the position of the atoms in the body-centered unit cell, and in Fig. 2.2-3(b) the links between Ti an O are shown. As in rutile, every Ti atom is between six O atoms, and every O atom is between three Ti atoms (Fig. 2.2-3(c)). Anatase and rutile are thus alternative forms of 6:3 coordination. Crystal form structure of anatase can be seen at Figure 2.2-4.
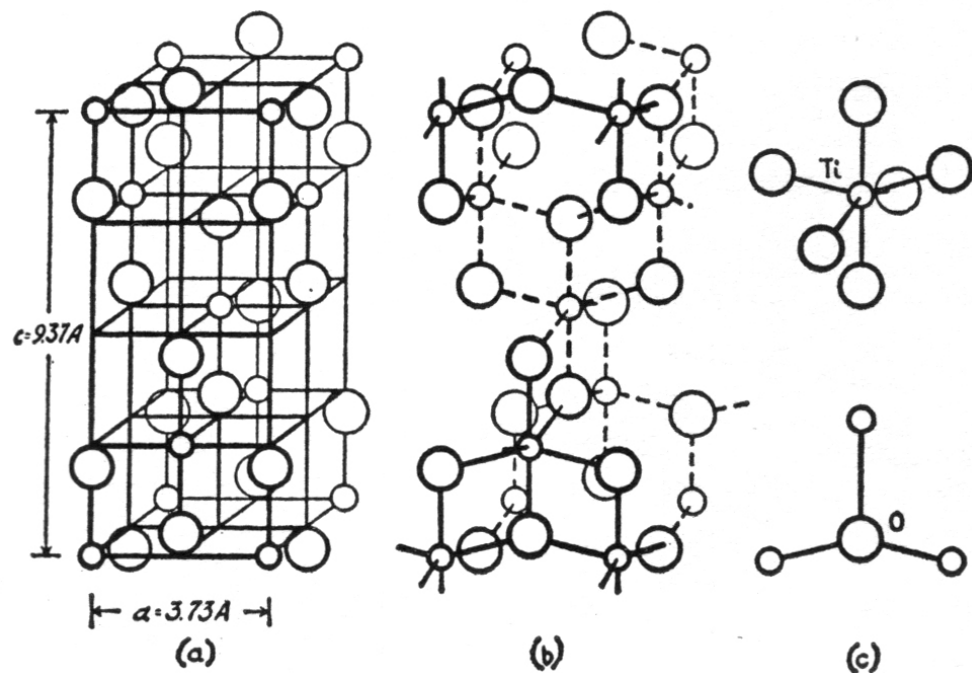
Fig. 2.2-3 The structure of anatase, TiO_2. (a) Unit Cell, (b) bonds between Ti and O, and (c) environments of Ti and O atoms which are closely similar to those in rutile.
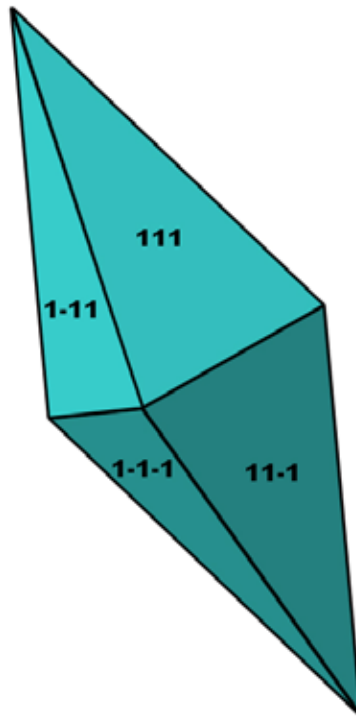
Figure 2.2-4 Crystal form structure of anatase

Some main XRD peaks of anatase and rutile are listed in Table 2.2-1.

Brookite has an orthorhombic structure and its a, b, and c dimensions are 9.14 Å, 5.44 Å, and 5.15 Å. The structure is shown in an idealized form in Fig. 2.2-5 and it can bee seen that the structure is quite complex compared to the other polymorphs. As is rutile and anatase, each titanium atom is surrounded by an octahedral group of oxygen atoms. In all three forms of TiO_2, the titanium-oxygen distance lies between 1.9 Å and 2 Å. Neighboring oxygen atoms are between 2.5 Å and 3 Å apart, the smaller distance obtaining when the pair of oxygen atoms are linked to the same two titanium atoms i.e. when the octahedra share an edge [92]. Crystal form structure of anatase can be seen at Figure 2.2-6.

Table 2.2-1 Main XRD peaks of anatase and rutile with copper source [93]

Anatase		Rutile	
2 Theta (Deg.)	Intensity (%)	2 Theta (Deg.)	Intensity (%)
25.27	100		
		27.70	100
		36.07	50
37.79	20		
		41.21	25
48.03	35		
53.87	20		
		54.30	60
55.04	20		
		56.62	20
		65.45	20
		68.98	20
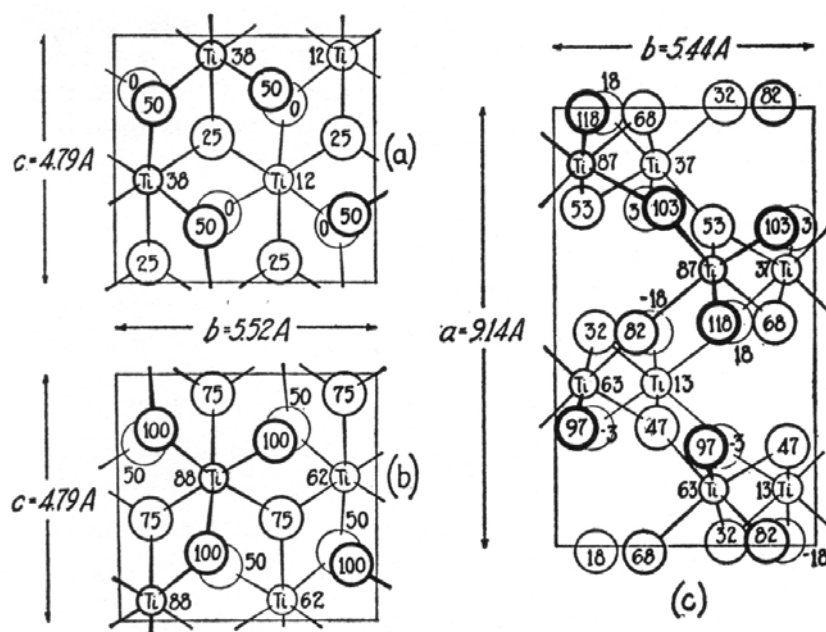
Fig. 2.2-5 (a), (b). The structure of brookite, TiO_2, in idealized form. (b) is to be superimposed on (a), the oxygen atoms at height 50 being common to both. (c) the actual structure projected on (001). Oxygen atoms which should be superimposed have been displaced symmetrically.
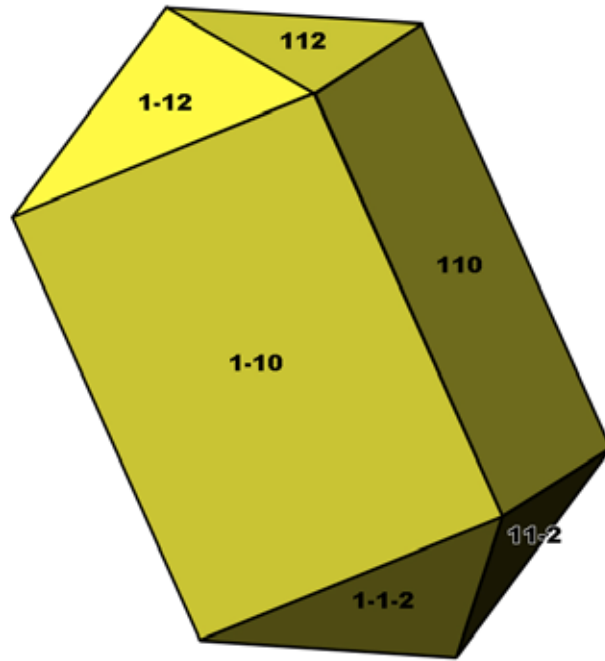
Figure 2.2-6 Crystal form structure of brookite

Some main XRD peaks of brookite are listed in Table 2.2-2.

Table 2.2-2 Main XRD peaks of brookite with copper source [93]

2 Theta (Deg.)	Intensity (%)
25.33	100
25.68	80
30.80	90
36.24	25
47.99	30
51.18	20
55.21	30

2.3 Photoinduced Properties of TiO$_2$

For nanoparticles, shape and size are key factors in determination of their chemical and physical properties. Some properties of nanocrystals are quite unique when compared with conventional materials [148, 149]. TiO$_2$, as an important photocatalytic semiconductor, have some unique properties and its photocatalytic activity increases remarkably at nanoscale.

Before mentioning photocatalysis in TiO$_2$ particles in detail, a definition of band gap should be made. In semiconductors and insulators, electrons are trapped to a number of bands of energy, and can not move to other regions. The band with the highest energy that an electron can move is the valence band. The next energy level is conduction band. The term band gap refers to the energy difference between the valence band and the conduction band. In order for an electron to jump from a valence band to a conduction band, it requires a specific minimum amount of energy for the transition. The required energy differs with different materials. Electrons can gain enough energy to jump to the conduction band by absorbing either heat or light. After an electron reaches the conduction band, a hole is created at the valence band and the material starts to conduct electricity.

Photocatalysis is one of the major application areas of TiO$_2$ materials. When photons have a higher energy than the band gap of TiO$_2$ nanoparticles, the photons can be absorbed and an electron of TiO$_2$ nanoparticles is send to the conduction band (CB), leaving a hole in the valence band (VB) (Figure 2.3-1).
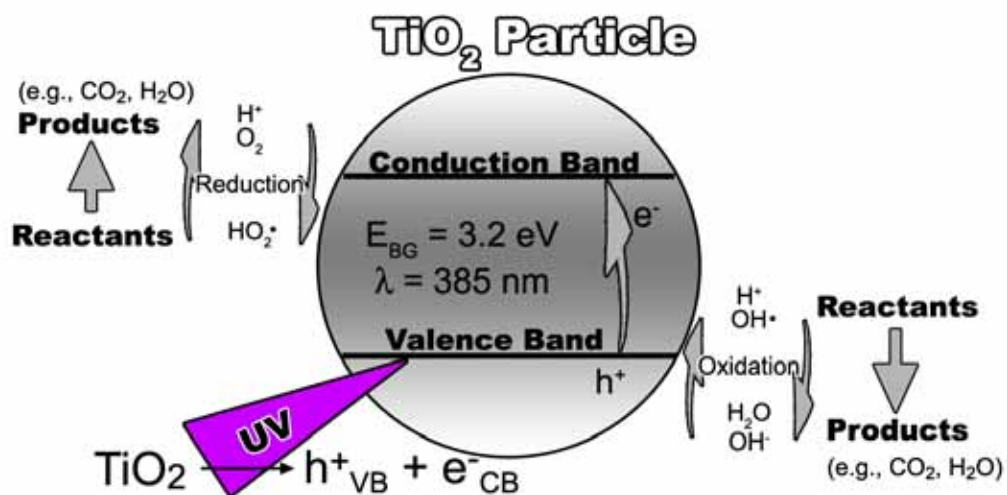
Figure 2.3-1 Photoinduction of a TiO_2 particle

2.3.1. Mechanism of TiO_2 Photocatalysis

The general equation of a photocatalyzed reaction can be given like:

$$(Ox_1)_{ads} + (Red_2)_{ads} \rightarrow Red_1 + Ox_2 \qquad <2.3.1>$$
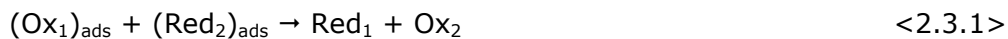
Where $(Ox)_{ads}$ is the adsorbed oxidant and $(Red)_{ads}$ is the adsorbed reducer.

Depending on the sign of Gibbs free energy, positive or negative, the reaction can be either oxidation or reduction reaction. In literature [163], a general mechanism is proposed for heterogeneous photocatalysis on TiO_2. Some steps of this mechanism are listed below:

a) Adsorption of Organic Materials:
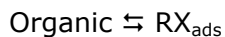
Organic $\leftrightarrows$ RX_{ads}

RX_{ads} represents the organic substrates.

13

b) Electron transfer from either the adsorbed substrate (RX_{ads}) or the adsorbed hydroxyl radicals ($\cdot OH_{ads}$) to the holes h^+:

$$h^+ + RX_{ads} \rightarrow RX^+_{ads}$$

$$h^+ + H_2O_{ads} \rightarrow \cdot OH_{ads} + H^+$$
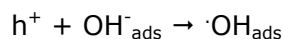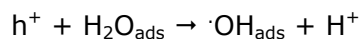
$$h^+ + OH^-_{ads} \rightarrow \cdot OH_{ads}$$

The most important steps are the second and the third one for the major oxidant, adsorbed hydroxyl radicals ($\cdot OH_{ads}$), are generated in these steps.

c) Molecular oxygen is presented in oxidative decomposition processes, because it is an electron acceptor in the electron transfer reaction:

$$O_2(g) \leftrightarrows O_{2ads}$$

$$O_{2ads} \rightarrow 2O_{ads}$$

$$O_{ads} + e^- \rightarrow O^-_{ads}$$

$$e^- + O_2 \rightarrow O_2^-$$
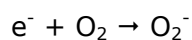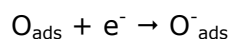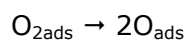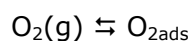
d) The superoxide anion can further be involved the following reaction and give more ($\cdot OH_{ads}$) groups:

$$H^+ + O_2^- + HO_2 \rightarrow H_2O_2 + O_2$$

$$H_2O_2 + h\nu \rightarrow 2\cdot OH$$
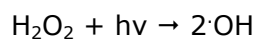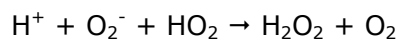
e) And lastly the active free radicals ($\cdot OH_{ads}$) oxidize organic substrate (RX_{ads}) adsorb onto the surface of the semiconductor particles.

$$\cdot OH_{ads} + RX_{ads} \rightarrow \text{Intermediate} \rightarrow \text{Alcohols, Ketones, Acids, } CO_2, H_2O$$

Although some models were proposed, the knowledge of photocatalysis mechanism on TiO_2 surfaces is not complete yet. The initial steps involving the reactive oxygen species and organic molecules are of particular interest. In most of the processes, oxygen acts as a primary electron acceptor and the electron transfer process is the rate determining process. According to the mechanism, the hydroxyl radical is the principal reactive oxidant in photocatalytic reactions of TiO_2 [165, 166]. Also H_2O_2 can act as an electron acceptor or as a direct source of hydroxyl radicals. Depending on the reaction conditions, hydroxyl radicals, superoxide, hydrogen peroxide and oxygen can play important roles in photocatalytic reactions.

The excited electrons and holes can be used directly to drive a chemical reaction, which we call photocatalysis [116]. The surface atoms of TiO_2 nanoparticles are more active than the bulk atoms because of less adjacent coordinate atoms and unsaturated sites. The surface defects can act as a hole trapping centers in the photocatalysis process. With decreasing size, surface to volume ratio increases and the surface effect becomes more active [150]. In TiO_2 nanoparticles, a high surface to volume ratio can be obtained.

Superhydrophilicty is a newly studied photoinduced property of TiO_2 films. Water uniformly spreads on the UV light illuminated TiO_2 surface and it can be explained by the oxygen vacancy generated on the photoexcited TiO_2 surface [151, 152]. The following adsorption of water after the generation of oxygen vacancies leads to the increase of Van der Waals forces and hydrogen bonding interactions between H_2O and –OH [203, 204]. Self-cleaning and anti-fogging surface can be synthesized according to the superhydrophilic effect. This extraordinary property shows promising applications to the preparation of anti-stain architectural materials, anti-fogging glass and accelerated drying materials [116, 205].

Schematic representation of superhydrophilicity of titania can be seen at Figure 2.3.1-1. a) The electrons in the conduction band have the affinity to reduce titania to form an intermediate species. b) In the following step, holes in the valence band pushes away oxygen atoms, creating vacant sites. If there are some surface defects, these vacant sites are more easily created c) Titania with vacant sites can dissociate water into H and OH groups. Migration of H and OH groups, lead to superhydrophilicity.
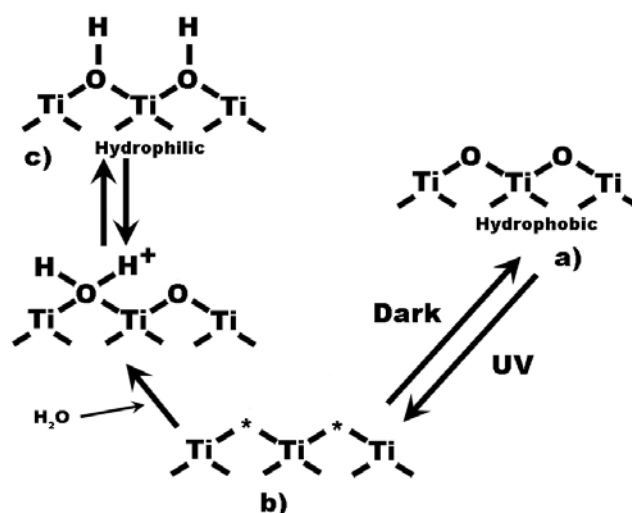
Figure 2.3.1-1 Superhydrophilicity of titania a) Hydrophobic titania, b) titania with vacant sites, c) hydrophilic titania

Studies have revealed that numerous organic materials can be mineralized into carbon dioxide and water under UV irradiation on TiO_2 nanoparticle suspensions. Although there are lots of parameters affecting the photocatalytic reactions, one of the key parameter is the preparation of particle suspensions with a high degree of homogeneousness and stability in the aqueous phase. The feasibility of organic substance removal can be improved by increasing the stability of nanoparticle suspension and the adsorption of various organic molecules onto TiO_2 nanoparticles surface sites [153].

In aqueous systems, nanoparticles always carry charge because of ionization, the adsorption of ions or the preferential substitution of ions from the particle surfaces [154, 155]. Physical properties of TiO_2 nanoparticles suspensions are mostly dependent on the behavior of aqueous suspensions, which are especially reactive to the electrical and ionic structure of the particle-liquid interface. The intensity of repulsive forces among particles and the stability of dispersion are defined by zeta potential. This parameter is crucial on the stability control of TiO_2 nanoparticles in suspensions and the adsorption properties of TiO_2 nanoparticles sites [154, 155].

Some studies showed the isoelectric points (IEP) could be correlated with the photocatalytic activity of TiO_2 particles and the surface charge of TiO_2

particles affected the inactivation kinetics of bacteria considerably [156, 157]. Samples with different chemical compositions had all different zeta potential dependence on pH values. It was seen that addition of alcohol strongly affected the zeta potential values of particles [157-160].

2.4. Photocatalytic Reactions and Applications of TiO$_2$ Nanoparticles

Recent studies on TiO$_2$ as a catalyst have revealed the photochemical conversion of solar energy, environmental photocatalytic reactions, self-cleaning surfaces and photoinduced superhydrophilicity potentials [161]. The most active field of TiO$_2$ photocatalysis is photocatalytic decomposition of organic molecules. A huge variety of organic substrates, viruses, bacteria, fungi and algae can be completely degraded and mineralized to CO$_2$ and H$_2$O [21, 162]. Some latest studies [163, 164] have presented the fundamental knowledge about heterogeneous photocatalysis of TiO$_2$.

2.4.1. Kinetic Model for Photocatalysis on TiO$_2$ Nanoparticles

Kinetics of the photocatalytic decomposition of organic substrates on TiO$_2$ surface can be described with Langmuir-Hinshelwood model [167, 168]. However, it was also reported that, for some conditions, this model should be modified since reaction rate and adsorption rate constants depend on the light intensity [241-243]. A first order kinetic versus initial substrate concentration was proposed by many studies [169-172]. In addition to that, when initial concentration of substrate is very large, then the rate becomes zero order [173]. Reaction rate after the adsorption equilibrium can be expressed as:

$$R = -\frac{d[C]}{dt} = \frac{k_c K_C [C]}{1 + K_C [C]}$$

<2.4.1>

Where [C] is the concentration of the substrate at time t, t is the reaction time, k_c is the Langmuir reaction rate constant and K_C is the adsorption equilibrium constant.

17

Photocatalytic decomposition reactions of substrate follow the pseudo-first-order kinetics with respect to the concentration of the substrate in the bulk solution [C]:

$$-\frac{d[C]}{dt} = \frac{k_c K_C [C]}{1 + K_C [C]} = k_{app}[C]$$

<2.4.2>

Where k_{app} is the apparent reaction rate constant.

After integration of Equation <2.6.3>, within the limits of t=0 → t=t and $[C]=[C]_0$ → $[C]=[C]$, the correlation of concentration and time can be expressed as:

$$-\ln\left(\frac{[C]}{[C]_0}\right) = k_{app}t$$

<2.4.3>

Where C_0 is the initial concentration of the substrate.

From the definition of k_{app} in Equation <2.4.2>, the relationship among k_{app}, k_c and K_C can be expressed as a linear equation:

$$\frac{1}{k_{app}} = \frac{1}{k_c K_C} + \frac{[C]_0}{k_c}$$

<2.4.4>

A plot of $-\ln([C]/[C]_0)$ vs. t will give a slope of k_{app}, which is the apparent reaction rate constant for that $[C]_0$. Likewise, a pot of $1/k_{app}$ vs. $[C]_0$ will give a slope of $1/k_c$ and an intercept of $1/(k_c K_C)$. Consequently, parameters k_{app}, k_c and K_C can be found from these plots.

In addition to that, operational parameters influencing the rate have also been studied [164, 174]. Most of the time, higher catalyst loading mass leads to a higher decomposition rate as a result of increase in surface area and active reaction sites. But above a certain level, rate becomes independent of loading. It is found out that rate is independent of wavelength as long as the energy of light is higher than the band gap energy. Also the rate of reaction is proportional to the radiant flux (ϕ). Above a certain value the rate becomes proportional to ($\phi^{0.5}$) [173]. An increase in oxygen concentration does not always lead to a higher decomposition rate, since hydroxyl products may prevent the contact of substrates with the photocatalytic surface [175]. The apparent activation energy is small in medium temperature conditions (293-353 K). The rate decreases with

temperature as the product desorption becomes the rate limiting step. At high temperature, the exothermic adsorption of reactant becomes rate limiting, leading to a lower activity compared to medium temperatures [173].

2.4.2. Some Examples of Photocatalysis Processes with TiO_2 Nanoparticles

The most important environmental application of TiO_2 photocatalysis is the photocatalytic degradation of organic materials. Photocatalytic degradation of organic materials on TiO_2 has some advantages over other purification processes:

1) It gives nonselective decomposition of organic and inorganic compounds under ambient temperature and pressure.

2) TiO_2 photocatalysis can work with very low concentrations of organics (ppb level of concentration).

3) Additional oxidants are not needed.

4) It is known to be effective against inactive substrates like surfactants and dyes.

In the studies of TiO_2 photocatalysis, many of them studied TiO_2 nanoparticles in suspension systems [180, 181]. But, as it is difficult to separate and recover TiO_2 particles in the suspension after the reaction, some groups began to work on immobilized TiO_2 films [182-184]. Also some studies have been focused on supported TiO_2 photocatalyst films [185].

In recent years, a large amount of processes of photocatalytic technology have been investigated. Mills et al. [186, 187] studied the photocatalytic decomposition of 4 chlorophenol in a TiO_2 suspension using the commercial photocatalyst P-25 with photocatalyst loading of 0.5 mg/mL. Photocatalytic decomposition of some other compounds like methyl blue [164] and stearic acid [188] were also studied. They also studied the functions of different electron acceptors for the oxidation of water photocatalyzed by TiO_2 [189].

Photocatalytic decomposition of phenol and its derivatives were also studied, because they are very important compounds regarding the industrial pollutants [190-192]. Decomposition of phenol gave different mechanisms

depending on the initial phenol concentration. Rodriguez et al. [190] observed two different mechanisms of phenol decomposition. The insertion of hydroxyl radicals is preferred at low phenol concentrations (0.1 g/ L). On the other hand, insertion of hydroxyl radicals did not change the decomposition reaction much at high phenol concentrations (1 g/L), because the decomposition took place on the TiO_2 surface by means of peroxocompound formation. In addition to that, it was found that types of substrates, electronic nature of the compound and the position of the aromatic ring can affect the photocatalytic reactivity [193].

Photocatalytic decomposition of other organic materials like methylene blue [194], methyl orange [169], dyes [195-196] and surfactants [197-198] have also been studied. When we examine the amount and the chemical composition of the industrial effluents, textile dyes are one the major pollutants in industrial effluents. Photocatalytic decomposition rate of different dyes were significantly different [195]. Depending on the nature of the substrate and the pH of the solution, there are three possible mechanisms for dye decomposition: hydroxyl attack, direct oxidation by holes and direct reduction with conduction band electrons. Surfactants are used more and more in domestic and industrial fields. Photocatalytic decomposition of ethylenediaminetetraacetic acid (EDTA) [197], dodecyl benzene sulfonates (DBS) and sodium dodecyl sulfate (SDS) [198] showed photocatalysis is an effective alternative to remove surfactants in wastewater.

As for the inorganic contaminants, photocatalytic purification leads to deposition of environmentally harmful toxic metals on the surface of the semiconductor. Some photocatalytic purification studies about metal ions like Cu^{+2}, Hg^{+2}, Cr^{+6} and Pb^{+2} have been reported [151, 152]. Mechanism analysis of photocatalytic decomposition of nitrate on TiO_2 surface suggested that the major product of photooxidation was nitrite [199]. Also it has been confirmed that the photocatalytic decomposition of hydrogen sulfide could occur on TiO_2 [200].

For inactivation or removal of pathogenic organisms like bacteria, fungi or viruses photocatalytic disinfection is a promising alternative process [201]. It has been confirmed that photocatalytic inactivation of bacteria with TiO_2 can be described with a first order kinetics [202]. It is reported that it is also possible to selectively kill organism using TiO_2 [202].

2.5. Synthesis of Titania Nanoparticles

The functional properties of TiO_2 are strongly dependent on crystal phase, particle size, crystallinity, surface area, pore size and distribution. For a catalyst, surface area and porosity are very important parameters. A higher surface area and porosity brings a better activity. However, titania with classic synthesis methods does not have that much surface area. Converting titania particles to nanoparticles with different shapes, and also synthesizing them with a template can increase the porosity and the surface area of the photocatalyst.

There are many studies aiming the control of size and shape of inorganic nanoparticles with methods like: sol-gel, hydrothermal and chemical vapor deposition techniques [64, 127, 129]. Yet, synthesis of shape-controlled nanocrystals with some surfactants is another method [64, 128, 130].

Different shapes of TiO_2 nanocrystals have been synthesized by using various procedures [131, 132]. In a research [133], elongated TiO_2 nanocrystals were synthesized from the hydrolysis reaction of titanium alkoxides. Short and long nanorods, bullet- and diamond-shaped nanocrystals, platelets, nanotubes and fractals have been prepared [22, 134-137]. The shape evolution on anatase TiO_2 nanocrystals from bullet- and diamond-shape to rods structures was explained by the modulation of surface energies of different crystal facets with use of surfactants [138]. The long axes of the nanocrystals were parallel to the c-axis of the anatase structure. The hexagonal nanorods truncated with two (001) and four (101) facets were observed. The branched shape was believed to be the product of growth along (101) direction starting from the hexagonal shape [139]. Zhu et al. [140] synthesized 50 nm TiO_2 cuboids by sol-gel method.

Recently, TiO_2 nanotubes have attracted a wide attention for their potential application in high efficiency photocatalysis and photovoltaic cells. Well-aligned TiO_2 nanotubes were synthesized by sol-gel method in various studies [141]. Leu et al. [142] developed a one step templating synthesis of TiO_2 arrays in solutions. Wang et al. [143] proposed a model for the formation of TiO_2 nanotubes. In this model, TiO_2 nanotubes were formed following a three-dimension, two-dimension to one-dimension process. They suggest that two-dimensional lamellar TiO_2 is crucial for the formation of TiO_2 nanotubes. Li et al. [141] synthesized TiO_2 nanotubes with anodic aluminum oxide as template. It was found that nanotubes or nanofibers could be obtained by controlling the immersion time of template membrane in precursor sol. Wei et al. [144]

synthesized TiO$_2$ nanotubes from layered titanate particles by a soft chemical process.

TiO$_2$ nanofibers have been synthesized by a templating process [145] and a wet chemical reaction [146]. To prevent agglomeration and excessive growth of TiO$_2$ nanoparticles, crystallized anatase and rutile TiO$_2$ nanoparticles have been synthesized successfully at low temperature [108, 148].

Mesoporous TiO$_2$ can also be synthesized with help of some carbon templates. During synthesis templates like activated carbon [169], poly (alkylene oxide) block copolymer [224], polystyrene [225] or hexadecylamine [226] can be added to the medium. TiO$_2$ network covers those templates and, after calcination, those templates gasify thus leaving pores behind. As a result the material becomes more porous.

Also it is reported that carbon can be used a doping material [227]. It sensitizes TiO$_2$ and reduces the band gap of TiO$_2$, increasing the photocatalytic activity under visible light irradiation [228]. In literature, some carbon sources were used as doping materials like: resins [227], ethylene glycol [229] and carbon nanotubes [212, 221, 222, 230]. Both as a template and as a dopant, carbon nanotubes are very promising sources.

Again for increasing the photocatalytic effectiveness of TiO$_2$, it can be synthesized with SiO$_2$. By dispersing TiO$_2$ nanoparticles on high surface area materials like SiO$_2$ aerogels, very effective catalysts can be made. Zhu et al. [231] reported that (SiO$_2$ aerogel)/TiO$_2$ composite have a much higher photocatalytic activity for increased hydrophilicty. Guan [232] showed that the presence of silica mixed to titania in a well-defined amount enhances both, the photocatalytic activity and the superhydrophilicity due to an increase of the acidity of the surface. This means that SiO$_2$ in the SiO$_2$/TiO$_2$ matrix acts as an adsorber. Zhang et al [233] and Bennani et al. [234] confirmed that situation. Increased adsorption of organics showed an increase in the photocatalytic activity.

In the following sub-sections, the general methods, the sol-gel synthesis and hydrothermal synthesis for nanostructured TiO$_2$ are briefly explained.

2.5.1 Sol-Gel Synthesis

Sol-gel synthesis has become the most common method for the synthesis of metal oxides with various advantages [94-97]. The final product has a superior homogeneity and purity. The microstructural control of the nanoparticles is easier and the resulting materials have higher BET surface area. It is much more flexible to dope the material, and finally, the solution enables to coat large and complex surfaces by spraying, dip coating or spin coating techniques.

A general process scheme of sol-gel synthesis can be seen at Figure 2.5.1-1.
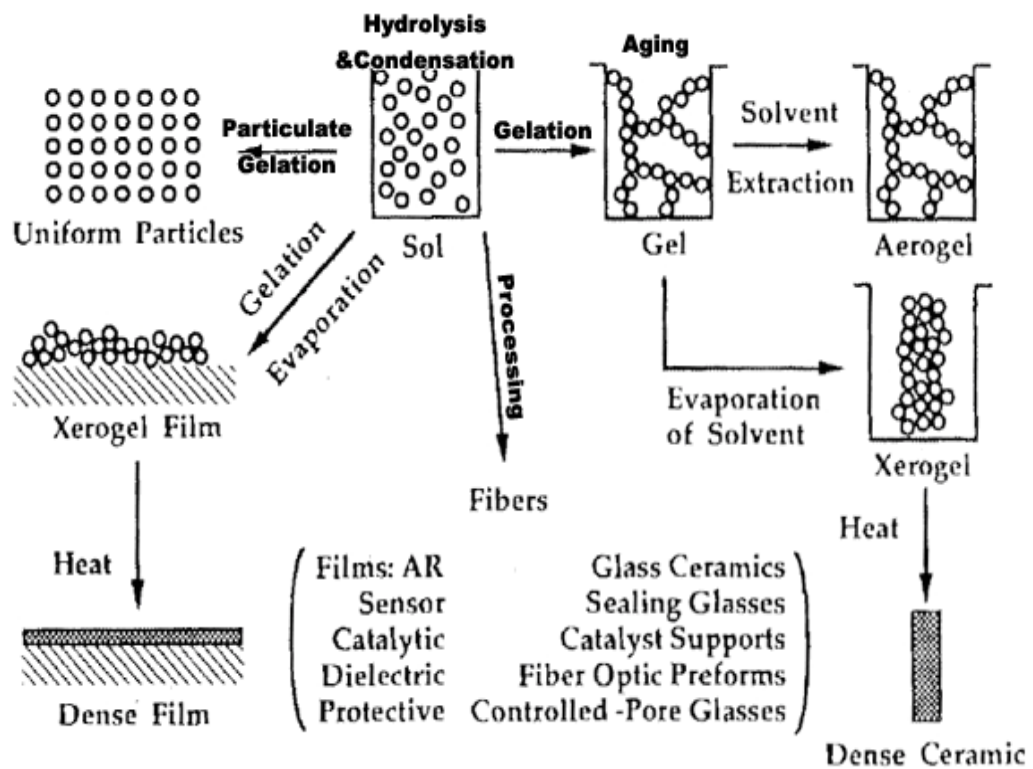
Figure 2.5.1-1. Process scheme of sol-gel synthesis [223]

Sol-gel methods have been extensively used in the synthesis of TiO_2 nanoparticles. In the synthesis of TiO_2 nanoparticles with sol-gel technique, titanium alkoxide or non-alkoxide can be used as titanium precursors. $Ti(i-OP)_4$ [94], $Ti(OBu)_4$ [95] and $TiCl_4$ [96] are the most commonly used alkoxide precursors. In sol-gel synthesis, TiO_2 is usually prepared by performing the hydrolysis and polycondensation reaction steps. Titanium alkoxides, $Ti(OR)_n$, form oxopolymers in aqueous phase, and then these oxopolymers are transformed into an oxide network. The reaction scheme can be described as follows [97]. The non-ionized titanium precursor molecules $Ti(OR)_n$ reacts with water (2.5.1.1):

$$Ti(OR)_n + xH_2O \rightarrow Ti(OH)_x(OR)_{n-x} + xROH \qquad (2.5.1.1)$$

The reactions proceed until titanium hydroxide ($Ti(OH)_n$) is formed. Then the polymerization reactions take place. Condensation dehydration (2.5.1.2):

$$Ti(OR)_n + Ti(OR)_{n-1}(OH) \rightarrow Ti_2O(OR)_{2n-2} + ROH \qquad (2.5.1.2)$$

Dealcoholation (2.5.1.3):
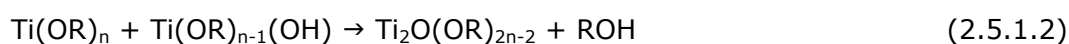
$$2Ti(OR)_{n-1}(OH) \rightarrow Ti_2O(OR)_{2n-2} + H_2O \qquad (2.5.1.3)$$

The overall reaction can be expressed as (2.5.1.4):

$$Ti(OR)_n + n/2\ H_2O \rightarrow TiO_{n/2} + nROH \qquad (2.5.1.4)$$

Condensation reactions pull the particles together into a compact form and build up the metal oxide crystal [98]. Gelation of the solute occurs and form a three dimensional network of gel. The gelation process step is a critical step since it controls the structure of the final product. After the gel is formed, the network starts to lose water and alcohol. This causes the gel to shrink and also creates pores. Also pH, concentration and the solvent used highly affects the structure of these pores. For example, if the pores are wetted under highly soluble conditions, the network may resist compression by capillary forces during drying; causing more porous material (223).

Various factors can change the morphology of TiO_2 nanoparticles during the synthesis. One is type of titanium precursor [99-101]. The other one is the pH and stoichiometry of the reactants [102]. In Addition to those, chemical complexation in the sol-gel system [103-106], drying processes and calcination temperature [107-108] are also important. The dried material is amorphous and

it should be calcined to crystallize the inorganic material. The calcination should be made with air pumped through the system for oxidizing the material. The calcination temperature is also very important to obtain the specific crystal. If the temperature is very high, the material may sinter which is not wanted for our purposes. Calcination at high temperatures leads to a decrease in surface area, loss of hydroxyl groups and growth of crystal size. Recently, in literature, some research showed that TiO_2 can be crystallized at lower temperatures [109, 110].

2.5.2. Hydrothermal & Solvotehrmal Methods

In these methods, synthesis occurs in an aqueous (hydrothermal) or organic medium under autogenerated pressures at relatively lower temperature than calcination. Dried particles obtained from sol-gel synthesis are mostly amorphous and a subsequent thermal treatment is required to crystallize them [111]. Unfortunately, the calcination step will cause crystal growth and reduction in specific surface areas by both sintering and crystal growth of the particles and even cause phase transformation. Hydrothermal synthesis can solve those problems encountered in sol-gel process, because crystallization of nanoparticles can occur under autogenerated pressure during the hydrolysis process. In addition to that, the hydrothermal method is environmentally friendly since the reactions are carried out in a closed system and the contents can be recovered and reused after cooling down to room temperature [112].

The hydrothermal methods are useful to control the size, morphology, crystalline phase and surface chemistry by adjusting the sol composition, reaction temperature, pressure, property of solvent and aging time [112]. Most of the hydrothermal synthesis processes need an accurate control of low temperature and pressure systems [113]. The temperature of hydrothermal processes is usually under 250 ºC and the pressure in the autoclave reaches to 2.0-6.0 atm. Complete hydrolysis could be obtained in the autoclave without adding excessive water [114].

2.5.2.1. Hydrothermally Treated Titania: Trititanate Nanoparticles

For synthesizing titanium nano particles, TiO_2 (anatase) particles should be treated with NaOH solution. The solution concentration should be at least 5 M while temperature should be 60 °C at minimum. After that the product should be washed with 0.1 N HCl and then with deionized water until the solution reaches to neutral pH conditions [40]. The product will be either a nanotube or a nanoplate with trititanate structure ($H_2Ti_3O_7$). As a basic medium, NaOH seems to be a crucial material and other bases do not promote the generation of nanotubes. Trititanate formation is not produced in a single step transformation of TiO_2 crystals where Na contained disordered material formation takes place as intermediate step. After an ion-exchange between Na^+ and H^+, a single layer of trititanate is formed [30]. When those sheets grow planarly, (two-dimensional), they simultaneously roll and form a nano tube. On the other hand, when those sheets grow three dimensionally, a nano plate formation is not occurring. In both cases, particles consist of several layers of trititanate [31, 32] and classified as nanostructured material.

Trititanate nanotubes are formed by scrolling up of multi layers of trititanate. For this reason, they have open ends, which are not seen in carbon nanotubes. The d-spacing of the layers is 0.78 nm, which can not be observed by XRD because the number of layers is not more than four. The crystal structure of the nanotubes fits $H_2Ti_3O_7$ (trititanate, monoclinic, a = 16.03, b = 3.75, c = 9.19 Å and β = 101.45º). Figure 2.3.2.1-1 shows a structural model of 2x2 unit cells of the $H_2Ti_3O_7$ crystal looking along the [010] direction. The structure of $H_2Ti_3O_7$ is seen to be composed of corrugated ribbons of edge-sharing TiO_6 octahedrons. The ribbons are three octahedrons wide, and these octahedrons join at the corners to form a stepped layered structure (Figure 2.5.2.1-1) [115].
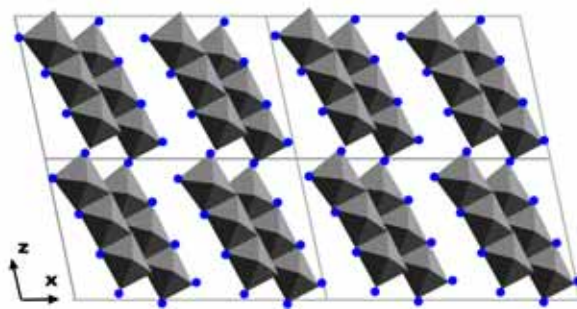
Figure 2.5.2.1-1 Structure model of 2x2 unit cells of $H_2Ti_3O_7$ on the [010] projection [115]

The structure of a layer of TiO_6 octahedrons is shown in Figure 2.5.2.1-2, together with the coordinate system. For the simplest tube structure, the tube axis is along [010] and the tube may be constructed by wrapping a (100) plane atoms along the line AA'. While a perfect nanotube, such as a carbon nanotube, may be formed by joining points A and A', a scroll nanotube may be constructed by displacing the point A' outward by a layer spacing of 0.78 nm, as shown in Figure 2.5.2.1-3. Figure 2.5.2.1-4 shows a cross-sectional view of a multi-walled scroll nanotube formed by four layers of atoms. As it can be seen mostly (001) plane is available for contact.
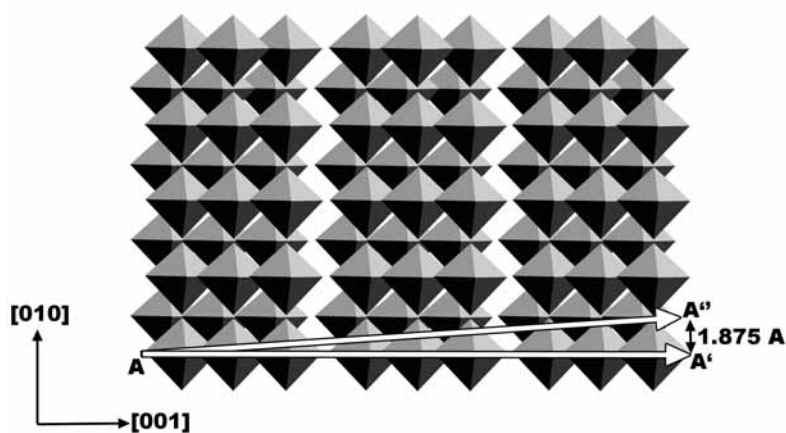
Figure 2.5.2.1-2 A layer of $H_2Ti_3O_7$ on the (100) plane [115]
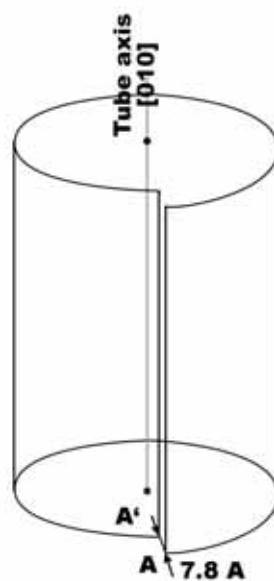
Figure 2.5.2.1-3 The displacement vector AA' when wrapping up a sheet to form a scroll-type nanotube [115]
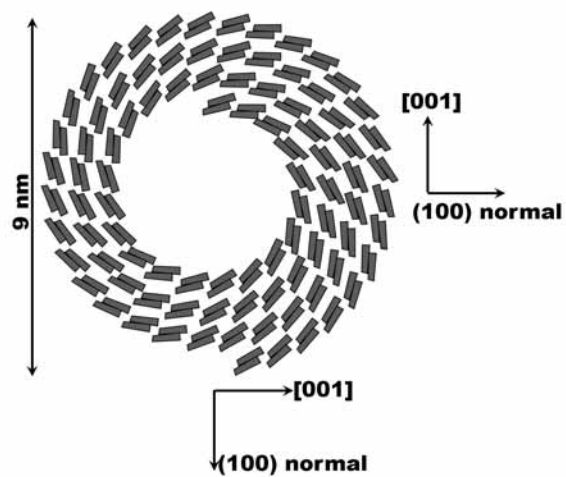
Figure 2.5.2.1-4 The structure of the trititanate nanotube [115]

XRD data of trititanate for room temperature is given at Table 2.5.2.1-1. The crystal structure of trititanate is stable until 200 ºC, after that temperature the reflection peak at 11.2, which corresponds to (200) plane, shifts towards a higher angle. (200) plane is the interlayer plane of reflection and shifting to a higher angle means that the d-spacing decreases. This is explained by dehydration of interlayers. Heating nanotubes to 700 ºC will change the structure to anatase and at higher temperatures they will be converted to rutile [32].

Table 2.5.2.1-1 XRD data for trititanate [115]

2 Theta (deg.)	Intensity (%)
9,54	60
11,2	100
24,4	40
29	70
32,3	30
33,5	40
37,9	30
48,4	70
60	20
61,8	30

2.5.3 Other Synthesis Methods

Titania can be synthesized with various methods. Since their details are beyond the focus of this study, they will be explained briefly.

One method is the precipitation method. In precipitation methods, hydroxides are precipitated by addition of a basic solution to a raw material followed by calcination to crystallize the oxide. The disadvantage of these methods is the difficulty of controlling particle size and size distribution. Uncontrolled precipitation often causes formation of larger particles instead of nanoparticles [116-120].

Another method is microemulsion. In this technique, nanoparticles can be obtained by mixing the microemulsion of the precursor and the microemulsion precipitating agents by mixing two microemulsions or it can also be obtained by simply adding the precipitating agent to the microemulsion of the precursor [121]. The synthesis of TiO_2 nanoparticles with microemulsion method is very similar to the reactions used in sol-gel methods and both anatase and rutile polymorphs can be synthesized with this microemulsion technique.

Gas phase synthesis is another important way for the synthesis of TiO_2 nanoparticles. There are lots of studies investigating the formation of TiO_2 nanoparticles films in gas phase. These techniques are: chemical vapor deposition (CVD), physical vapor deposition (PVD), inert gas condensation, pulsed laser ablation spark discharge generation, ion sputtering, spray pyrolysis, laser pyrolysis/photothermal synthesis, thermal plasma synthesis, flame and flame spray pyrolysis techniques [122-127].

2.6. Recent Progresses on TiO_2 Catalysts for Photocatalysis

Photocatalytic TiO_2 reaction systems has mainly focused on utilizing either suspensions or immobilized TiO_2 films in batch or continuous flow systems. Each system has its own advantages and disadvantages.

There are some works investigating TiO_2 suspensions [180, 181]. When compared with the immobilized TiO_2 systems, mass transfer and adsorption of the organic substrates on the TiO_2 surface are much better in the suspension system. When the reaction system is stirred, photocatalysts move with the reaction solution and it is hard to concentrate light on the TiO_2 photocatalyst. So, when stirring, a light concentrating reflector may be required. The major concern for the applications of TiO_2 suspensions is the separation and recovery of the suspended TiO_2 nanoparticles after the reaction. Because of the tiny size of the nanoparticles, it is hard to separate and recover the TiO_2 catalyst from the liquid medium through conventional separation methods such as sedimentation, filtration or centrifugation. In addition to that, the suspended nanoparticles tend to aggregate at high concentrations which leads to a decrease in the surface are of the photocatalyst. The difficulty in the recovery of the TiO_2 photocatalyst limits the application of the TiO_2 suspension systems.

This problem of photocatalyst separation can be overcome by using TiO_2 films on different substrates. Various studies were made on immobilized TiO_2 films [206-208]. Also some other studies have been focused on supported TiO_2 photocatalyst films [203]. On immobilized TiO_2 film, TiO_2 nanoparticles were usually immobilized on inert stationary supports such as glass, fiberglass, sand, silica gel, activated carbon, stainless steel, anodized iron, woven fibers and ceramic membranes. Immobilized TiO_2 systems are generally favored in scaling up because these systems can exclude the expensive secondary recovery of catalyst and are more suitable for continuous flow reaction systems. The most important concern when designing immobilized TiO_2 system is the photocatalytic reaction rates may be limited by the mass transfer rates in the solutions. Another important problem is the light scattering phenomenon for an immobilized TiO_2 system. In addition to that, TiO_2 catalyst coated on some supports may detach [204].

Also there are some examples that carbon nanotubes are used as a support. Boccacini et al. [235] reports that CNT's are excellent carrier substrates for TiO_2 nanoparticles, because of their high structural integrity and the high surface area they provide due to the possibility of building a mesoporous structure. In literature, the CNT/TiO_2 system was prepared with various methods like electrophoretic deposition [235], simply mixing and drying [236], and addition of CNT's during gelation of TiO_2 [237, 238]. All these articles showed that CNT's are very stable as a support and helping the photocatalytic activity.

CHAPTER 3

EXPERIMENTAL PROCEDURE

The photocatalytic activity of TiO_2 samples in powder and thin film form were studied. The effect of hydrothermal treatment temperature, treatment time and pH on catalytic activity of TiO_2 was examined and the surface and bulk properties of the samples were characterized with XRD, SEM, BET and TGA. The photocatalytic methylene blue degradation reaction and *E.Coli* inactivation methods were chosen as a probe technique for activity tests. Also the effect of CNT addition on activity and textural properties was studied. The textural properties of the catalyst samples were tried to be altered by the catalytic removal of CNT's by thermal oxidation.

3.1. Preparation of Titania Gel

The TiO_2 samples were synthesized by using sol-gel technique. Titanium tetraisopropoxide (TTIP, Aldrich, extra pure grade, CAS: 546-68-9), ethanol (C_2H_5OH, 99.5%) and 35% $HCl_{aq.}$ (CAS: 7647-01-0) were utilized as precursors. On the synthesis, 8.4 ml of TTIP was first dissolved in 20 ml ethanol and hydrolyzed with drop wise addition of ethanol–HCl–water mixture (130:0.24:0.5 ml) in thermostated bath at 0 °C, under continuous stirring. The final solution was kept at the same temperature for 30 min to ensure for complete hydrolysis. After that the sol is ready and should be stored in an airtight container.

3.2. Pretreatment of Microscope Slides and Coating of the Slides with Sol

The microscope slides to be coated should first be cleaned with a liquid detergent (CIF, 20-35 % active component) and then rinsed with deionized water. Later on the slides are left in saturated NaOH solution for 16 hours. Cleaning of slides performed first by rinsing with deionized water in ultrasonic bath for 10 minutes and washing with a boiling solution of 50 % ethanol and 50 % chloroform and rinsed in the ultrasonic bath for 10 minutes again. Finally, the slides are rinsed with deionized water and left for drying.

The glass slides are coated with colloidal solutions of TiO_2 which are synthesized by sol-gel technique by using dip coating technique (Figure 3.2-1). The coating was performed with pulling the sample from solution at 1.5 cm/min speed. The five consecutive layers of coating were applied with the same speed followed by the drying of samples in oven at 120 °C for 20 minutes. Slides which are coated with titania gel (T) are dip-coated 5 times and calcined at 600 °C for 10 minutes then left for cooling in the oven. In order to test the effect of calcination temperature, some of the titania coated samples were calcined at 500 °C for 2 hours and left in the oven until cooled (TT).

Figure 3.2-1 Dip coating apparatus

3.3. Synthesis of Titania with Carbon Nano Tubes (CNT's)

The photocatalytic activity of TiO_2 over CNT's and the use of CNT's as nanostructured 3D templates were also examined. The synthesis of TiO_2 by using sol-gel technique is the initial step of this method and the same procedure above was applied. The appropriate amount of CNT suspension (Nanocyl, NC 7000) was added to the solution to achieve 40% CNT loading. Thus titania solution containing 0.467 g of CNT for 100 mL of titania solution was formulated. On CNT loaded TiO_2 samples, the heat treatment were carried out under N_2 atmosphere at 400 °C for 120 minutes. For CNT 3D templated samples, the calcination was carried out under air flow at 400, 500 and 570 °C for 120 minutes. In order to decrease the oxidation temperature of CNT's, various amounts of $FeCl_3$ (CAS: 7705-08-0), $CoCl_2$ (CAS: 7646-79-9), NaCl (CAS: 7647-14-5) and Na_2CO_3 (CAS: 497-19-8) were added into the formulation which are catalyst promoters for carbon oxidation. This solution can again be used in dip-coating or dried and used as a powder. For dip-coating, before every new layer was coated, solution was ultra-sonically stirred for 5 minutes. After coating the slides for 5 times, slides were calcined at 500 ºC for 5, 10 and 15 minutes.

3.4. Hydrothermal and Post Treatment of the Samples

Synthesized titania sol was dried in the oven at 60 ºC overnight, and after mashing the aggregates in mortar, the samples were calcined at 600 ºC for 2 hr and kept in desiccator for further use. In addition to the sol-gel synthesized TiO_2 samples, commercial TiO_2 samples (Anatase, Aldrich 99.9%, CAS: 1317-70-0) were also tested as starting material for comparison. Trititanate nanoparticles were both synthesized from commercial TiO_2 (99.9+ % anatase, Aldrich) and sol-gel synthesized TiO_2. For the synthesis of trititanate samples, similar procedure of Kasuga et al. [28, 29] and Idakiev et al. [27] was applied. In the synthesis, 1.5 g of either commercial or sol-gel synthesized samples with 100 mL of 10 N NaOH (NaOH, MERCK, pure, CAS: 1310-73-2) were sealed in autoclave with Teflon insert (Figure 3.4-1). The autoclave was kept in an oven at 130 ºC for 24 and 48 hr. The resulting suspension was filtered, and washed several times with 0.1 N HCl solution until the pH of filtrate is reduced to 1 to perform protonation. The excess HCl was removed by washing with distilled water until the neutral filtrate (pH=7) was observed. After drying at 60 ºC for 2 hr, the cake was mashed in the mortar, and stored in a desiccator

for further analyses and hydrothermal treatment. In the post hydrothermal treatment of trititanate particles, 1 g of the as-prepared trititanate nanoparticles were mixed with 100 ml of distilled water followed by hydrothermal post-treatment of the mixture at 200 ºC in a Teflon-lined autoclave for 12, 24 and 48 hr. After the hydrothermal post-treatment, the obtained samples were filtered and dried in an oven at 80 ºC for 4 hr. The catalysts preparation and the samples prepared using different treatment methods are summarized in Table-3.4-1.

Table 3.4-1 Sample preparation methods and catalyst samples

	Treatment -1 Time[a] (h)		Post Treatment-1 Time[b] (h)			Post Teratment-2 Time[c-d] (h)		
			12	24	48	4	4	4
Commercial TiO$_2$	24	Com24	Com24-12	Com24-24	Com24-48			
	48	Com48	Com48-12	Com48-24	Com48-48			
Sol-Gel Synthesized TiO$_2$	24	SG24	SG24-12	SG24-24	SG24-48			
	48	SG48	SG48-12	SG48-24	SG48-48	SG48-24R[c]	SG48-48R[c]	SG48-24C[d]

a) The commercial and sol-gel derived samples were treated with 10N NaOH solution at 130 ºC.
b) The samples were further treated with distilled water at 200 ºC.
c) These samples were treated with distilled water under 0.1mW/m^2 irradiation at room temperature.
d) This sample was treated with distilled water in dark at room temperature.

Figure 3.4-1 Autoclave setup for hydrothermal treatment of TiO$_2$

To increase the photocatalytic activity of the coated slides, after the calcination, they were hydrothermally treated. Some of the slides are hydrothermally pos-treated with deionized water at 200 °C for 24 hours (TH, TTH).

3.5. Characterization

The X-ray diffraction (XRD) patterns were collected for samples by a X-ray powder diffractometer (Philips, PW 1840) with Cu target and Ni filter (λ_{Cu} K_{α} = 1.5418 nm) between 5 and 80 Bragg angle values. Also scanning electron microscopy (SEM, Gemini Leo 32 Supra 35VP) and atomic force microscopy (AFM, Nanosurf Easyscan) were used for surface imaging. The BET specific surface area and the pore size distribution were determined by gravimetric absorption analyzer (IGA-200 Hiden) and Gemini V Series surface area analyzer (Micromeritics) with N_2 sorption technique. Since hydrophilicity is an important parameter for titania, contact angle measurements were made. Also for some samples, TGA (Shimadzu DTG-60H) and DTA (Shimadzu DSC-60) analyses were performed.

3.6. Photocatalytic Antimicrobial Activity

Photocatalytic activity of sol-gel synthesized, commercial, and their hydrothermally treated counterparts was tested on *E. coli*. A Pyrex glass container of 100 ml (3 cm in diameter and 6 cm high) was used as a batch reactor. Total reaction mixture volume was 20 ml. The reaction mixture contained 3.5 g/l TiO_2 and *E. coli* of about 10^3 cells/ml in 0.1 % peptone water. The mixture was agitated with a magnetic stirrer at 250 rpm at ambient temperature while artificial irradiation source was illuminated vertically. Photocatalysis was performed up to 4 hr. Osram Ultra-Vitalux (Product number: 03313) 300 W bulb with similar spectral distribution to solar spectrum between 280 and 780 nm was used as artificial irradiation source. The light intensity over the test bench was adjusted to achieve 10 mW/cm^2 within the visible range by adjusting the distance between the sample and light source. Sample of 1 ml reaction mixtures were removed at various time intervals and 200 μl of it was directly spread onto the agar plates and incubated at 35 °C for 24 hr to determine the survivors by counting the colony-forming units (CFUs). Two

36

control experiments carried out for each set of data, one without TiO_2 under irradiation and the other one with TiO_2 but in the dark [21].

3.7. Photocatalytic Activity

Photocatalytic activities of the coated samples were tested by the deactivation of 200 ppm methylene blue (MB, MERCK, 82 %). For this purpose, the coated glass samples were stained with methylene blue solution and exposed to light in artificial sun light simulator (Suntest CPS+, Atlas) under 300 W/m^2 irradiation flux for 24 hours. The simulator was equipped with a soda glass filter. On the other hand, the quantitative measurements were also carried out with 300 mL of 2 ppm methylene blue. On the reaction experiments, the solution containing catalyst sample was stirred under artificial irradiation (Figure 3.7-1). The samples taken at 30 minutes interval were analyzed by UV-Vis spectrometer. The absorbance wavelength of samples was 665 nm. The concentration of methylene blue in samples was determined by comparing the measured absorbance with calibration data.
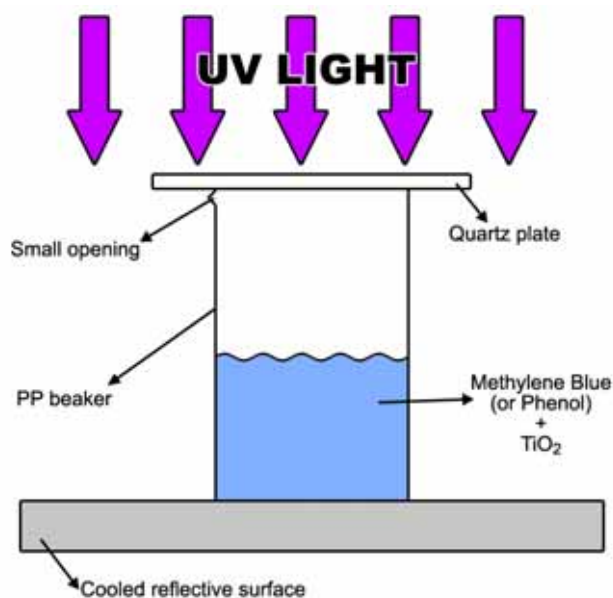
Figure 3.7-1 Photocatalytic activity test setup

CHAPTER 4

RESULTS & DISCUSSION

In the first part of the research, TiO$_2$ particles were synthesized with sol-gel technique. To obtain high surface area nano particles, TiO$_2$ were hydrothermally treated under alkali conditions. During the treatment, anatase particles converted to trititanate. Since trititanate is not photocatalytically active, a further treatment was needed. This treatment was hydrothermal treatment under neutral condition. After that treatment, anatase nano particles with high surface area were obtained. Also to compare the results of sol-gel based samples, same procedures were applied to commercial anatase.

4.1. Characterization of trititanate nanoparticles

SEM analysis revealed that commercial anatase (Com) has spherical particles with an average size of 170 nm. The sol-gel (SG) synthesized particles are comprised of large clumps around 10 μm size and aggregates consist of 50 nm spherical particles (Figure 4.1-1). After hydrothermal treatment of both samples under alkaline conditions obtained with 10 N NaOH (treatment-1), commercial anatase and sol-gel anatase transformed into different structures significantly. Commercial anatase hydrothermally treated for 24 hours (com24) has fibrous structure resembling the presence of nanotubes or wires. As it is presented in Figure 4.1-2, these particles have a diameter of about 30 nm and 650-700 nm long. Further hydrothermal treatment of commercial anatase for additional 24 hours (Com48), this fibrous structure transforms into rod-like particles with 25 nm diameter and their length is about 100 nm (Figure 4.1-2). Conversely hydrothermally treated sol-gel anatase transformed to nano-sized lamellar structure. The sol-gel synthesized sample hydrothermally treated for 24 hours (SG24) yielded 50 nm thick flat lamellar particles with a wide particle size

distribution. An additional 24 hour hydrothermal treatment (SG48) thickened the lamellar particles to about 600 nm (Figure 4.1-2).

The samples which were hydrothermally treated under alkaline conditions were further treated with distilled water hydrothermally (post treatment-1). Prominent change in the particle morphology was observed. 12 hours of hydrothermal treatment of commercial anatase which was treated for 24 hours under alkaline conditions (Com24-12) was converted into dispersed particles with particle size of about 120 nm. When the post treatment time increased further, for 24 and 48 hr, results crystal growth, and octagonal particles were obtained. The growth of crystals can be explained by the thermal stabilization of nanostructured crystallites under the hydrothermal conditions. Also the crystal growth under the elevated temperatures might be attributed to the thermodynamically controlled Ostwald ripening process [209] (Figure 4.1-3).

Com48-12 first formed curvy spiked nanoparticles with thickness of about 60 nm, and further increase of treatment time for 24 and 48 hr yield crown like ridged larger particles (Figure 4.1-3). Similarly, crystal growth was observed with post treatment-1 time.

SG24, after post treatment-1, showed a drastic change in particle morphology. The samples after 12, 24 and 48 hr post treatment-1 have distinct octagonal shape. 12 hr post-treated particles are about 150 nm thick and 600 nm long. Crystal growth is much more apparent than the commercial anatase samples which were treated same way (Figure 4.1-4).

The particle morphology after 48 hr hydrothermal treatment with NaOH and post treatment-1 yield smaller particles than 24 hr hydrothermally treated counterpart. SG48-12 particles are about 100 nm thick and 500 nm long. When compared with the 24 hr counterpart, particles do not have distinct octagonal shapes. Like the previous 24 hr counterpart, crystals growth was also observed (Figure 4.1-4).
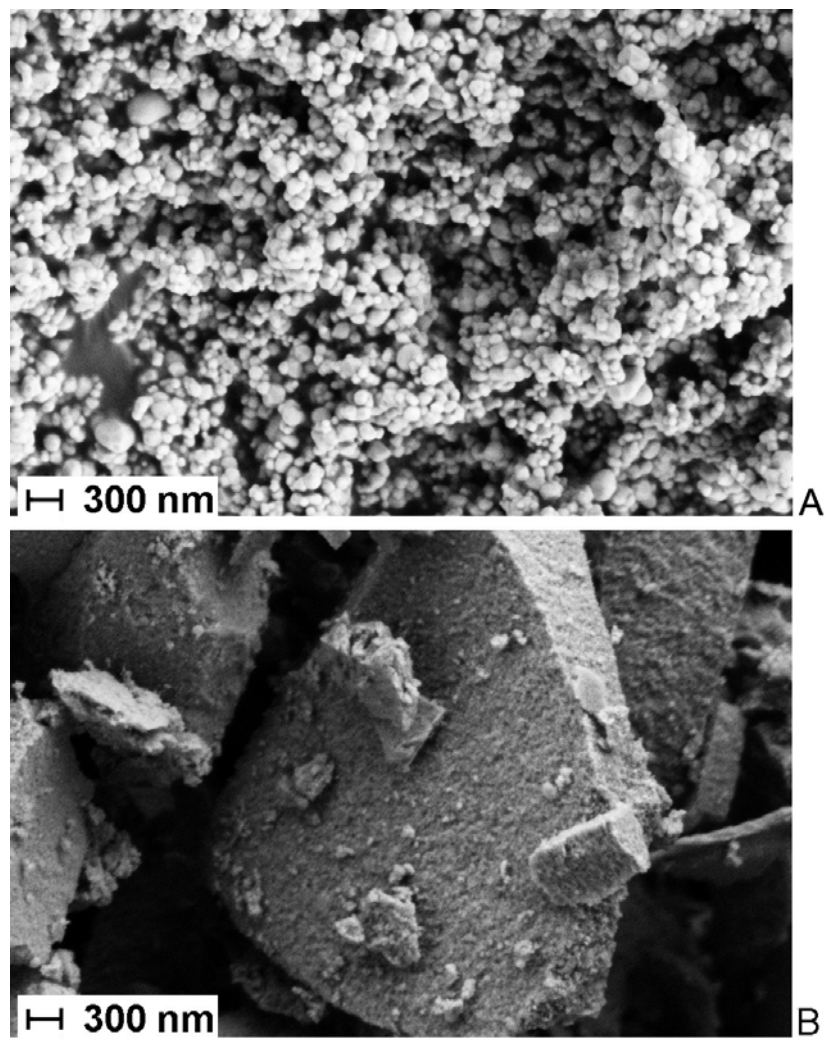
Figure 4.1-1 50 KX magnification of commercial anatase (a) and calcined
sol-gel TiO_2 (b)
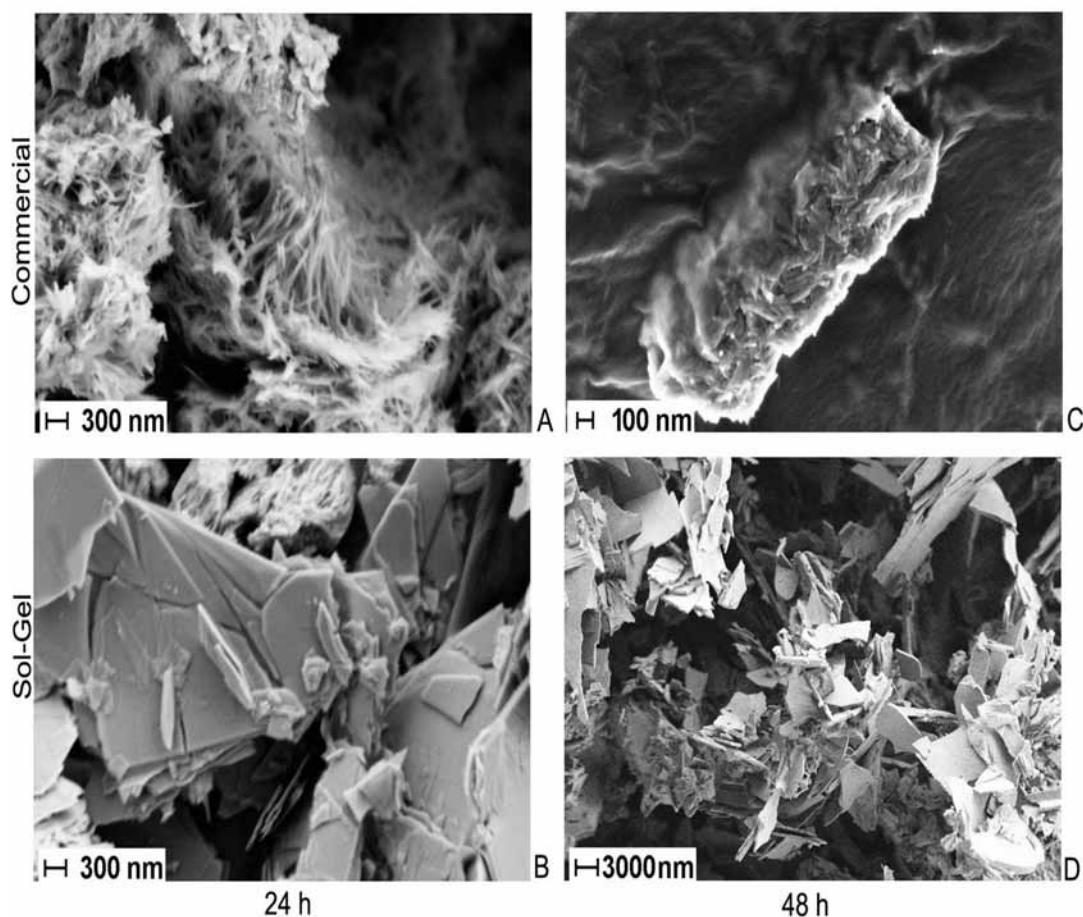
Figure 4.1-2 SEM images of hydrothermally treated commercial and sol-anatase for 24 and 48 h. (a) Commercial anatase treated for 24 h, (b) Sol-gel anatase treated for 24h, (c) Commercial anatase treated for 48 h, (d) Sol-gel anatase treated for 48 h

Anatase and trititanate have similar crystalline structures; anatase consists of TiO_6 octahedrons and trititanate consists of TiO_6 octahedrons attached to each other by protons [31, 33]. Similar to the study of Yu et al. [33], by post hydrothermal treatment, trititanate particles were dehydrated and the trititanate structure began to convert to anatase. A reaction was suggested by Zhang et al. [215] for layered trititanate (Equation 4.1-1); according to that H^+ combines with OH^- at the neighbor trititanate layer and leaves the structure (Figure 4.1). At the end of dehydration process, anatase is formed.
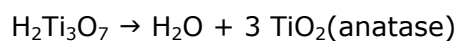
$$H_2Ti_3O_7 \rightarrow H_2O + 3\ TiO_2(\text{anatase}) \hspace{3cm} (4.1\text{-}1)$$
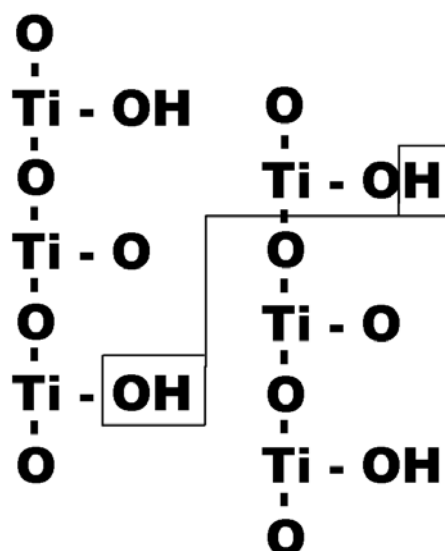
Figure 4.1. Dehydration of layered trititanate with neutral hydrothermal treatment

XRD pattern of SG and Com samples are shown in Figure 4.1-5. Commercial TiO2 sample comprised of pure anatase as it can be seen from the diffraction pattern presented in 4.1-5.b. The sol-gel synthesized sample has traces of 27.70 º which can be attributed as the main diffraction peak of rutile (Figure 4.1-5.a) After hydrothermal treatment under alkaline conditions, all the samples transformed into the mixture of anatase, trititanate and rutile (Figure 4.1-6). The nanotube and nanostructured lamellar structure is clearly identified with diffraction line at 9.5°. From Figure 4.1-6, it can be seen that anatase content decreases with hydrothermal treatment duration. After post treatment with distilled water, the diffraction peak of nanotubes (or nanoplates) located at about 9.5° was diminished considerably and the anatase peak at about. 25.3° became more intense, indicating the destruction of trititanate structure and the formation of anatase phase as a result of crystal growth which was also observed in SEM analysis.
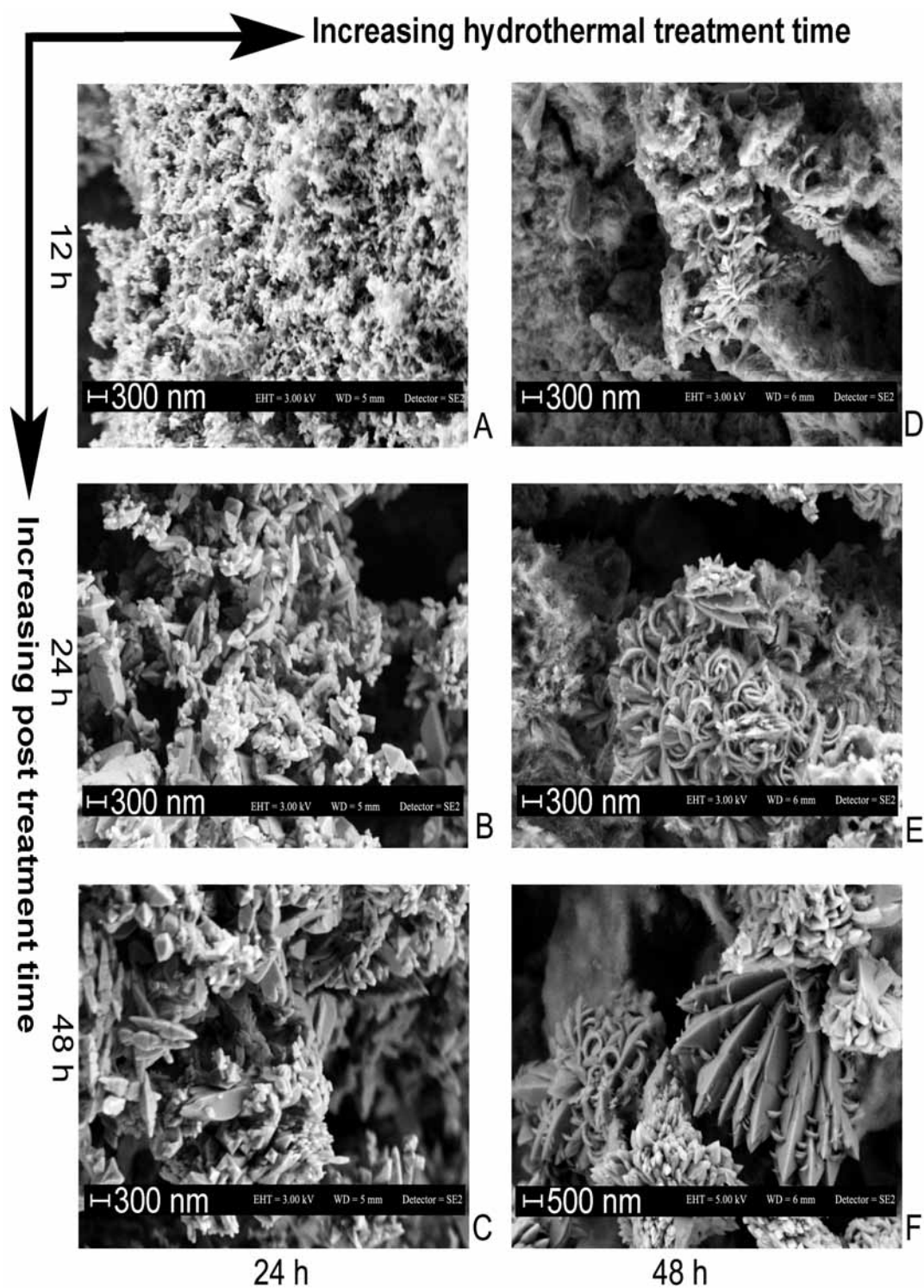
Figure 4.1-3 Commercial anatase after 24 hr hydrothermal treatment and (a) 12, (b) 24, (c) 48 hr of post treatment. Commercial anatase after 48 hr hydrothermal treatment and (d) 12, (e) 24, (f) 48 hr of post treatment
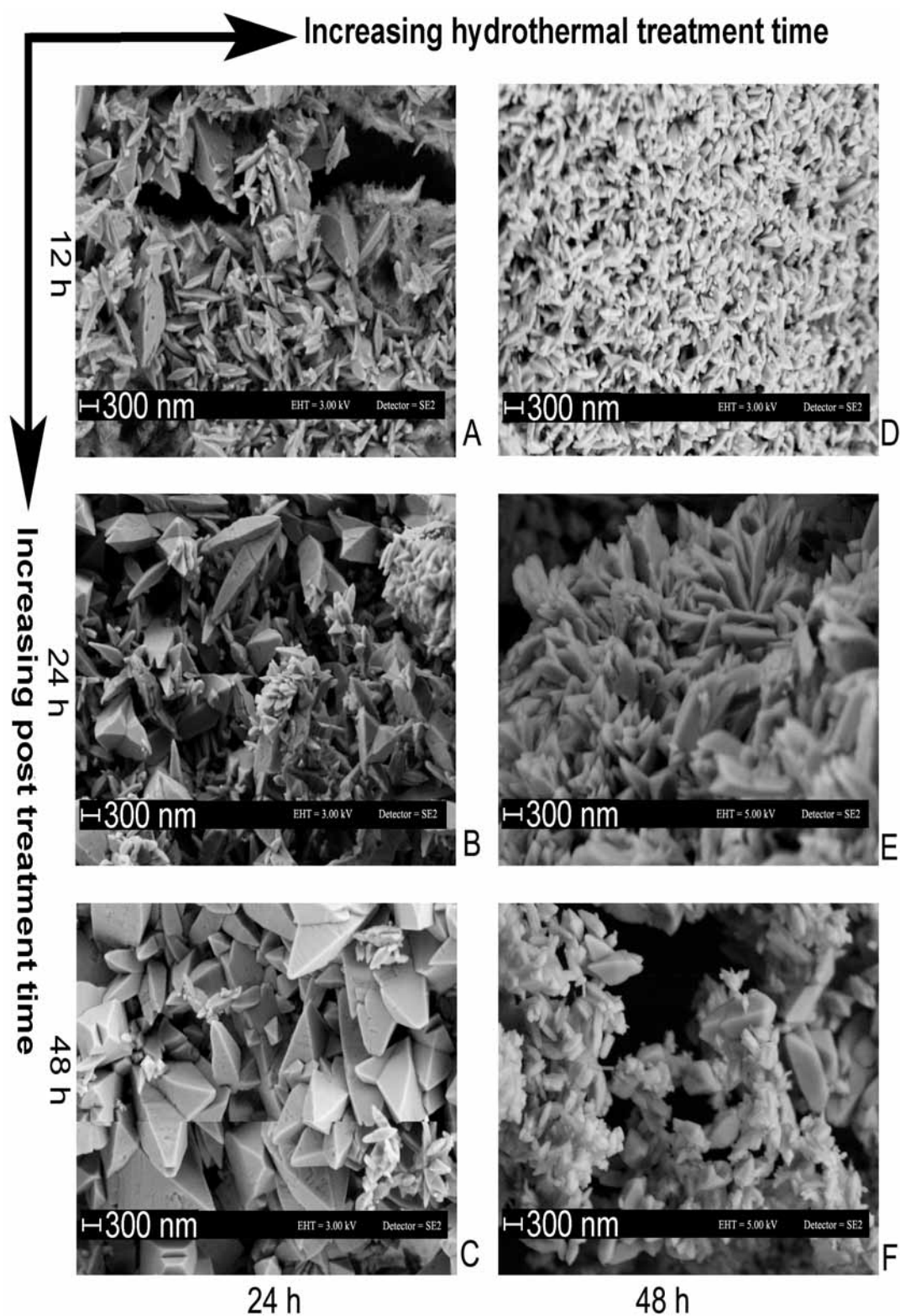
Figure 4.1-4. Sol-gel anatase after 24 hr hydrothermal treatment and (a) 12, (b) 24, (c) 48 hr of post treatment. Commercial anatase after 48 hr hydrothermal treatment and (d) 12, (e) 24, (f) 48 hr of post treatment
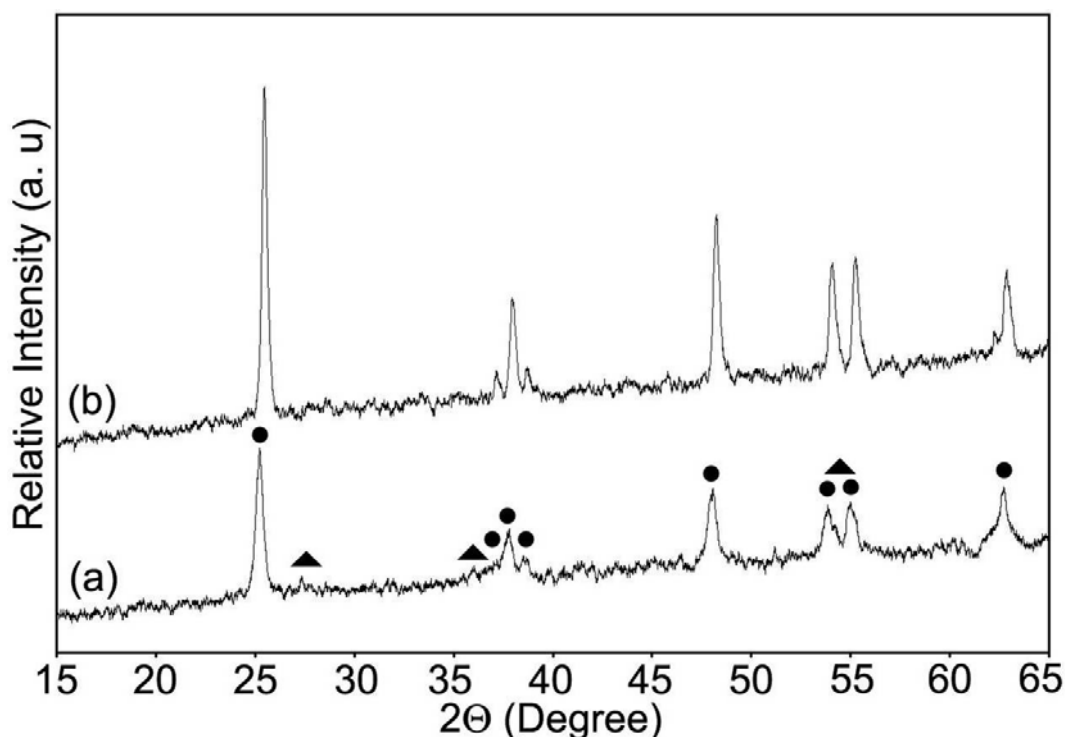
Figure 4.1-5. XRD pattern of (a) calcined sol-gel TiO_2 and (b) commercial TiO_2 (•, anatase; ▲, rutile)

The increase in hydrothermal treatment under neutral conditions caused the transformation of trititanate phase into anatase phase. It is clear that (Figure 4.1-7, 4.1-8); the crystallization of anatase phase or crystal growth is favored by hydrothermal treatment. It is observed that increase in hydrothermal treatment under alkaline conditions, suppresses the formation of anatase phase by hydrothermal treatment. This may be attributed to the formation of more trititanate crystallites during alkaline treatment. Sol gel synthesized sample yield higher anatase phase compared to the commercial counterpart. With increasing alkaline hydrothermal treatment time, all of the diffraction peaks of anatase shift to a higher degree. This is also reported by Teng et al. [43], and attributed to the dehydration and the conversions of nanotubes are to the turbostratic anatase, which have higher d-spacing. After post treatment under neutral conditions, turbostratic particles formed and converted to anatase, with smaller d-spacing. As result, XRD peaks become more intense and shift to a higher degree.
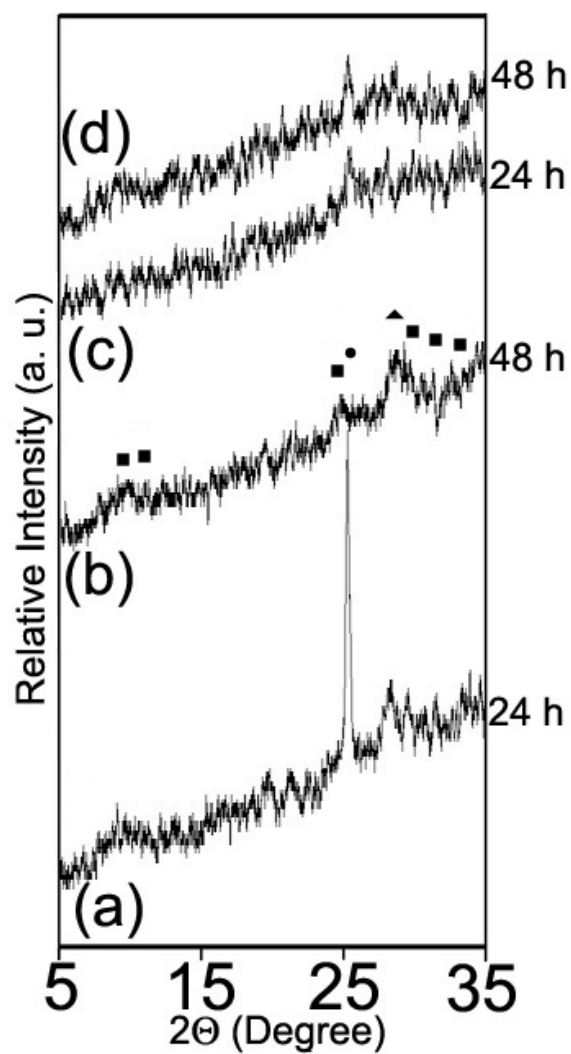
Figure 4.1-6 XRD pattern of the samples after hydrothermal treatment.
Commercial TiO_2 treated for (a) 24 h and (b) 48 h. Sol-gel TiO_2 treated for (c)
24 h and (d) 48 h. (•, anatase; ▲, rutile; ■, trititanate)
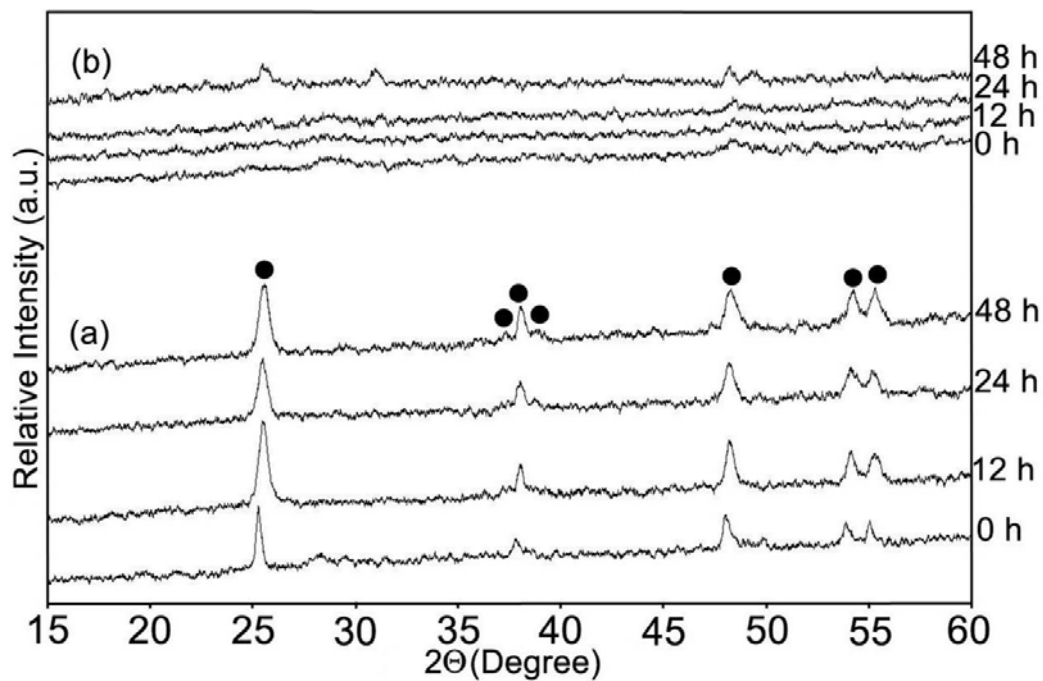
Figure 4.1-7 XRD patterns of hydrothermally and post-treated commercial TiO$_2$ samples with respect to time. Set (a) treated hydrothermally for 24 h and set (b) hydrothermally treated for 48 h. (•, anatase)
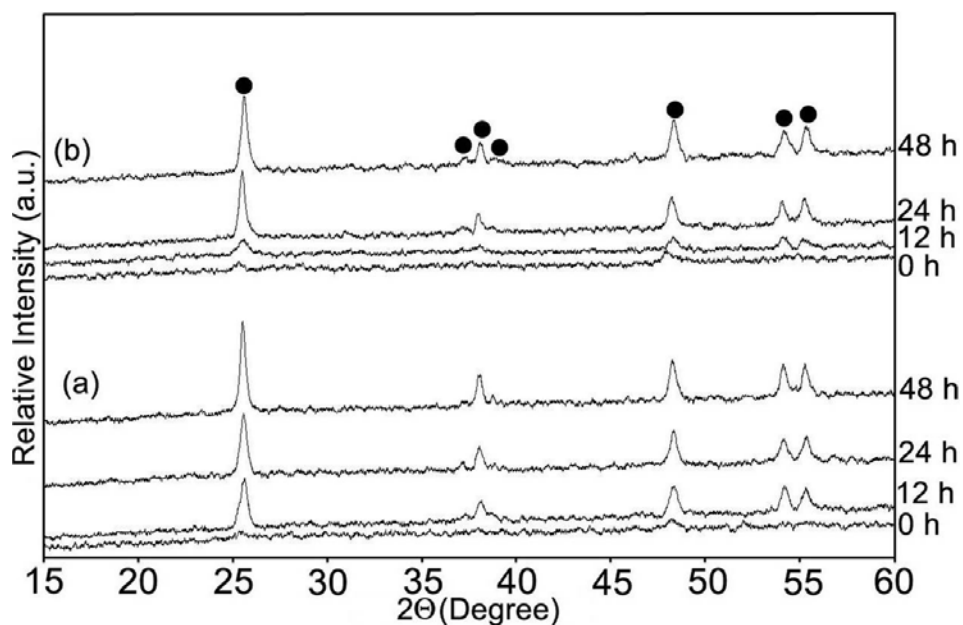
Figure 4.1-8 XRD patterns of hydrothermally and post-treated sol-gel TiO$_2$ samples with respect to time. Set (a) treated hydrothermally for 24 h and set (b) hydrothermally treated for 48 h. (•, anatase)

47

4.2. Structure of Dip-Coated Samples

AFM analysis showed that titania coating before calcination does not have any uniform structure and, after the calcination spherical particles started to appear over the surface (Figure 4.2-1). The sizes of the particles are about 40 nm for the samples which are dip-coated with titania gel and calcined for 10 minutes (T) (Figure 4.2-2.a) while it is 50 nm when dip-coated samples are calcined for 2 hours (TT) (Fig. 4.4-2.b). Also it was seen that TT samples are closely packed when compared with the T samples. After alkaline hydrothermal treatment, most of the coating flaked. Analyses with SEM and AFM showed that remained samples over the surface have highly porous structure. The structure is comprised of fibrous (Figure 4.2-3. a & b) structure.
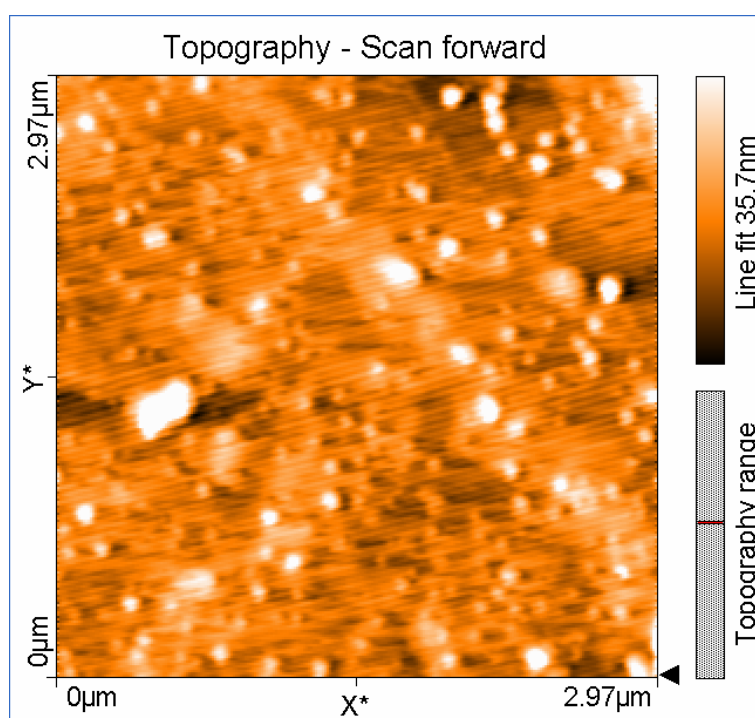
Figure 4.2-1 AFM image of titania coating before calcination
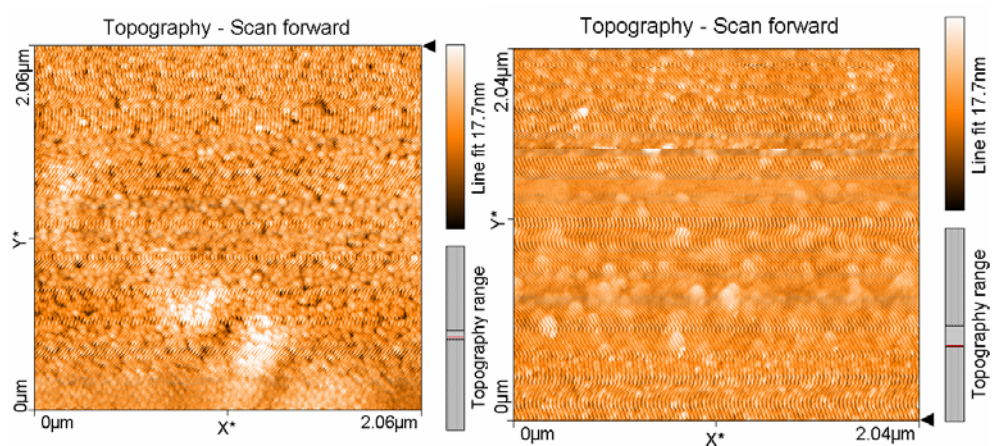
a)   b)

Figure 4.2-2 AFM image of the a) T coating and b) TT coating
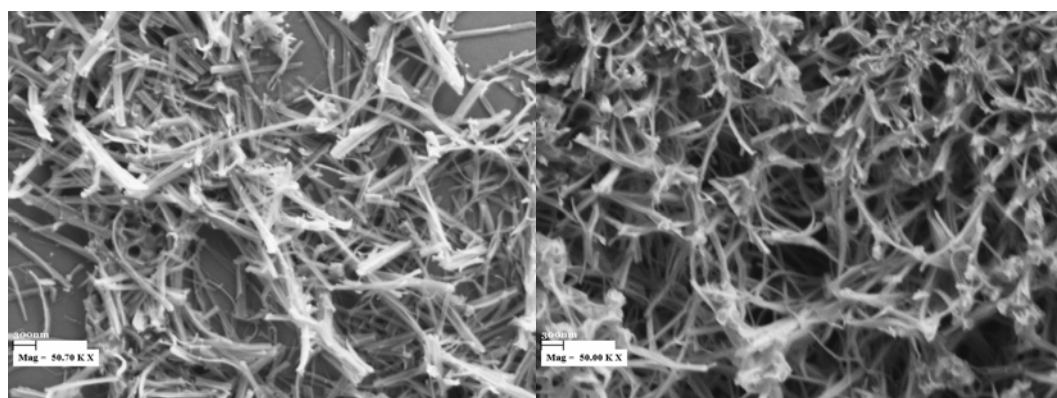
a)   b)

Figure 4.2-3 50 KX SEM images of a) TH coating and b) TTH coating

The specific surface area and pore size distribution of powder samples were determined by using BET N_2 adsorption technique. Since the amount of coatings was very low in thin film samples and detaching coatings from the slides is very difficult, surface area analyses for thin films were not possible to be carried out. For hydrothermal treatment, samples after treatment-1 and post treatment-1 showed Type-IV isotherms with type H3 hysteresis loops indicating

49

the presence of mesoporous structure. The results of surface area measurements are given in Table 4.2-1.

Table 4.2-1 Surface areas of hydrothermally treated samples

Sample	Surface Area (m^2/g)
SG	19
SG24	22
SG48	22
Com	50
Com24	110
All Post Treated Com24 samples	150
Com48	110
All Post Treated Com48 samples	150

Surface area of Com and SG are about 50 and 19 m^2/g respectively. After the treatment-1, higher surface area was measured for the Com24 and Com48 (110 m^2/g) while the sol-gel counterpart (SG24 and SG48) slightly increased to 22 m^2/g. After post treatment with distilled water, the surface areas of commercial samples were measured as 150 m^2/g.

All of the samples following treatment-1 have an average pore size of 17 ºA with a sharp peak at that point (Figure 4.2-4.a). Lan et al. [209] synthesized trititanate nanotubes from rutile and obtained similar peak but with an average pore size of 3 nm. Also in literature many nano structured particles were synthesized from titania by different techniques; having an average pore size of in the range of 9-45 nm [44, 45, 220] which is quite higher than our results. However Antonelli et al. [214] synthesized mesoporous TiO_2 with average pore size of 20 ºA which is close to ours. Observing small pore size may be attributed to capillary condensation in the hollow tubes. After post treatment-1, the

porosity of the samples was reduced drastically (Figure 4.2-4.b). As can be seen from SEM images, post treatment with distilled water results with surface restructuring; nanotubes and nanoplates form ditetragonal (bipyramidal) structures which may explain the widening of the peak at Figure 4.2-4.b.
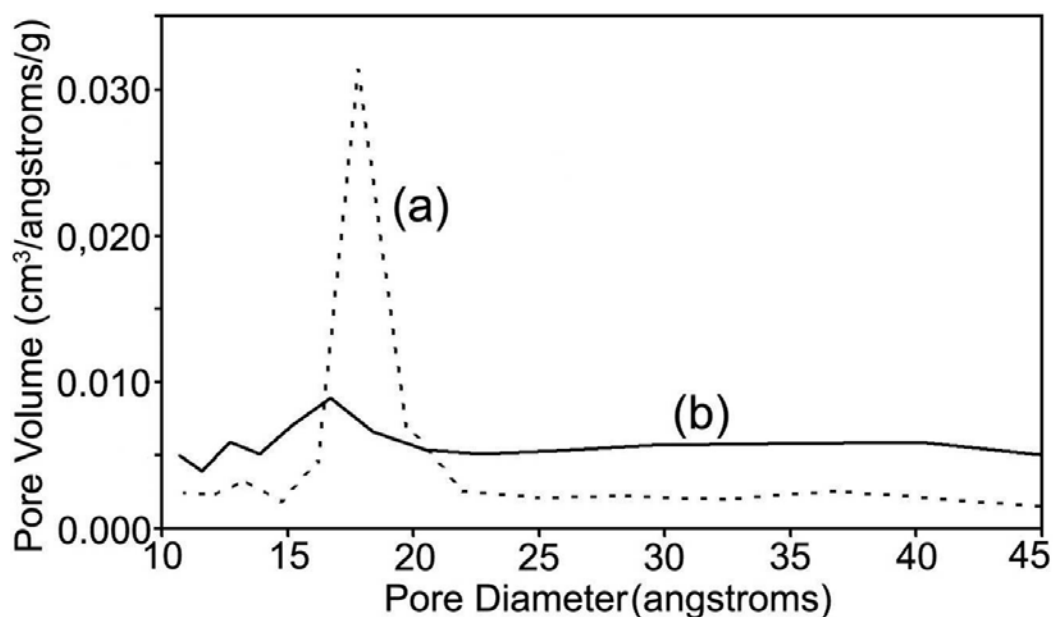
Figure 4.2-4 Pore size distribution diagram of (a) 48 h hydrothermally treated commercial TiO$_2$, (b) 48 h post treated (a)

4.3. Photocatalytic Antimicrobial Activity

In order to characterize the antimicrobial effect of the commercial (Com) and sol-gel synthesized (SG) samples and their hydrothermally treated counterparts, *E. coli* was selected as a model microorganism and the photocatalytic inactivation was examined under 10 mW/cm^2 irradiation by using 3.6 mg/l catalyst at room temperature. The effect of UV radiation on the dose applied and the non-photocatalytic toxic effect of TiO$_2$ were tested by control experiments. No microbial inactivation was observed in these control

experiments indicating neither the effect of UV irradiation nor the TiO_2 in the dark is effective alone on the microbial inactivation.

The antimicrobial performances of the commercial (Com) samples and their hydrothermally treated derivatives are presented in Figure 4.3-1. Commercial anatase sample and its hydrothermally treated counterparts (Com24 and Com48) under alkaline conditions exhibited antimicrobial activity and complete inactivation was obtained within 4 hr period for all samples. In literature, there is no agreement on the photocatalytic activities of the alkali- and protonic- titanates. Yu et al. [33] reported that protonic titanate does not possess any photocatalytic activity on the degradation of acetone in air. Similarly, no significant activity was reported for the propylene oxidation over the alkali- and protonic- titanates [215]. In both studies, thermal [215] and hydrothermal [33] treatments which alter the crystalline structure to anatase enhanced the photocatalytic activity. However in the present study, the hydrothermal treatment under alkaline conditions enhanced the antimicrobial activity (Figure 4.3-1.a). The initial rate constants of photocatalytic inactivation of *E. coli* were calculated as 0.6, 1.3, 1.3 hr^{-1} for Com, Com24, Com48 samples, respectively which is in the same order with the specific surface area of the samples (50, 110,110 m^2/g). Considering the surface area of the samples and photocatalytic activity, it could be suggested as; longer hydrothermal treatment more than 24 hr does not contribute a significant change. Following hydrothermal post treatment with distilled water (Post Treatment-1), no significant affect was observed on the initial microbial inactivation rate. However, both Com24-24 and Com48-24 samples demonstrated limited antimicrobial activity. Especially Com24-24 sample has significant loss of activity after 1 hr operation.

The antimicrobial performances of the Sol-Gel (SG) samples and their hydrothermally treated derivatives are presented in Figure 4.3-2. A limited antimicrobial activity was observed for SG samples. Although the initial inactivation rate of Sol-Gel synthesized was nearly same with commercial anatase, a complete inactivation could not be assessed, which might be related to its lower specific surface area in comparison with commercial anatase while their crystal structures are almost the same (Figure 4.1-5). However, the alkali treatment enhanced the activity (SG24 and SG48) and complete inactivation was achieved within 3 hr period (Fig.4.3-2.a). The initial inactivation rate

constants were evaluated as 0.6, 0.7 and 1.4 hr^{-1} for SG, SG24 and SG48, respectively.

The effect of post treatment with distilled water at 200 °C on the antimicrobial activity was also investigated and post treatment-1 was applied to the SG24 and SG48 samples for 12, 24 and 48 hr. Similar initial inactivation rates were observed with hydrothermally post treated samples, however the initial activity have not been sustained after the first 20 minutes of reaction (Fig.4.3-2.b) and reaction proceeds with a much slower rates for a period. During that period the number of surviving cells remains almost constant with respect to time. Notably, the activity replenished after 150 to 200 minutes and proceeded with higher rate (Fig.4.3-2.b). A similar trend was also observed for 12 and 48 hr post treatment-1 derivatives (SG24-12, SG24-48, SG48-12, and SG48-48) which is in good agreement with the results in literature for *E. coli* and Bacillus species [216]. This behavior was attributed to the concentration of oxidative species which directly influence the microbial inactivation rate. Moreover the competitive consumption of .OH species between alive and dead cells, the continuation of cell growth by using nutrients released from dead cells, and sporulation were attributed to describe the time lag mechanism [216]. All these suggestions may partially explain our results, but observing a lag phase only in Sol-Gel derivatives and the inability of sporulation of *E. coli*, bring us the opinion that there might be a different mechanism for the explanation of the time lag. Under this situation, the lag period in microbial inactivation might be attributed to the density of active surface sites and active species.
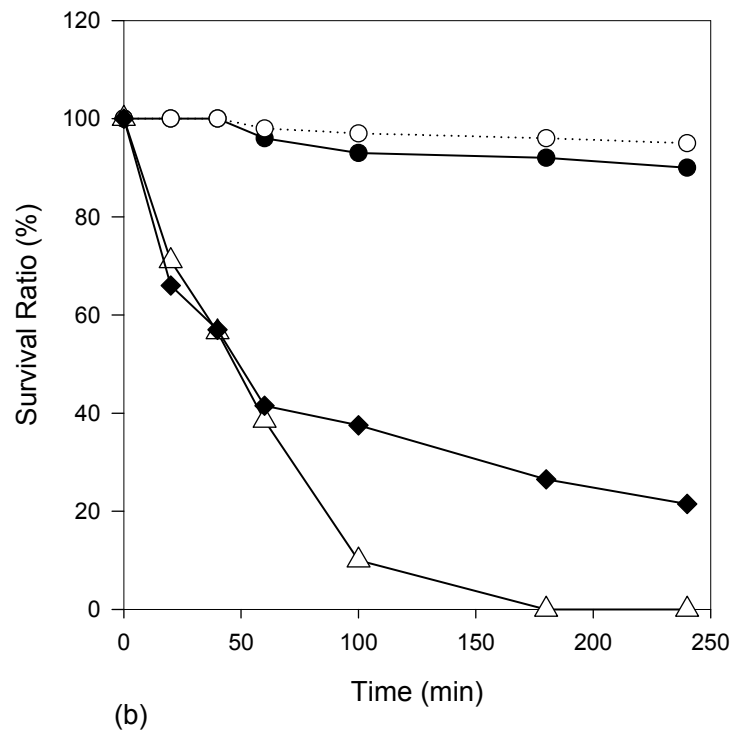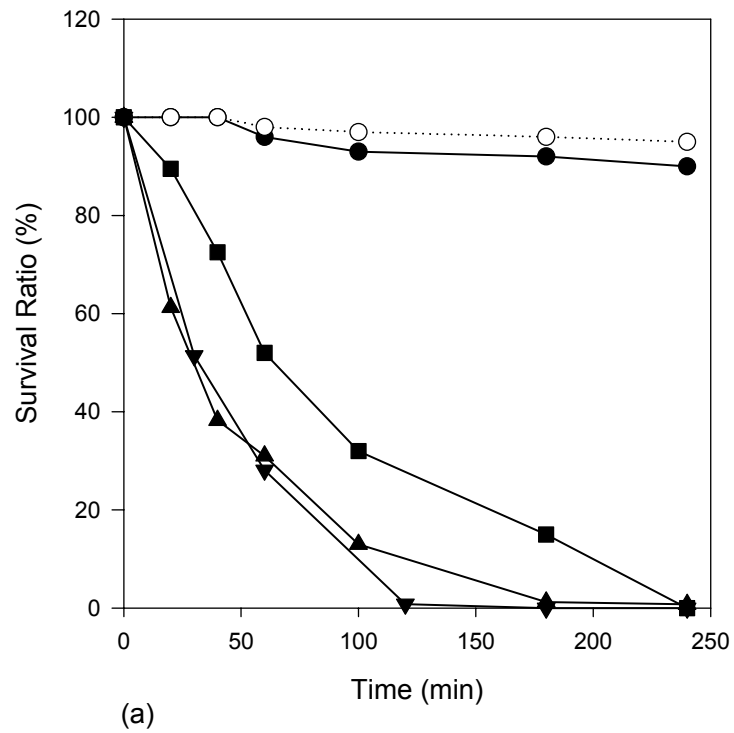
Figure 4.3-1 Effect of hydrothermal treatment on antimicrobial efficiency of commercial samples under irradiation (10 mW/cm^2) (a) After hydrothermal treatment ; (b) after post hydrothermal treatment-1 (■, Com; ▲, Com24; ▼, Com48; ♦, Com24-24; △, Com48-24; o, dark; •, under irradiation)
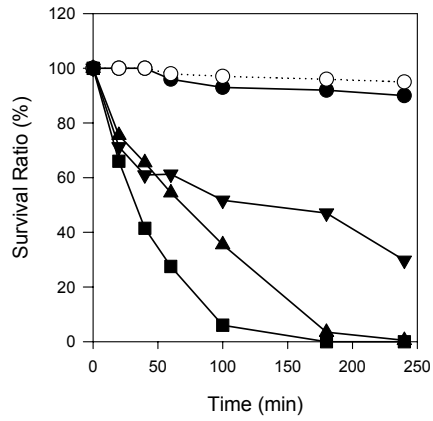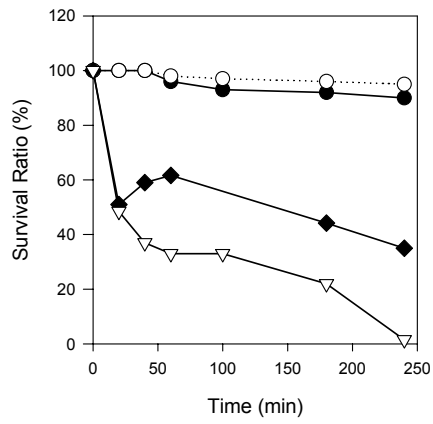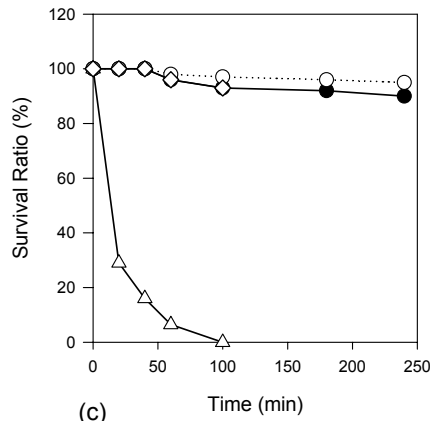
Figure 4.3-2 Effect of hydrothermal treatment on antimicrobial efficiency of sol-gel samples under irradiation (10 mW/cm^2) (a) After hydrothermal treatment ; (b) after post hydrothermal treatment-1 (c) after post hydrothermal treatment-2 (▼, SG; ▲, SG24; ■, SG48; ♦, SG24-24; ♦, SG48-24; △ , SG48-24R; ◇, SG48-24C ; o, dark; •, under irradiation)

Over the anatase surface, the reactions between the active sites and the formation of surface species can be described [19] as (Eqs.4.8-1~4);

$$TiO_2 + h\nu \rightarrow h^+ + e^-$$ (4.8-1)

$$h^+ + OH^- \rightarrow \bullet OH_{ads}$$ (4.8-2)

$$h^+ + H_2O_{ads} \rightarrow \bullet OH_{ads} + H^+$$ (4.8-3)

$$e^- + O_2 \rightarrow O_2^-$$ (4.8-4)

The concentration of $\bullet OH_{ads}$ species depends on the consumption rate by microbial inactivation and production rate by hole generation. Over the time lag period, the microbial inactivation rate might be limited with the lower concentration of active species. In order to validate this mechanism, control experiments were designed. To increase the surface density of $\bullet OH_{ads}$ species, two SG 48-24 samples were stirred in water for 4 hr under illumination (Post treatment-2) (SG 48-24R) and in dark (SG 48-24C). After a 4-hr period, *E. coli* was inoculated to both mixtures and the antimicrobial efficiencies of two samples were followed. As shown in Figure 4.3-2.c, a high inactivation rate (2.9 hr^{-1}) was observed and complete microbial inactivation was achieved at the end of 100 min for the sample which was treated with water under UV irradiation (SG 48-24R). The inactivation rate obtained for this sample was superior over both Com and SG samples. However, keeping the substrate with water in dark (SH 48-24C) results in no antimicrobial activity which indicates the surface sites are occupied with molecular water and UV radiation is essential for $\bullet OH_{ads}$ formation. The active surface of anatase is (101) plane and water adsorption with (101) surface takes place molecularly [1, 68]. After post treatment-1, trititanate structure is destroyed and anatase octahedrons start to grow (Figure 4.3-3). At this stage (101) surface grows and (001) surface shrinks resulting in all 8 faces of octahedrons become (101) surfaces [217, 218] (Figure 4.3-4). With increasing post-treatment-1 period, more water may start to be adsorbed over the surface. This may describe the reason why effectiveness of the catalyst decreases with increasing post-treatment-1 time and early reaching to incomplete inactivation stage. When anatase is irradiated with UV, adsorbed molecular water dissociates [1, 68] and the concentration of oxidative species such as $\bullet OH_{ads}$ or H_2O_2 form over the surface which directly influences the photocatalytic microbial inactivation rate.
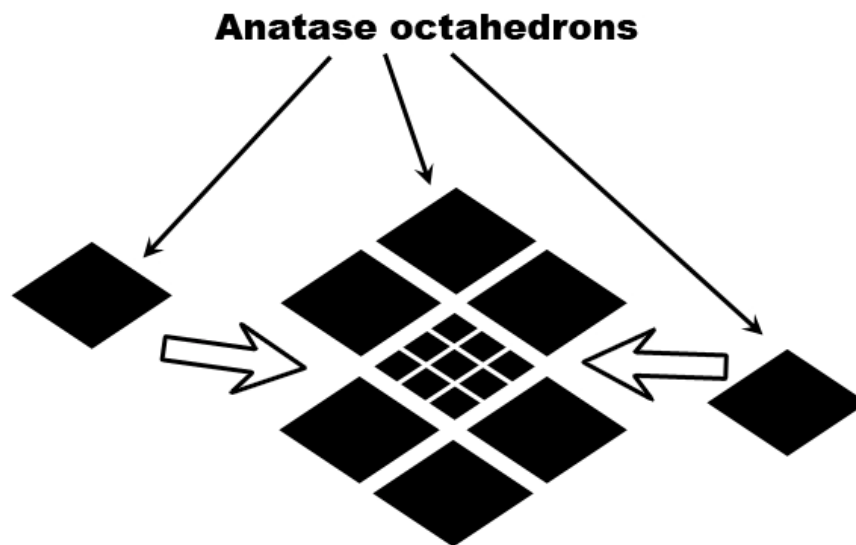
Figure 4.3-3 Growth of anatase octahedrons
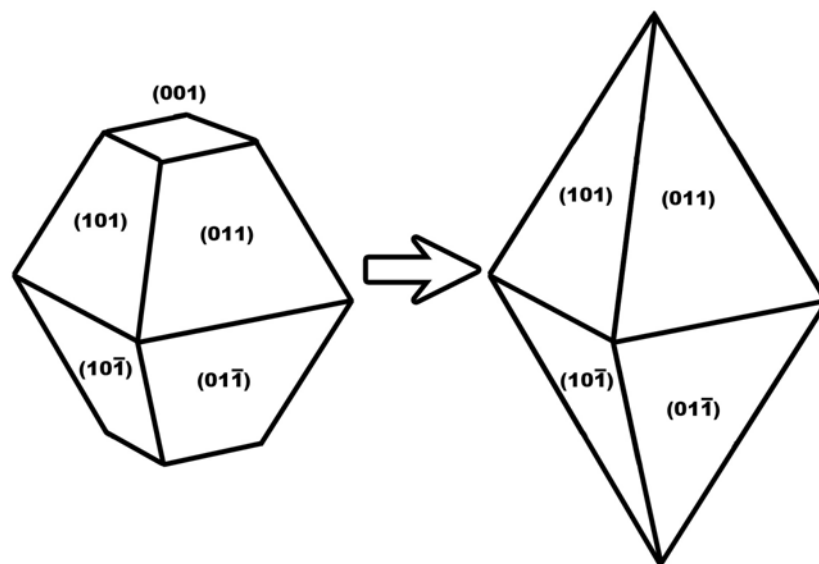
Figure 4.3-4 Shrinking of (001) face on anatase

4.4. Structure of Titania and the use of Carbon Nano Tubes (CNT's) as nanostructured templates

Two sets of CNT-TiO$_2$ samples were prepared; the first set covers the samples which are dip-coated and the second set of samples were prepared as powder form. TiO$_2$, CNT-TiO$_2$ and CNT-TiO$_2$-1%Fe colloidal solutions were applied to glass substrates with dip coating and calcined for 5, 10 and 15 minutes. The AFM images of these sample surfaces are presented in Figure 4.4-1. Before calcination, the sample surface is formed by small particles with approximate diameter of 15 nm and growth of particles was observed with calcinations time. AFM images of titania-CNT coatings are presented Figure 4.4-2 and fibrous structure was observed before calcinations. When these samples were calcined, particle formation was observed. Addition of Fe^{+3} seems to affect the structure drastically (Figure 4.4-3) and porous structure was observed with the calcined samples.

(a) (b)

(c)
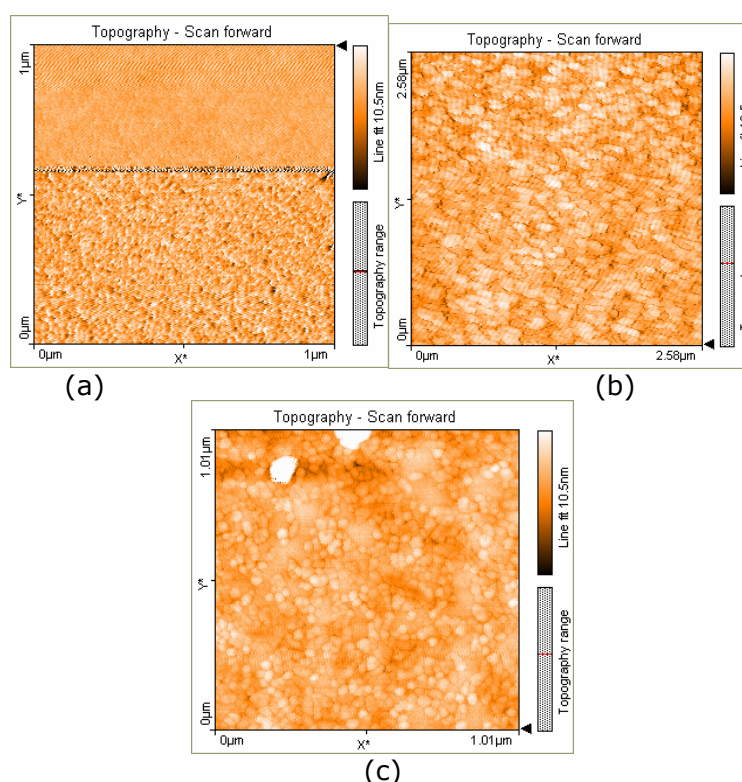
Figure 4.4-1 AFM images of titania coated glass samples,
a) Before calcination, b) after 10 minute calcination and c) after 15 minute calcination
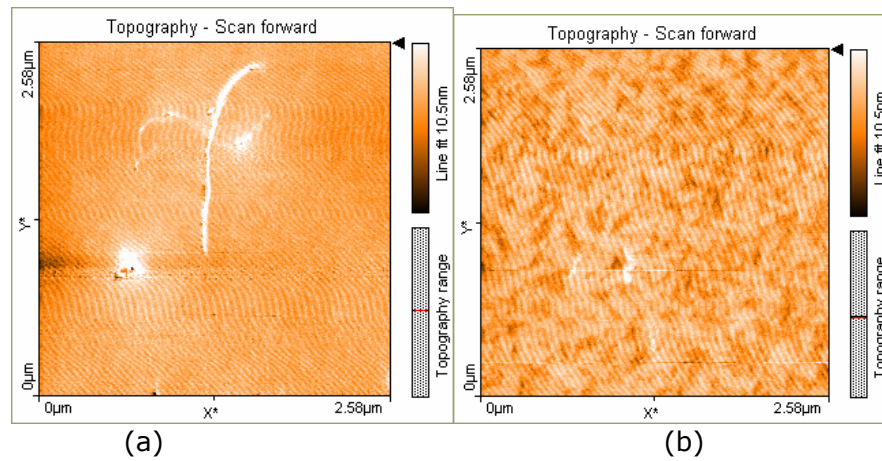
Figure 4.4-2 AFM images of titania-CNT coated glass samples, a) Before calcination, b) after 10 minute calcination
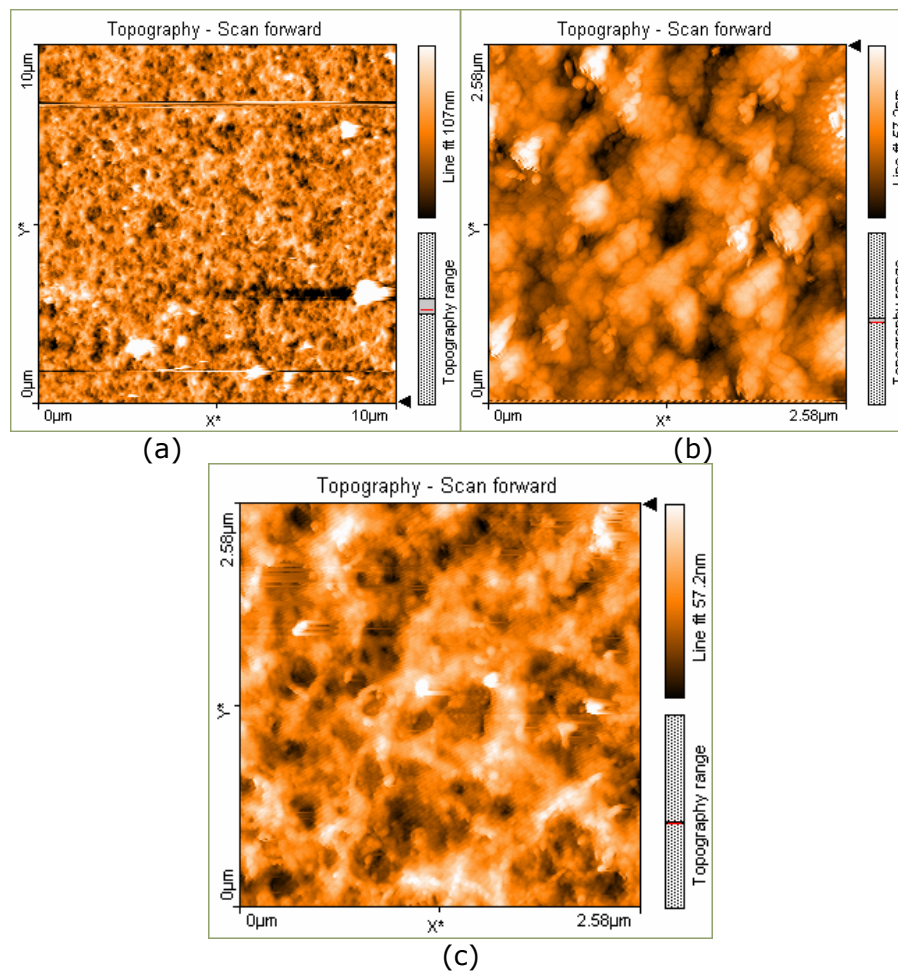
Figure 4.4-3 AFM images of titania-CNT-Fe coated glass samples, calcined for a) before calcination, b) after 5 minute calcination and c) after 15 minutes calcination

For dip coated samples, contact angle measurements were also carried out (Table 4.4-1). As it is seen from the table, contact angle drops with the calcination time which indicates the formation of more hydrophilic surface.

Table 4.4-1 Contact angle values of CNT samples

Calcination time (min)	Sample	Contact Angle	Sample	Contact Angle	Sample	Contact Angle
5		52,27		53,34		41,74
10	Ti	25,77	CNT	43,46	CNT-Fe	31,98
15		27,44		17,26		34,61

The removal of CNT by calcination might be a viable method to obtain nanostructured micro- or meso- porous thin films. However, CNT is very heat resistant material and the reaction of CNT's with oxygen takes place at temperatures above 700 °C which is higher than the transformation temperature of anatase to rutile (600-700 °C) [239]. So addition of catalyst to lower the activation energy of CNT oxidation is necessary. However, there are few publications in literature regarding the catalytic oxidation of CNT's and their thermal stability in the presence of air [210]. On the other hand, there are some recent studies which report the synergic effect of the presence of CNT's on TiO_2 formulations [235-238]. Thus the use of catalysts for CNT oxidation under calcination conditions and the effect of the presence of CNT in TiO_2 catalyst deserve the specific experimental study. A set of experiments were designed in order to investigate the effect of cobalt (Co), sodium (Na), and iron (Fe) as CNT oxidation catalyst to lower the CNT oxidation temperature. On the other hand, the effect of the presence of oxygen in calcination was also tested. The samples TiO_2, CNT-TiO_2, CNT-TiO_2-1%Na, CNT-TiO_2-3%Na, CNT-TiO_2-5%Na, CNT-TiO_2-1%Co and CNT-TiO_2-1%Fe were prepared. The mass ratio of CNT:TiO_2 was adjusted to 40:60 in all samples. All of the samples were heat treated at 400 ºC without oxygen under nitrogen flow also samples were calcined under three different temperature in the presence of air flow (400 ºC, 500 ºC and 570 ºC).

The non-oxidative heat treatment was planned to test the effect of the presence of CNT on photocatalytic performance of TiO_2. The SEM images of CNT-TiO_2 can be seen in Figure 4.4-4. Sample which is heat treated at 400 °C with N_2 has a heterogeneous structure with fibrous CNT's (Figure 4.4-4.a) and 1 μm particles. The fibrous structure and particles can be attributed to the CNT'S and TiO_2 particles respectively. When this sample is calcined with air at 400 ºC (Figure 4.4-4.b), the fibrous structure is preserved. The entangling of CNT's with TiO_2 particles is still visible at 400 ºC. The increase of calcination temperature to 500 °C, (Figure 4.4-4.c) resulted with the disappearance of CNT's and the formation of more homogeneous and porous structure. Very small fibrous structure is still visible representing the presence of some CNT residuals. When the calcination temperature is further increased to 570 °C, completely dense structure was observed (Figure 4.4-4.d).

SEM images of CNT-TiO_2-1%Na treated under different conditions is presented in Figure 4.4-5. At 400 °C with N_2 (Figure 4.4-5.a), the case is very similar to the CNT-TiO_2 sample. Again when air is introduced, no significant change in structure was observed (Figure 4.4-5.b). However, the calcination temperature increased to 500 °C, (Figure 4.4-5.c) more porous and fibrous structure was obtained. At the 570 ºC, (Figure 4.4-5.d), the structure resembling the Figure 4.4-4.c was obtained.

In order to test the effect of Na concentration on the structure and activity, CNT-TiO_2-3%Na and CNT-TiO_2-5%Na samples were also examined. SEM images of CNT-TiO_2-3%Na samples which were treated under different conditions are presented in Figure 4.4-6. Again at 400 °C with N_2, structure is very fibrous. As a different situation, there are very small particles at sides of CNT's (Figure 4.4-6.a). The structure is not altered when air is introduced at 400 ºC (Figure 4.4-6.b). However, at 500 °C, all of the fibers vanished, completely (Figure 4.4-6.c). The SEM images of samples containing 5%Na (CNT-TiO_2-5% Na) are shown in Figure 4.4-7 with very similar morphologies observed with 3% and 1% Na samples.

a) @ 400 °C with N₂

b) @ 400 °C with air

c) @ 500 °C with air
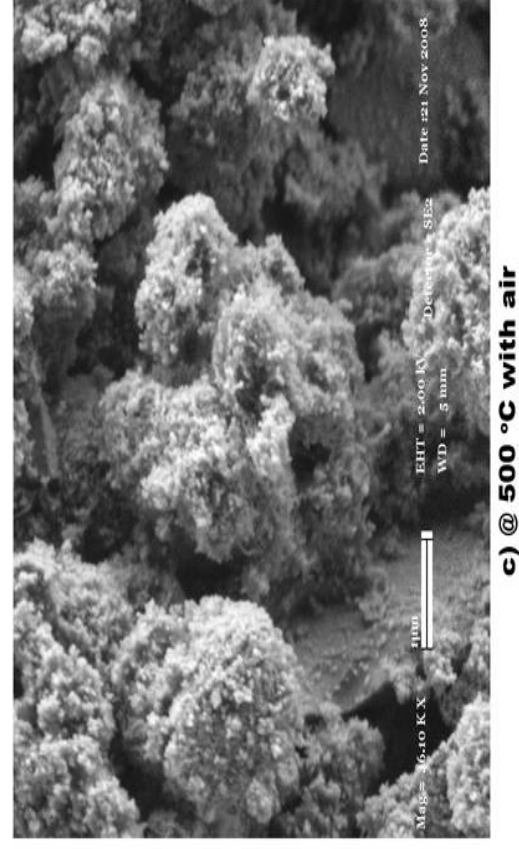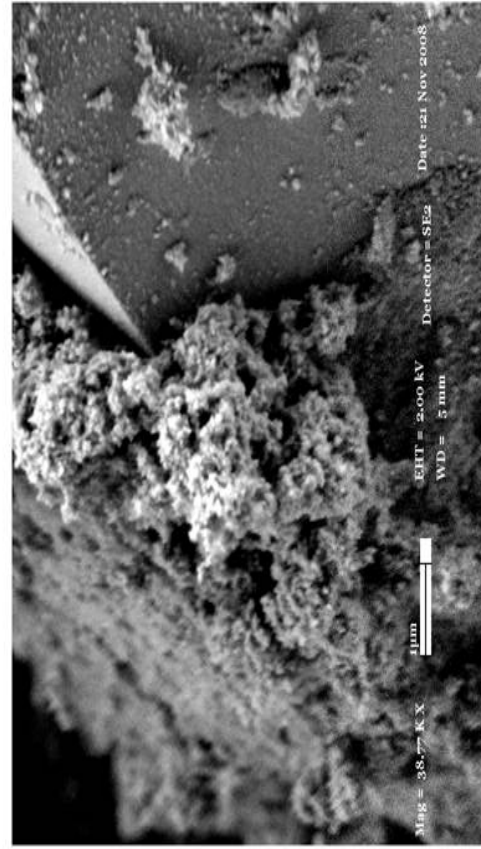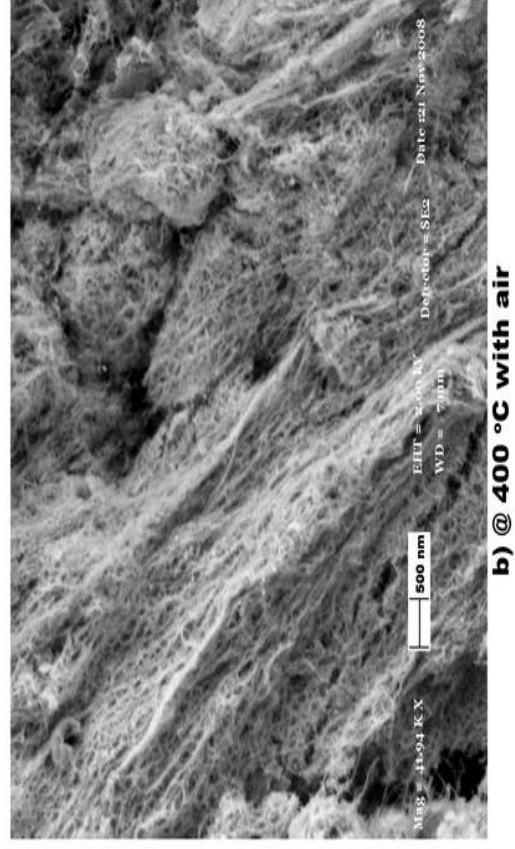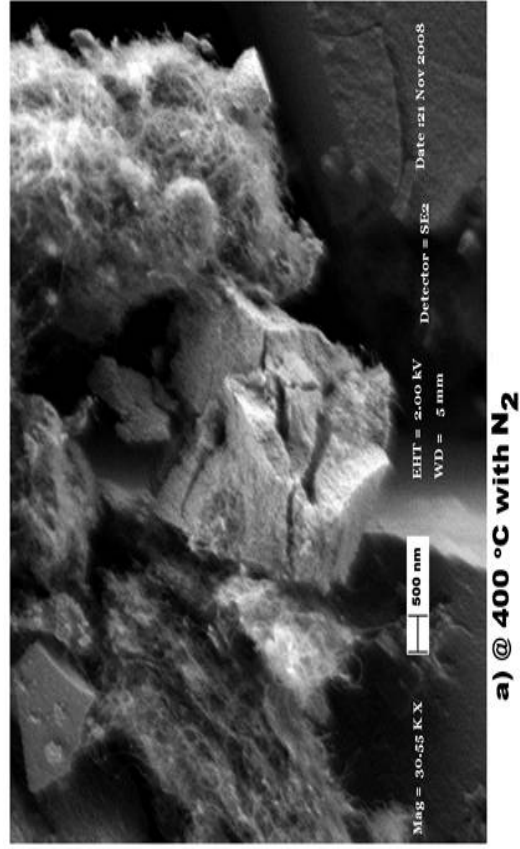
d) @ 570 °C with air

Figure 4.4-4 SEM images of CNT-TiO$_2$ heat treated at a) 400 °C with N$_2$, and calcined at b) 400 °C, c) 500 °C and d) 570 °C

62
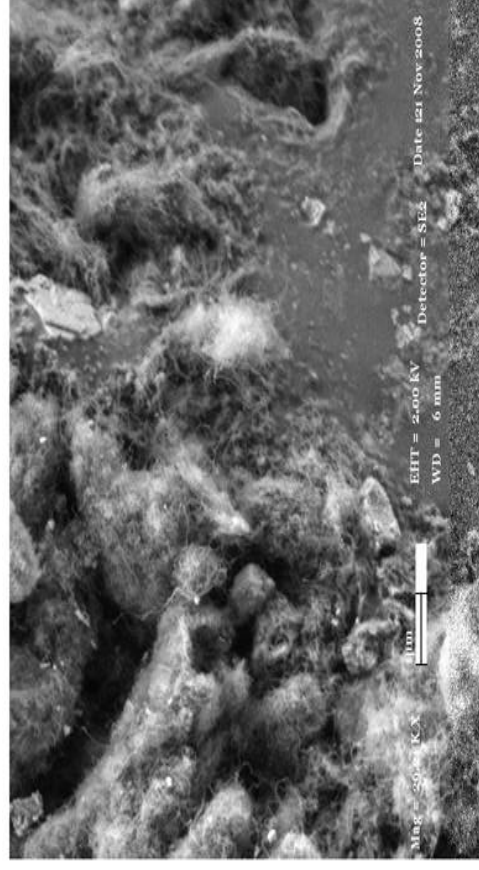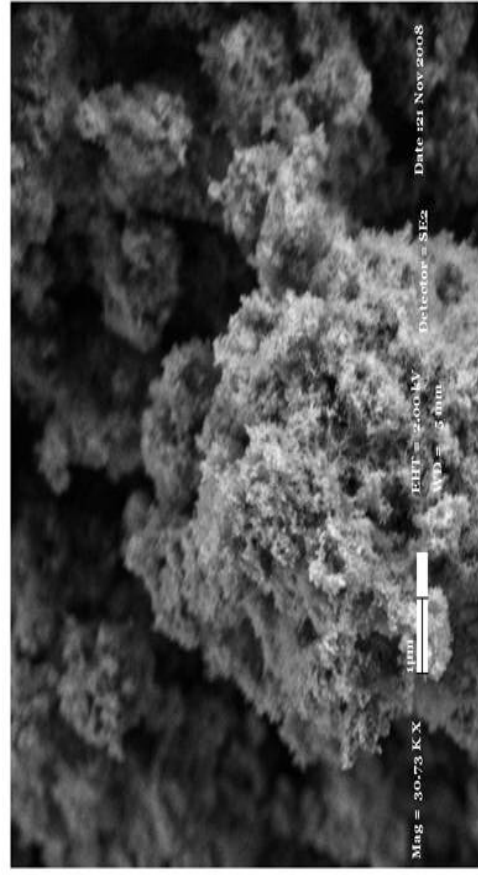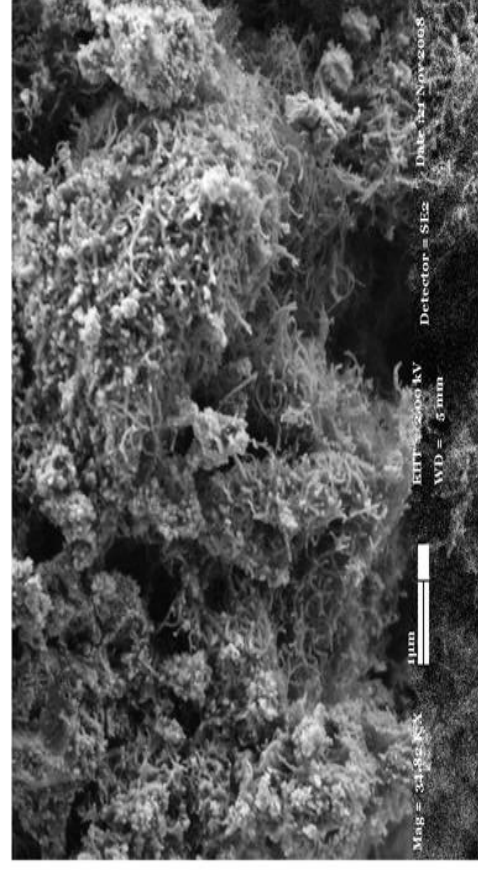
Figure 4.4-5 SEM images of CNT-TiO$_2$-1%Na heat treated at a) 400 ºC with N$_2$, and calcined at b) 400 ºC, c) 500 ºC and d) 570 ºC

a) @ 400 ºC with N$_2$

b) @ 400 ºC with air

c) @ 500 ºC with air

d) @ 570 ºC with air

63

Images CNT-TiO$_2$ samples doped with Co and Fe are shown in Figure 4.4-8, and Figure 4.4-9 respectively. At 400 °C without air, the fibrous structure was observed (Figure 4.4-8.a). However, CNT's are not entangled with TiO$_2$ particles when compared with the previous undoped and Na doped samples. When air is introduced, the sample became less fibrous (Figure 4.4-8.b), suggesting that the oxidation of CNT's. Increasing the temperature to 500 °C all fibrous structure is vanished (Figure 4.4-8.c). Although the sample is porous, it is more compact from its previous counterparts at the same temperature. At the final temperature, the structure became even denser (Figure 4.4-8.d) resembling the sintering. Very similar results were observed with Fe doped CNT-TiO$_2$ samples (Figure 4.4-8).

SEM images of CNT-TiO$_2$-1%NaC is in Figure 4.4-10. At 400 °C with N$_2$ (Figure 4.4-10.a), the structure is very similar to CNT-TiO$_2$-1%Na; a completely fibrous material with some small particles attached to them. Again when air is introduced, we can not observe a major change in the structure (Figure 4.4-10.b). Nevertheless at 500 °C, all of the fibers disappear, even short fibers are gone (Figure 4.4-10.c), but particles which were in contact with CNT's are porous. At 570 °C, the structure is still porous but denser (Figure 4.4-10.d). If we compare 1% NaC series with the previous ones, the structure is something between CNT-TiO$_2$ and CNT-TiO$_2$-1%Na. However there is a difference, there are some large pores inside titania particles which can not be seen in other materials.

SEM images of CNT-TiO$_2$-5%NaC is in Figure 4.4-11. In contrast to all other samples, the material, when heat treated at 400 °C with N$_2$, has some crystal shards (Figure 4.4-11.a). These shards are probably Na$_2$CO$_3$ crystals. Other than that, the structure is quite similar to the samples which are calcined at similar conditions; CNT's with small particles attached to them. After the introduction of air at 400 °C, crystal shards still can be seen, but CNT's are gone, leaving porous titania particles behind (Figure 4.4-11.b). This is a new result; at every other sample which is calcined at same conditions, CNT's could be observed. At 500 °C, crystal shards are lost and titania particles became denser (Figure 4.4-11.c). Lastly at 570 °C, titania particles are sintered a little bit more.

b) @ 400 °C with air

c) @ 500 °C with air

a) @ 400 °C with N₂
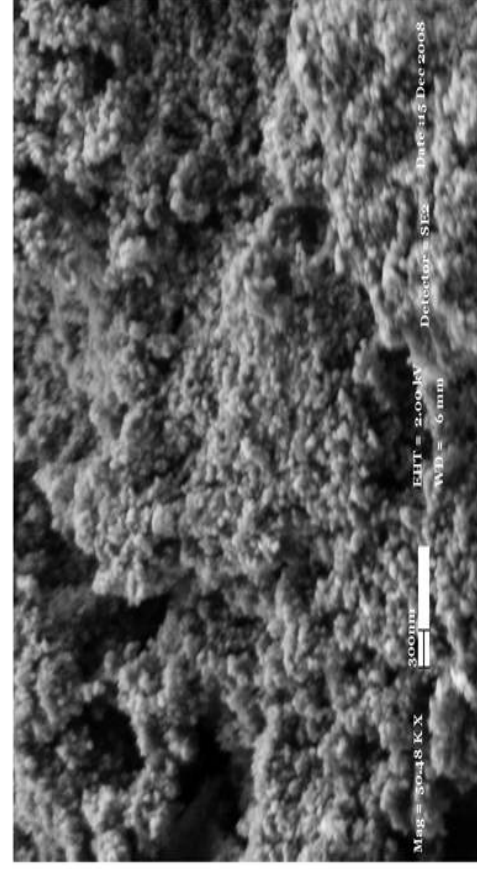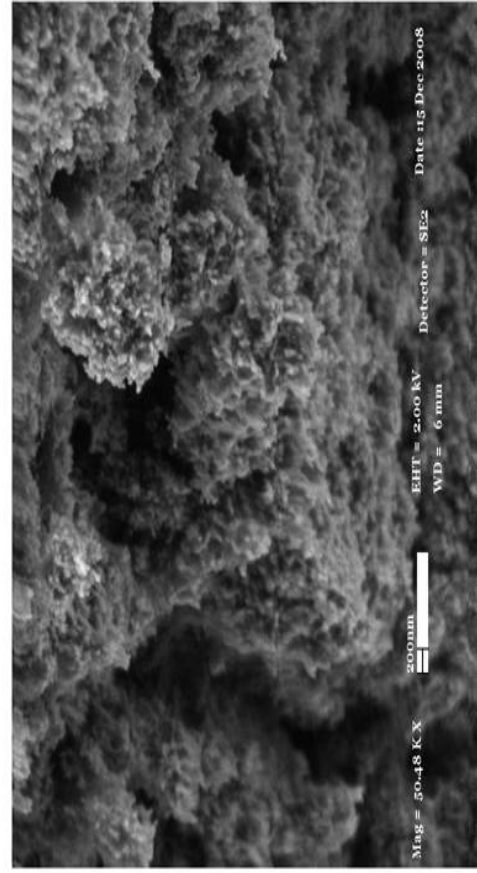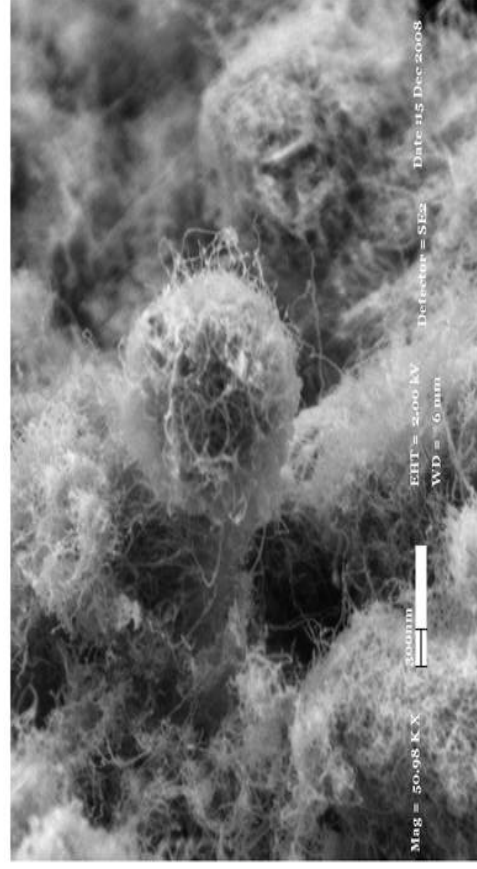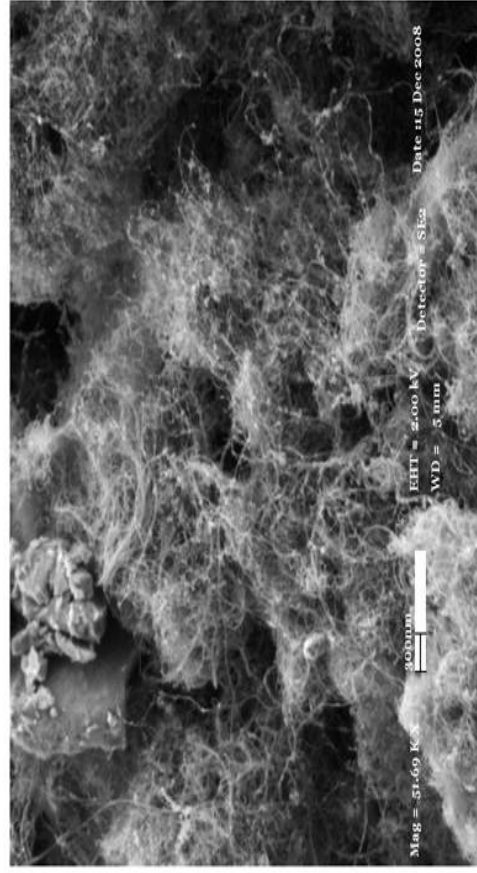
d) @ 570 °C with air

Figure 4.4-6 SEM images of CNT-TiO₂-3%Na heat treated at a) 400 °C with N₂, and calcined at b) 400 °C, c) 500 °C and d) 570 °C

65
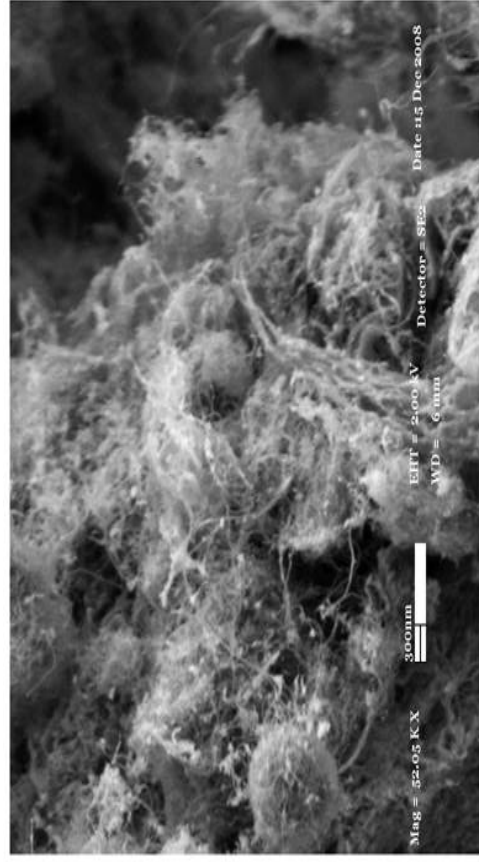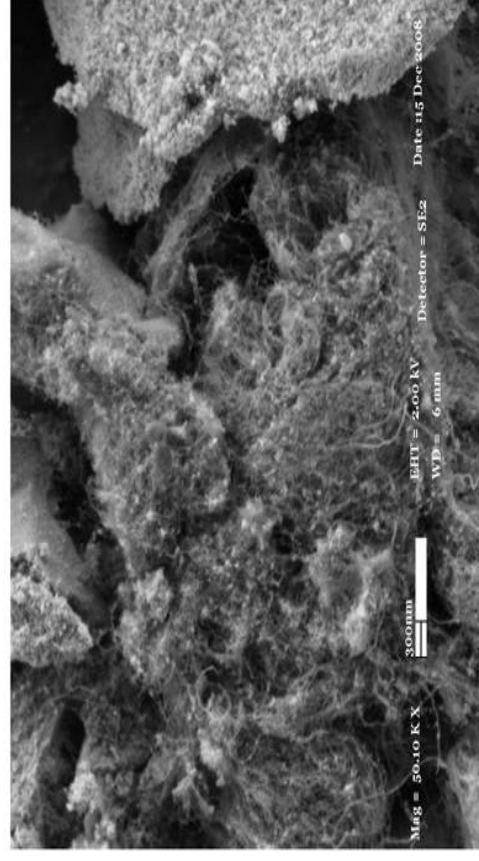
b) @ 400 °C with air
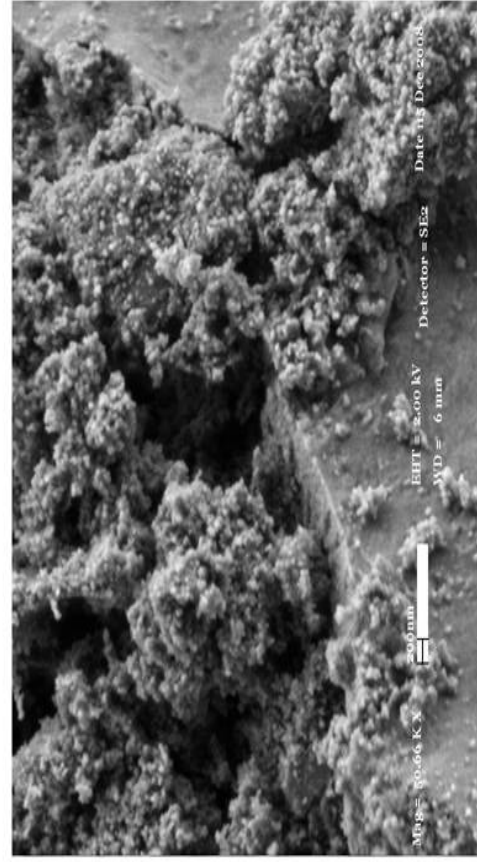
c) @ 500 °C with air
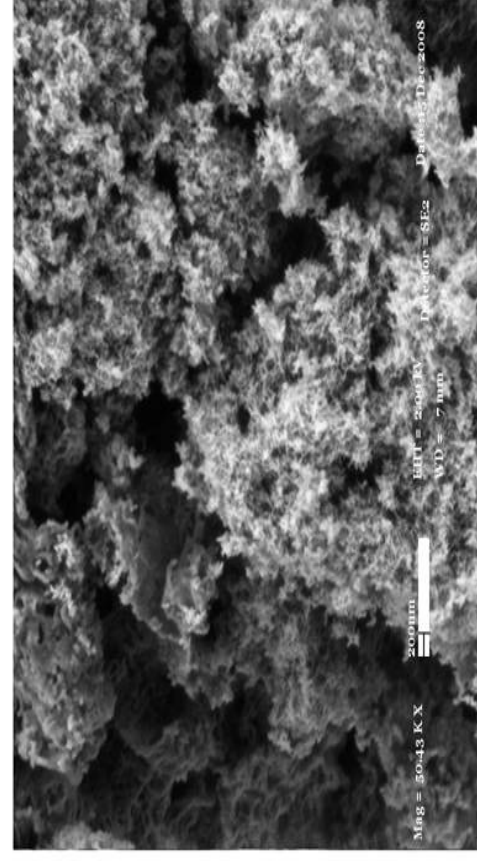
a) @ 400 °C with N$_2$

d) @ 570 °C with air

Figure 4.4-7 SEM images of CNT-TiO$_2$-5%Na heat treated at a) 400 °C with N$_2$, and calcined at b) 400 °C, c) 500 °C and d) 570

66
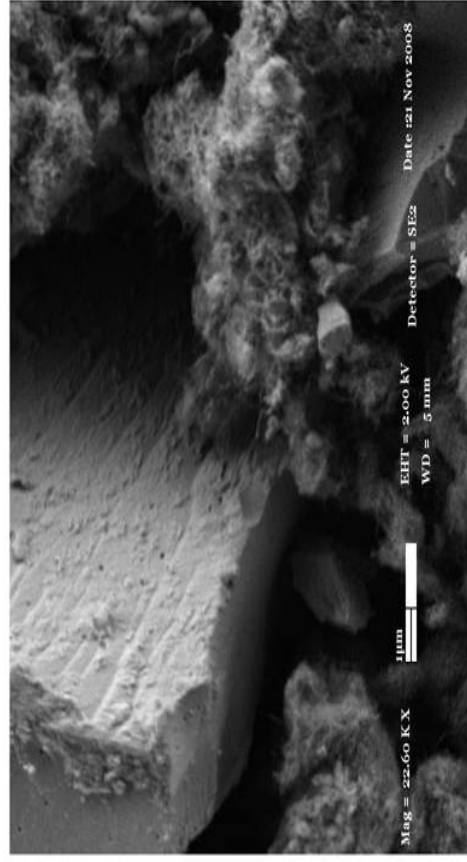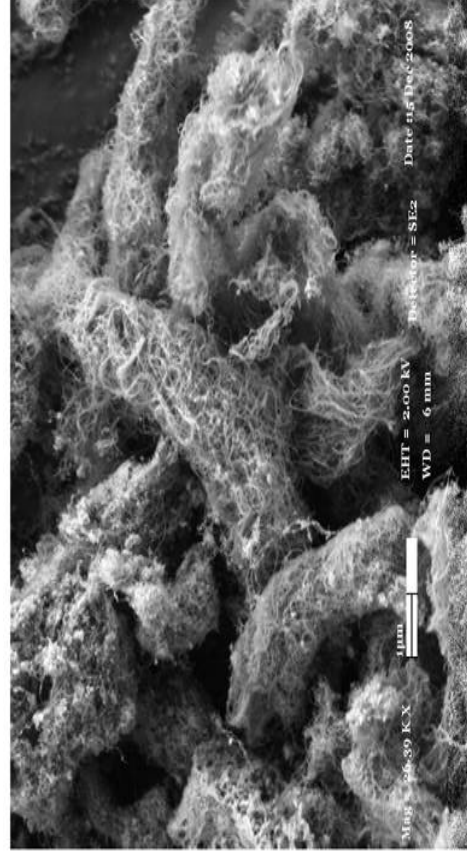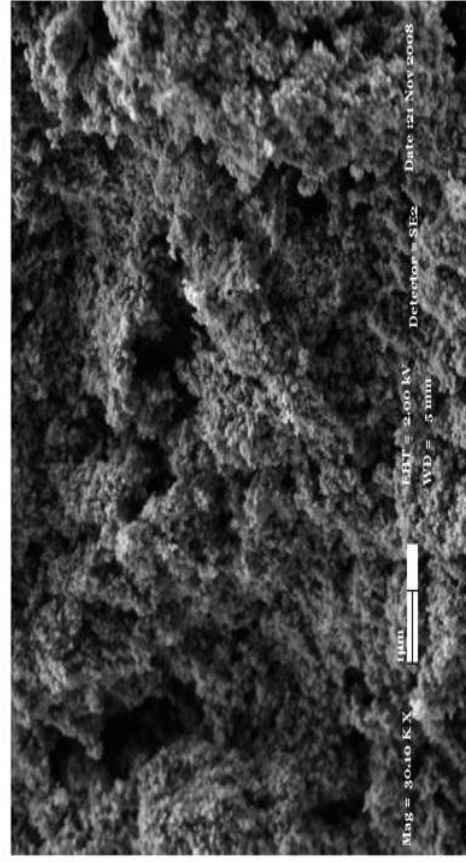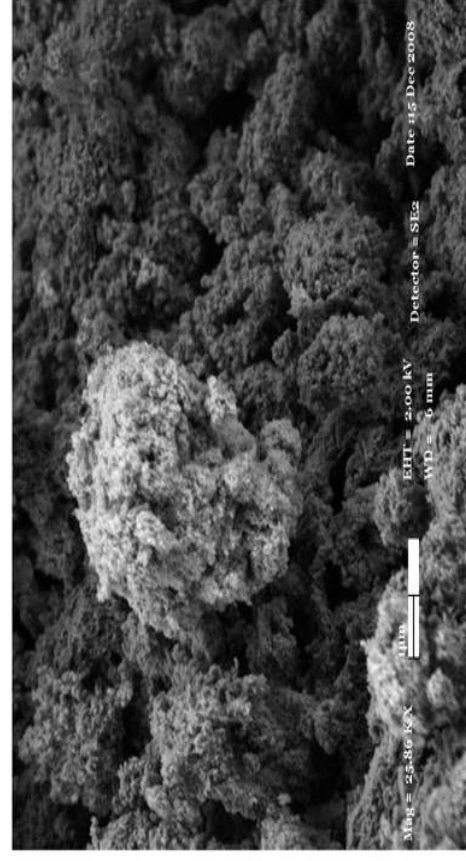
Figure 4.4-8 SEM images of CNT-TiO$_2$-1%Co heat treated at a) 400 °C with N$_2$, and calcined at b) 400 °C, c) 500 °C and d) 570 °C
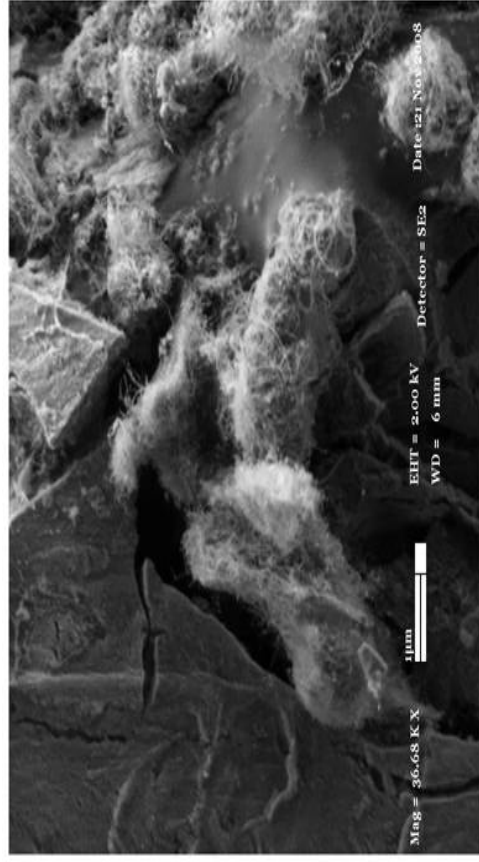
a) @ 400 °C with N₂
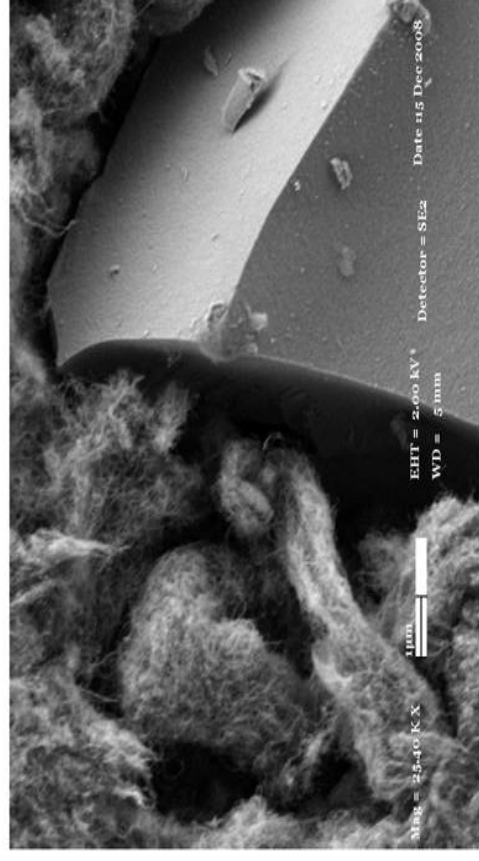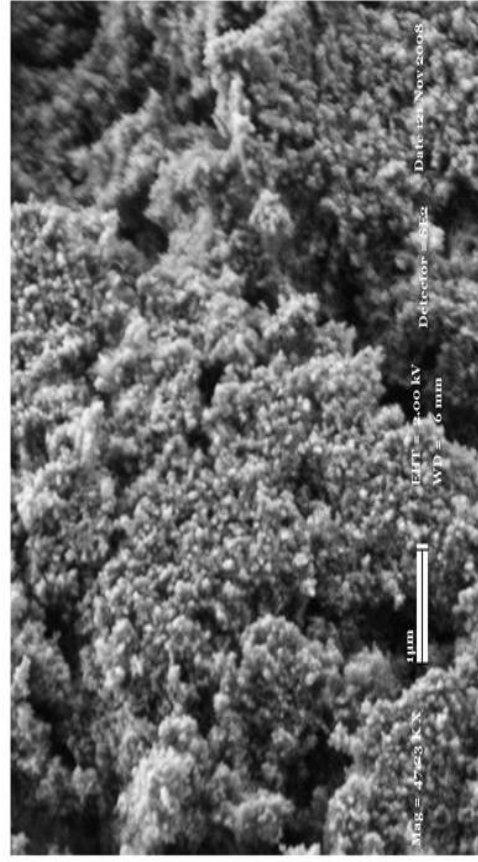
b) @ 400 °C with air
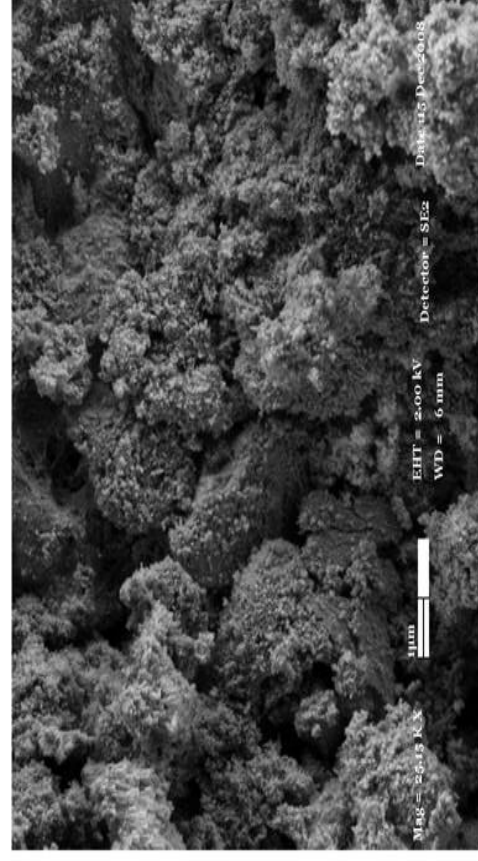
c) @ 500 °C with air

d) @ 570 °C with air

Figure 4.4-9   SEM images of CNT-TiO₂-1%Fe heat treated at a) 400 °C with N₂, and calcined at b) 400 °C, c) 500 °C and d) 570 °C

XRD analysis of undoped, Na, Co, and Fe doped CNT-TiO$_2$ samples were also examined to check the possible effect of dopant and heat treatment or calcination conditions on the crystallinity (Figure 4.4-12, 13, 14, 15, 16, 17, 18 and 19). As it is seen from the diffractograms, all samples have anatase structure (2theta = 25.27°) and the presence of oxygen and dopant does not effect the crystallinity in a great extend. In all samples, the increase of calcination temperature increased the crystallinity except the iron (Fe) doped sample. Similarly, the calcinations under the oxidative atmosphere favors the increase of crystallinity. In addition to that, samples with 3 % and 5 % Na (NaCl source), after calcination, have NaCl peaks. Also, in Co and Fe doped samples, traces of rutile formation was observed at 2theta = 27.7° at 570 °C.

To compare series with each other, XRD patterns of samples heat treated at 400 ^{0}C with N$_2$ were drawn around 25.27 °. When the main peak was examined, one can conclude that the degree of crystallinity decreases with the addition of dopant as it is shown in Figure 4.4.20.

4.5. Thermal Analyses of Sol-Gel Titania Synthesized with Carbon Nano Tubes (CNT's)

To check the possible oxidation reaction of CNT's in the presence of various dopants TGA and DTA analyses were carried out. Thermogravimetric analyses of the samples were performed at a heating rate of 10 °C min^{-1} under air flow from room temperature to 1000 °C. After the analyses, samples were visually examined. Also the gravimetric data was compared with the amount of CNT added into the sample to check the success of the use of dopant and air on CNT removal.

The pure TiO$_2$ gel was tested in order to set a background for TGA-DTA analysis (Fig. 4.5-1). When the TGA-DTA data is examined, the weight changes at 106 ºC and 140 ºC were attributed as the evaporation of water, and the oxidation of organic precursor respectively. The reaction at 417 ^{0}C is the removal of –OH species from oxide phase and the crystallization of TiO$_2$. These results were in good agreement with literature [212]. Similarly, the TGA-DTA analysis of pure CNT's was carried out (Figure 4.5-2). The TGA curve reveals

a) @ 400 °C with N₂
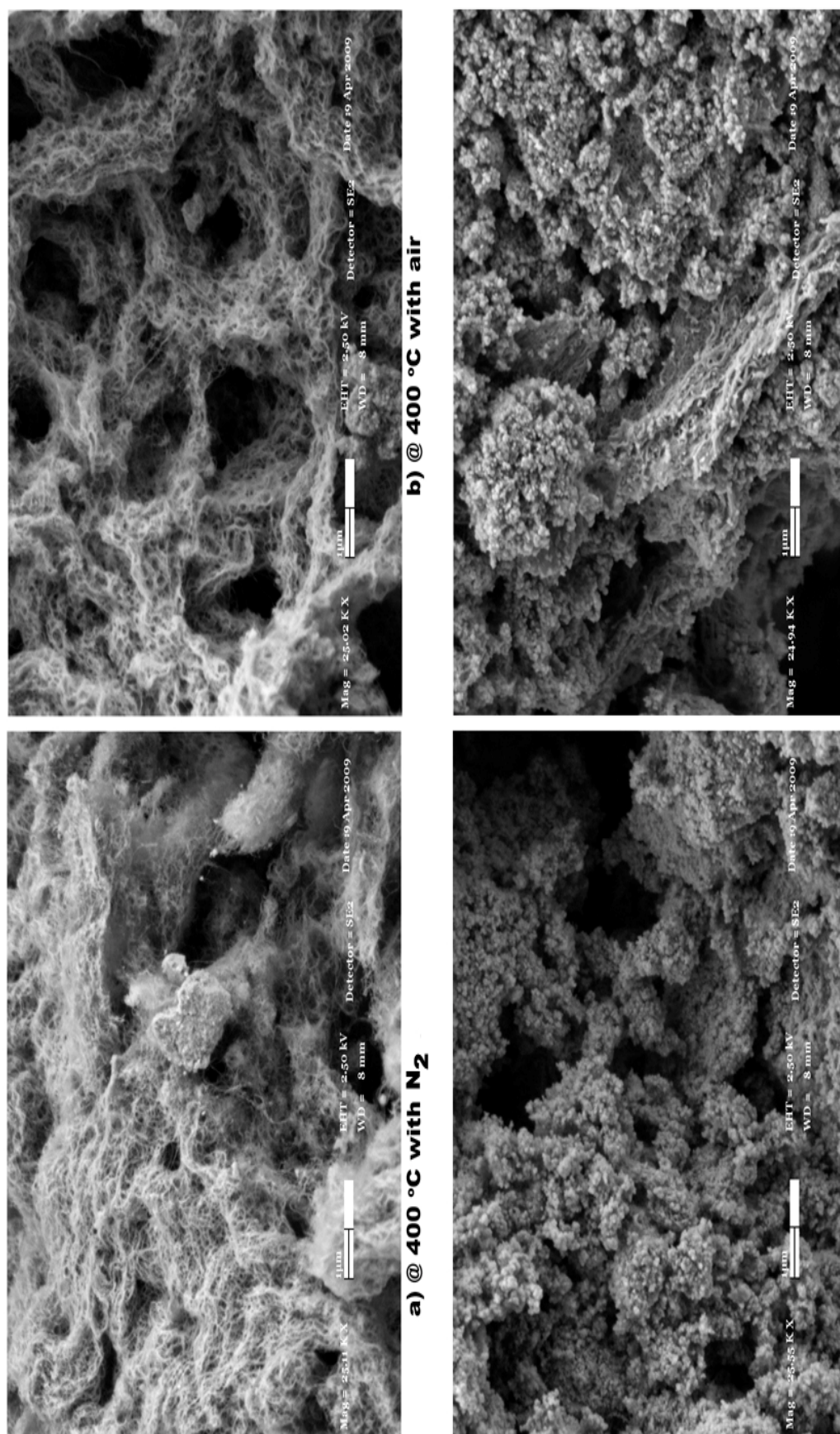
b) @ 400 °C with air

Figure 4.4-10 SEM image of CNT-MnNaC heat treated at a) 400 °C with N₂, and calcined at b) 400 °C with air c) 500 °C and d) 570 °C
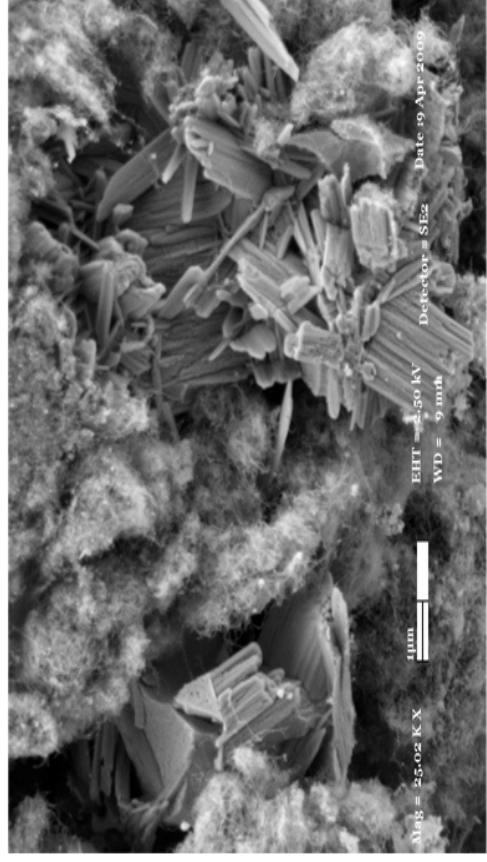
a) @ 400 °C with N₂
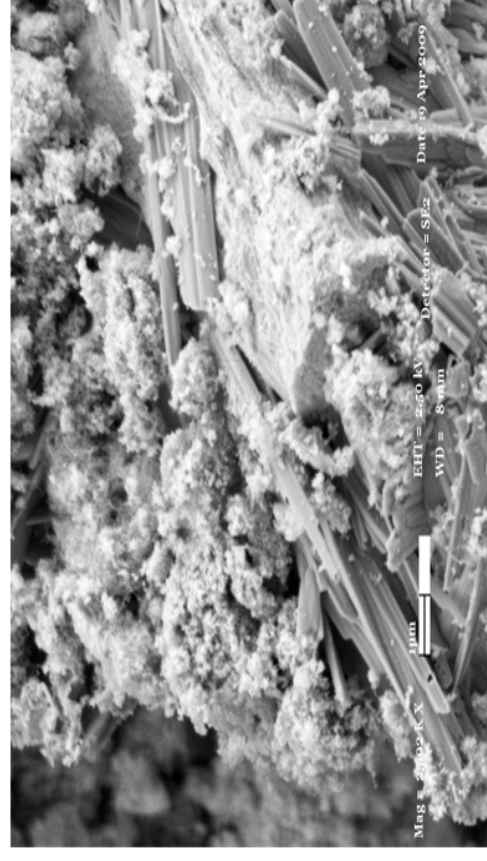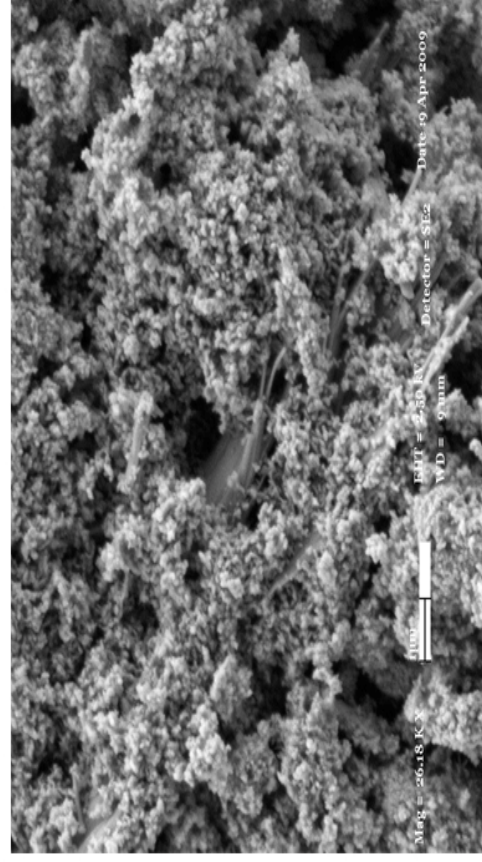
b) @ 400 °C with air

c) @ 500 °C with air

d) @ 570 °C with air

Figure 4.4-11 SEM images of CNT–TiO$_2$–5%NaC heat treated at a) 400 °C with N$_2$, and calcined at b) 400 °C, c) 500 °C and d) 570 °C

71
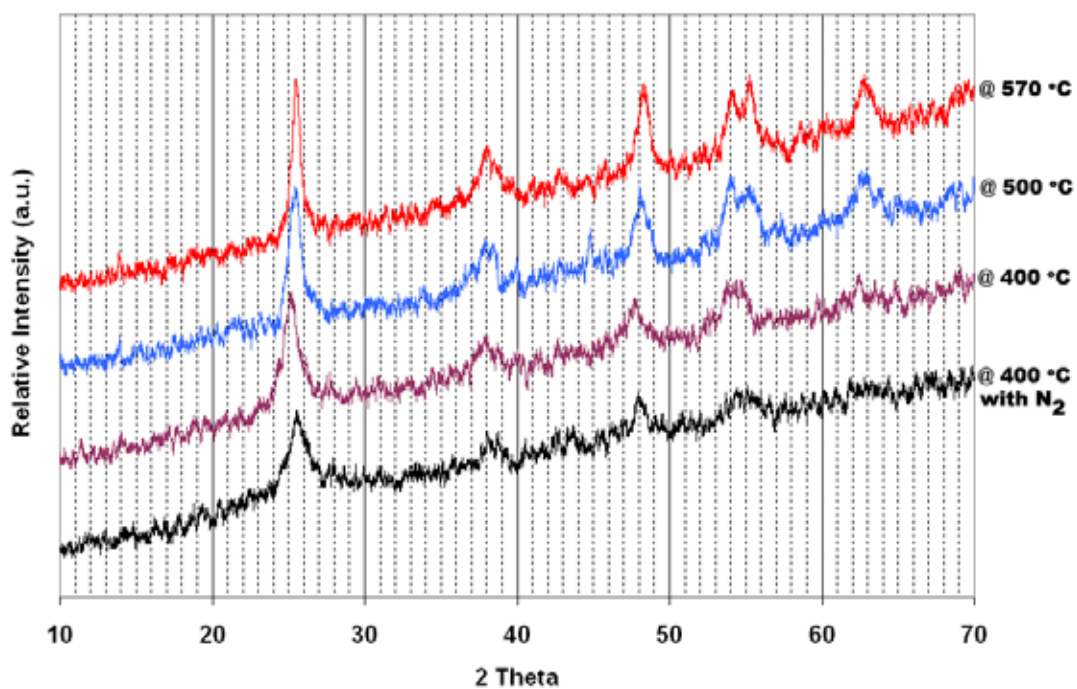
Figure 4.4-12 XRD patterns of CNT-TiO$_2$ at various treatment temperatures
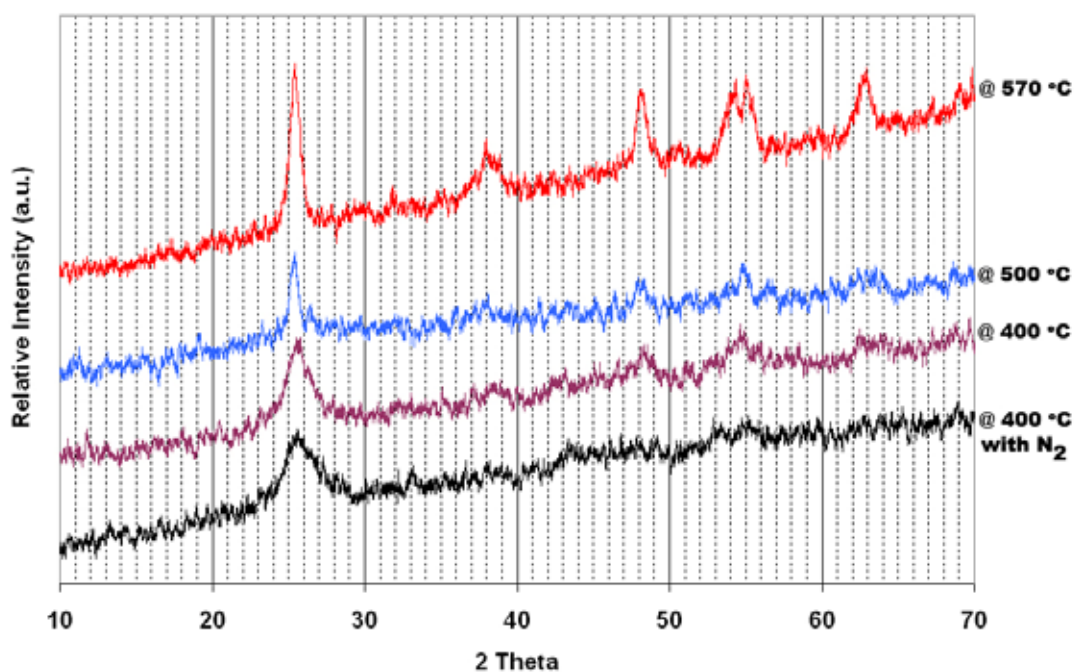
Figure 4.4-13 XRD patterns of CNT-TiO$_2$-1%Na (NaCl source) at various treatment temperatures
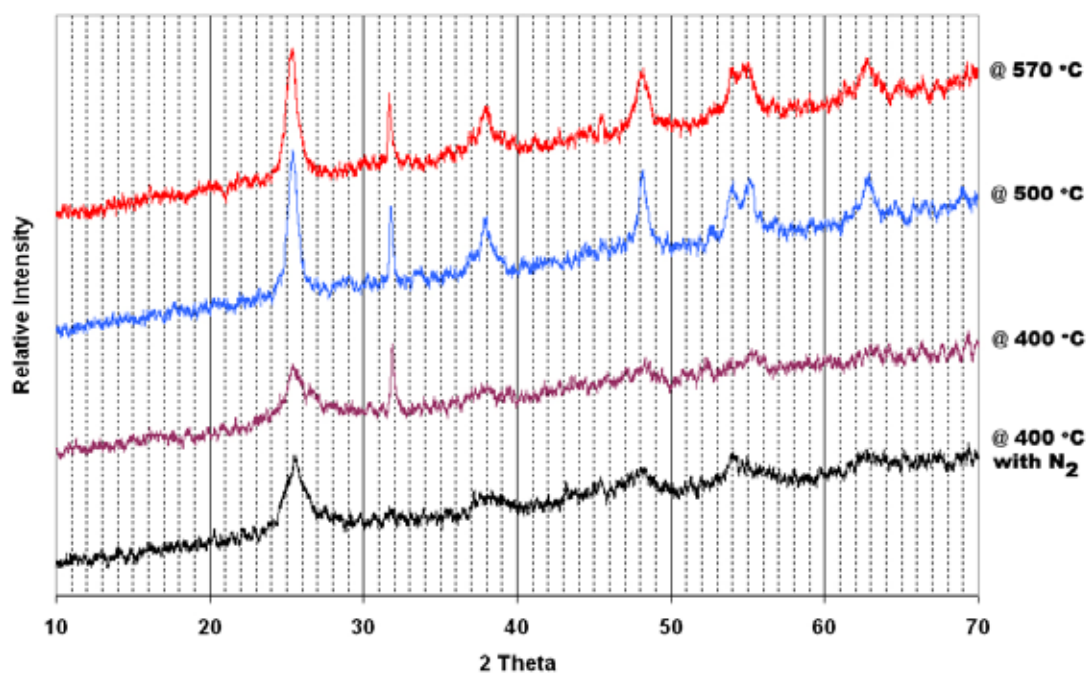
Figure 4.4-14 XRD patterns of CNT-TiO$_2$-3%Na (NaCl source) at various treatment temperatures
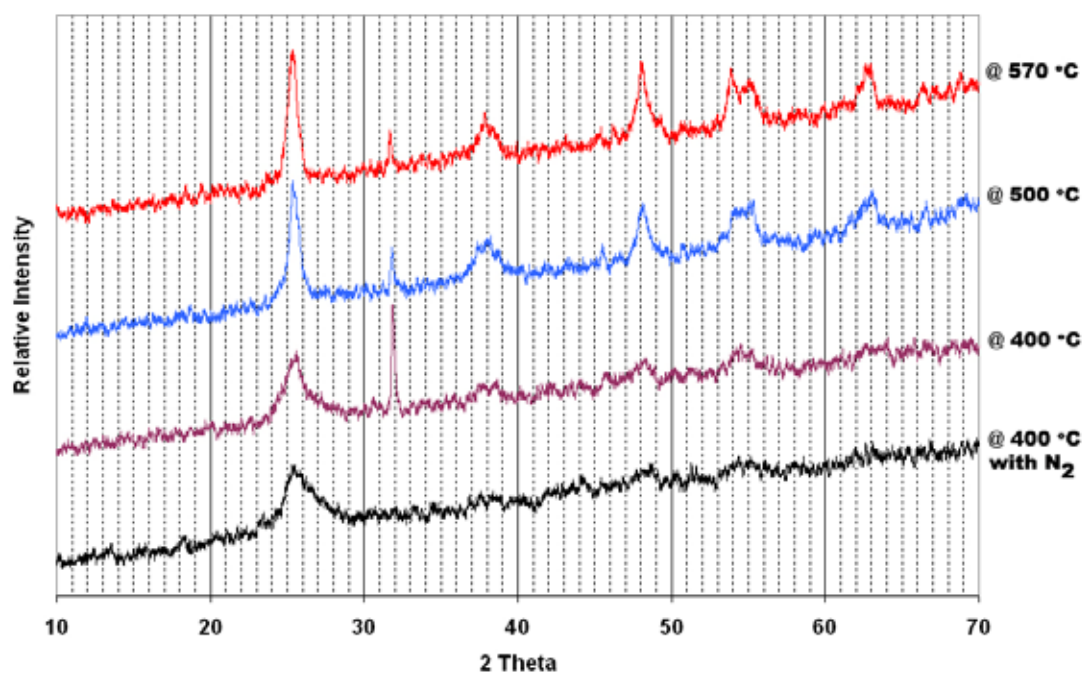
Figure 4.4-15 XRD patterns of CNT-TiO$_2$-5%Na (NaCl source) at various treatment temperatures

73
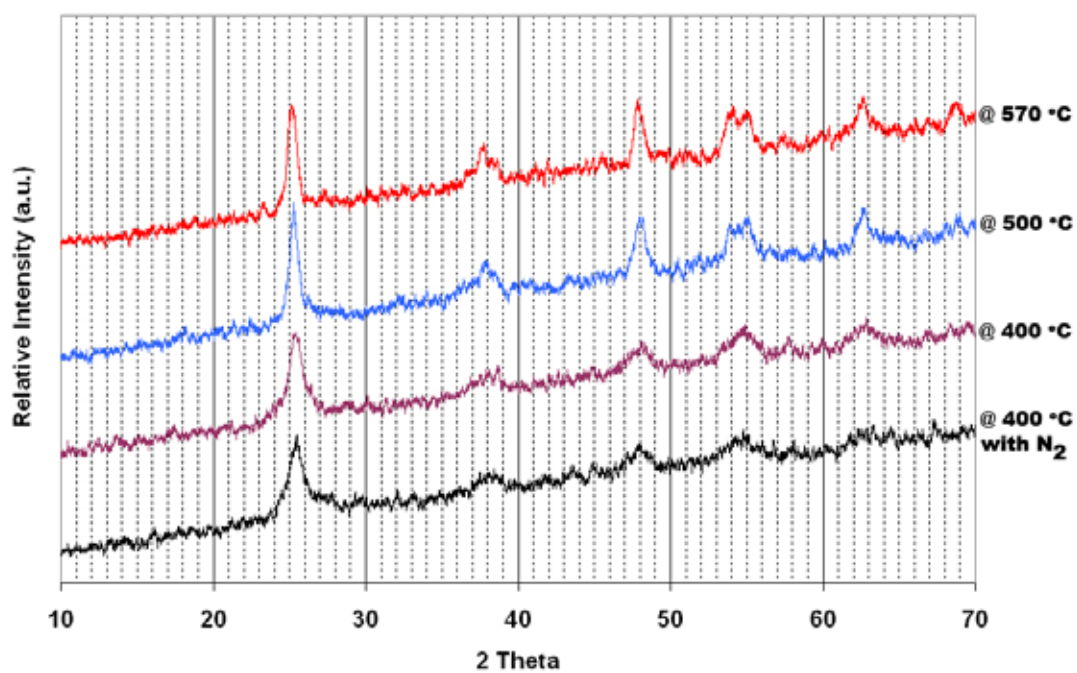
Figure 4.4-16 XRD patterns of CNT-TiO$_2$-1%Co at various treatment temperatures
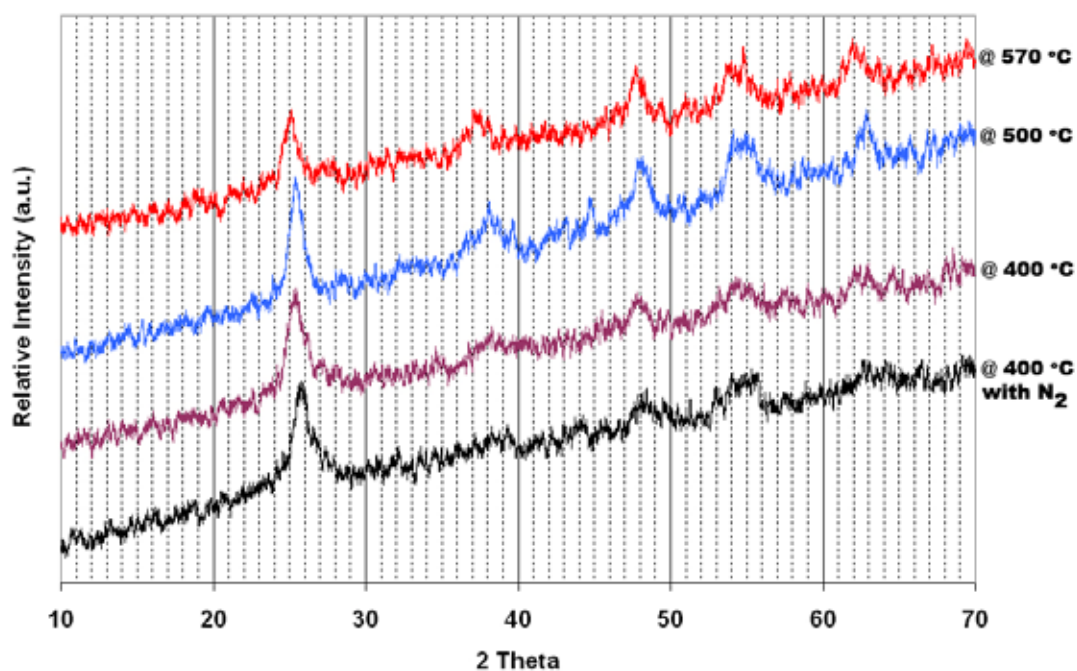
Figure 4.4-17 XRD patterns of CNT-TiO$_2$-1%Fe at various treatment temperatures

74
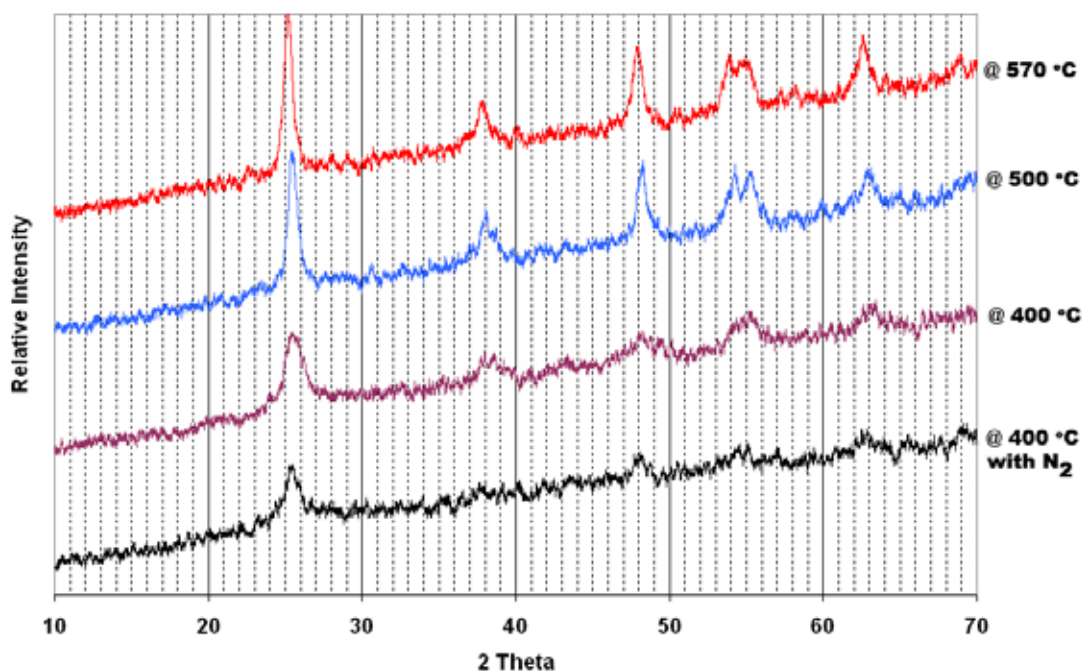
Figure 4.4-18 XRD patterns of CNT-TiO$_2$-1%Na (Na$_2$CO$_3$ source) at various treatment temperatures
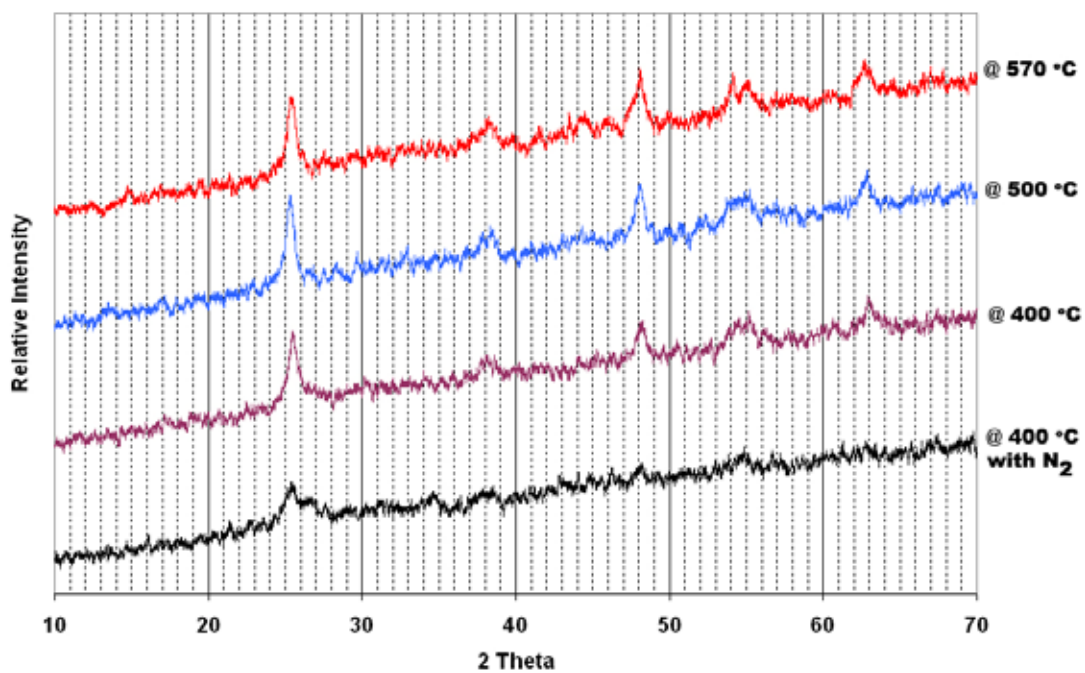
Figure 4.4-19 XRD patterns of CNT-TiO$_2$-5%Na (Na$_2$CO$_3$ source) at various treatment temperatures
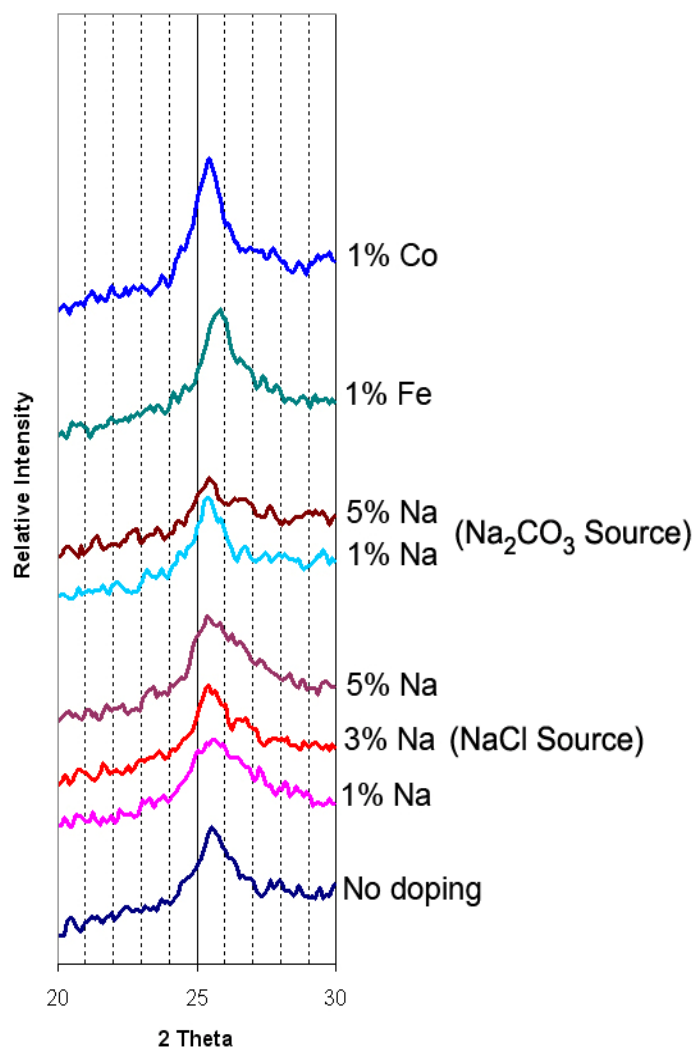
Figure 4.4-20 Crystallite size comparison of CNT series samples heat treated at 400 °C with N_2

that, the CNT is not pure and contains 13% ash. There is only one peak at 652 ºC and it is attributed as the oxidation temperature of CNT's. There is no agreement in literature about the oxidation of CNT's because of the change of activation energy with the number of walls and the presence of impurities. One study reported that value as 750 °C [210], while the other one as 550-650 °C [211].
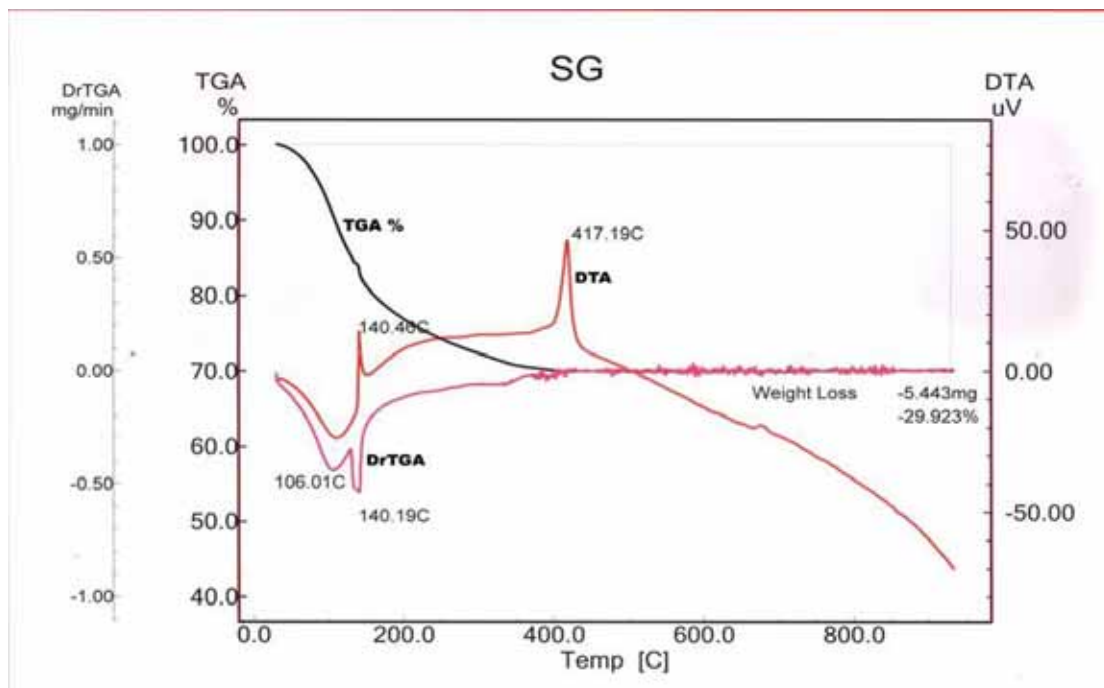
Figure 4.5-1 Thermal analyses of sol-gel titania
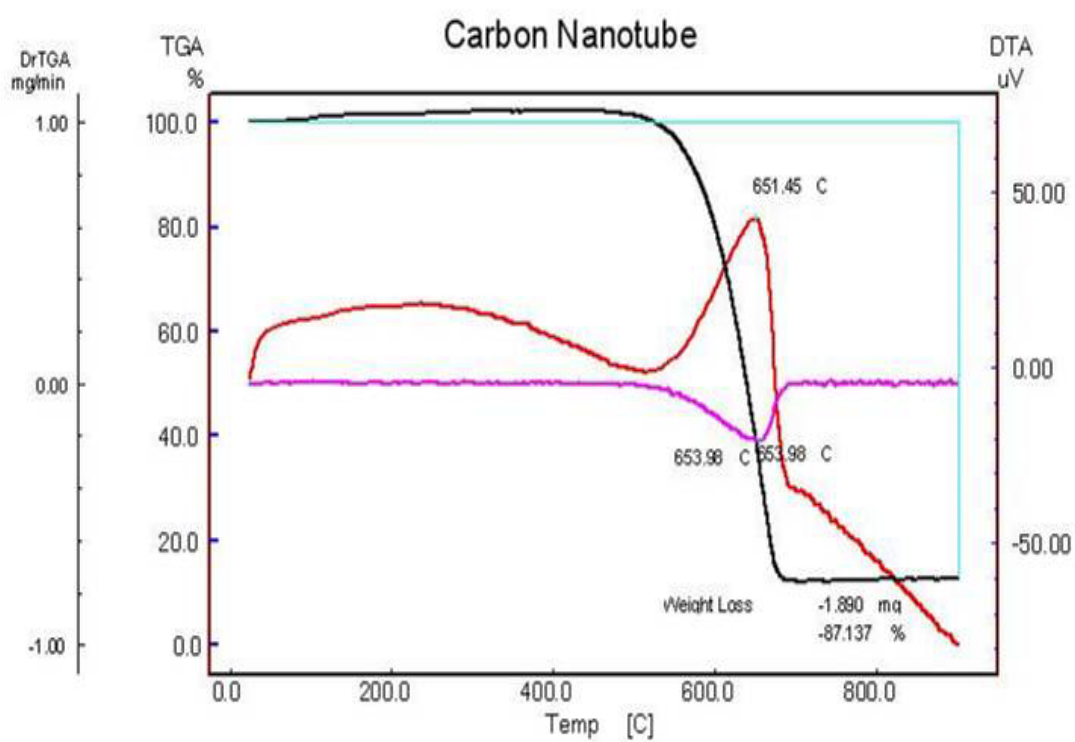
Figure 4.5-2 Thermal analyses of pure CNT

77

The effect of the presence of CNT in titania sol-gel formulation was tested by TGA-DTA of CNT-TiO_2 gel (Fig. 4.5-3). Three peaks were observed; at 35, 267 and 524 °C. The peaks before 400 °C can be assigned to sol-gel precursors. The major weight change which might be attributed to the CNT oxidation. As it is seen from the figure, the CNT oxidation was observed at 524 °C. Interestingly, the oxidation temperature of CNT's reduced significantly in the sol-gel recipe. From the XRD patterns, the formation of anatase phase is very clear even under the non-oxidative calcinations conditions. However, the exothermic reaction of crystallization was not resolved in DTA curve.

The TGA-DTA curves for Fe, Co and Na (NaCl source) doped CNT-TiO_2 gels are presented in Figures 4.5-4, 5, and 6 respectively. In all thermograms, three peaks were identified and presented in Table 4.5-1. Very Similar CNT oxidation temperatures were observed from the DTA curves of Fe^{+3} and Co^{+2} doped samples as 528 and 531 °C respectively while it is suppressed significantly Na doping (597 °C). However, the crystallization or phase transformation peak is resolved at 449 °C for Na doped CNT-TiO_2 sample. These results are contradictory with the results of Endo et al. [210]. They have reported the catalytic effect of Na impurity on the CNT oxidation and the reduction of oxidation temperature of CNT's from 770 °C to 660-690 °C in the presence of Na.

These results indicate that the CNT decomposition temperature is significantly lowered by the chemical environment of the sol-gel recipe. This effect might be explained by the detailed study and TiO_2 itself may catalyze the CNT oxidation. Li et al. [213] explains the shift of the maximum CNT gasification temperature by the reaction between carboxylic acid groups present at CNT's defect sites and TiO_2's surface hydroxyl groups.
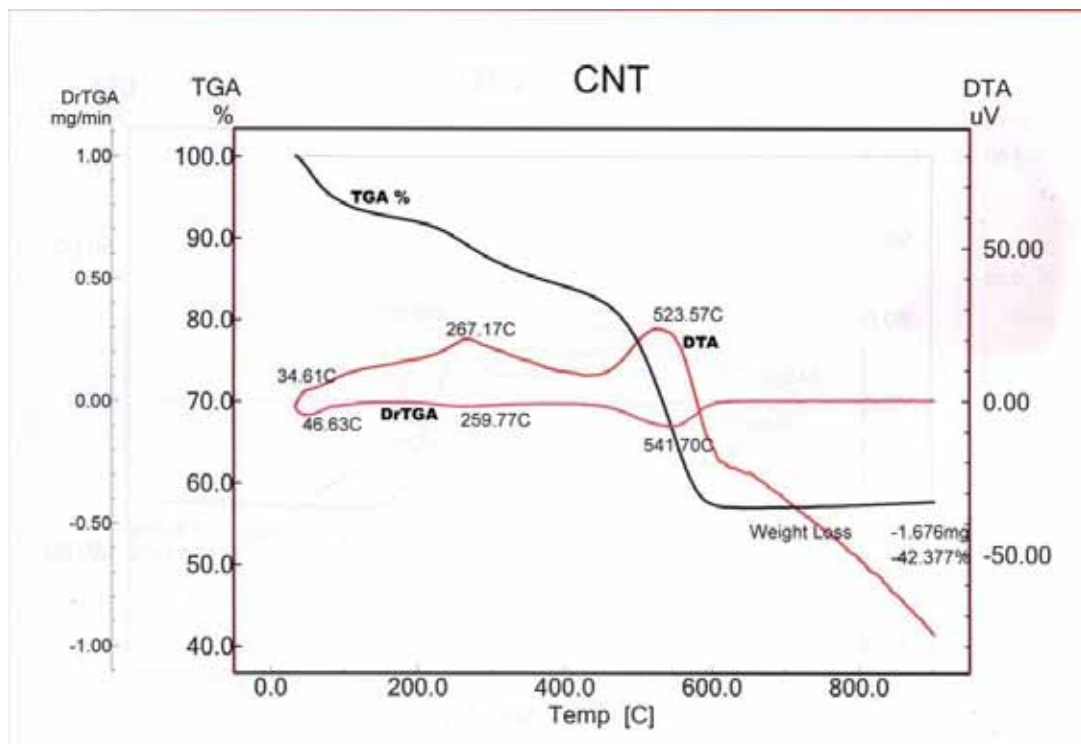
Figure 4.5-3 Thermal analyses of sol-gel titania with CNT
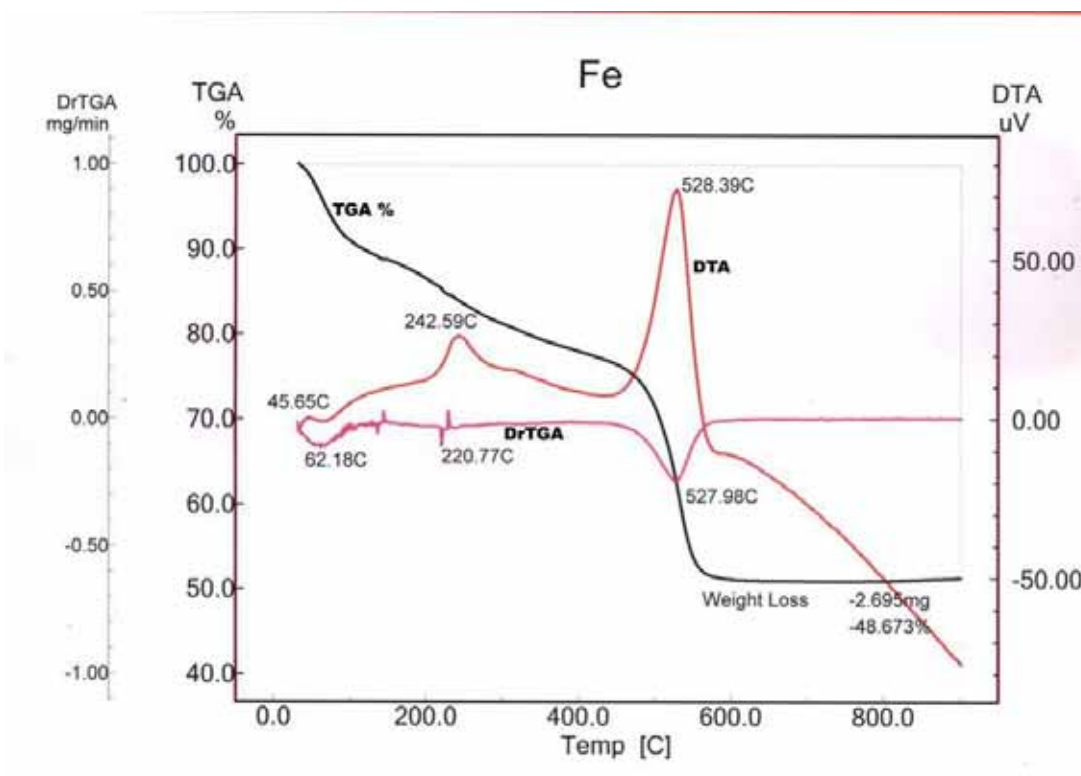
Figure 4.5-4 Thermal analyses of sol-gel titania with CNT and Fe
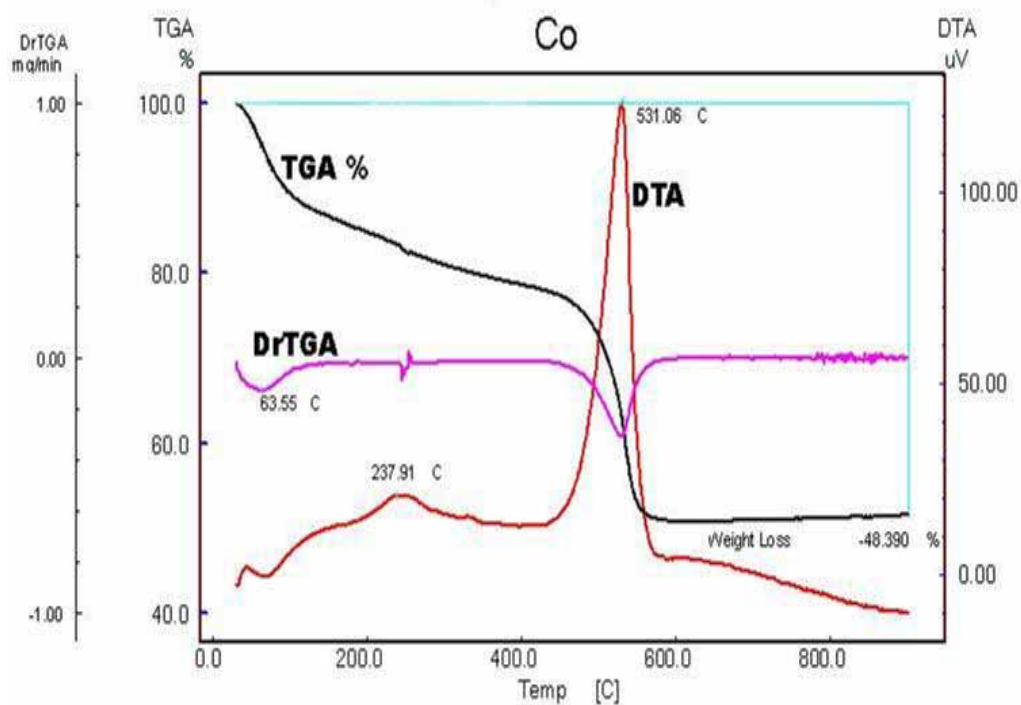
Figure 4.5-5 Thermal analyses of sol-gel titania with CNT and Co
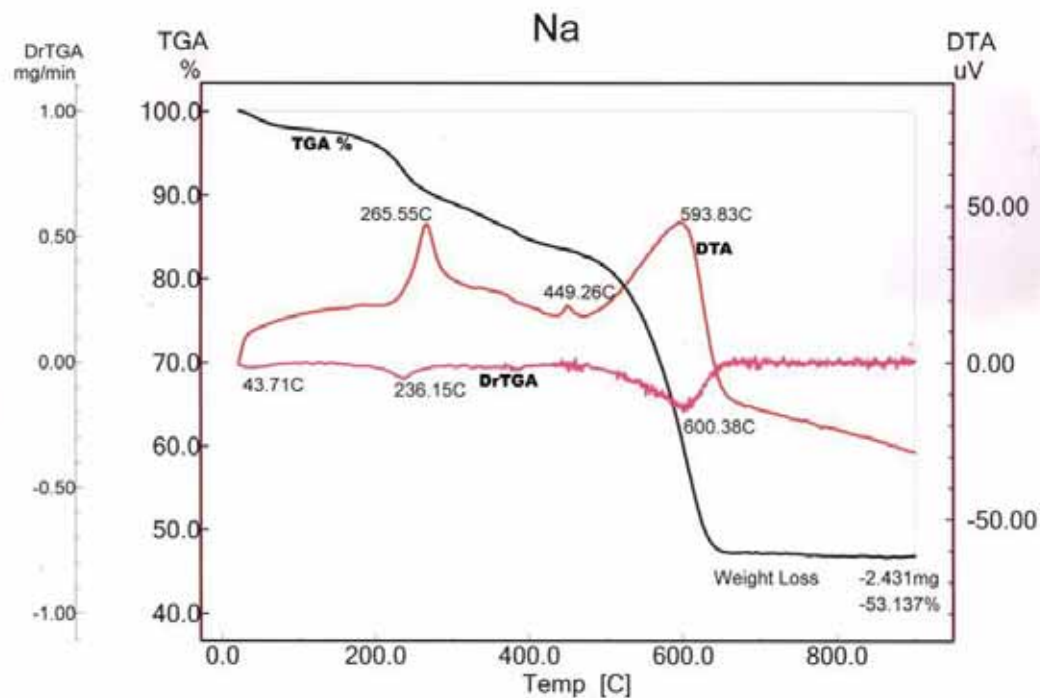
Figure 4.5-6 Thermal analyses of sol-gel titania with CNT and 1% Na (NaCl source)

80

Table 4.5-1 CNT Oxidation Temperatures

Sample	CNT oxidation temperature (°C)
CNT	652
CNT-TiO$_2$	524
CNT-TiO$_2$-1%Na (NaCl source)	597
CNT-TiO$_2$-3%Na (NaCl source)	518
CNT-TiO$_2$-5%Na (NaCl source)	522
CNT-TiO$_2$-1%Co	531
CNT-TiO$_2$-1%Fe	528
CNT-TiO$_2$-1%Na (Na$_2$CO$_3$ source)	515
CNT-TiO$_2$-5%Na (Na$_2$CO$_3$ source)	520

Addition of extra Na$^+$ to the mixture reduces the oxidation temperature of CNT's. Increasing the content to 3% decreases this temperature to 518 °C (Figure 4.5-7). This value is smaller than the iron doped one and when the Na$^+$ content is increased further to 5%, similar result was obtained as 522 °C (Figure 4.5-8). Changing the Na$^+$ source seems to change the oxidation temperature of CNT's (Figure 4.5-9). While the source was NaCl and the percentage is 1%, oxidation temperature was recorded as 597 °C. On the other hand, when the source is Na$_2$CO$_3$ with the same percentage, oxidation temperature is 515 °C. However, when the Na$^+$ percentage is 5 with Na$_2$CO$_3$ source, the oxidation temperature is 520 °C (Figure 4.5-10). Actually all Na$^+$ results are close to each other except the 1% NaCl sample.
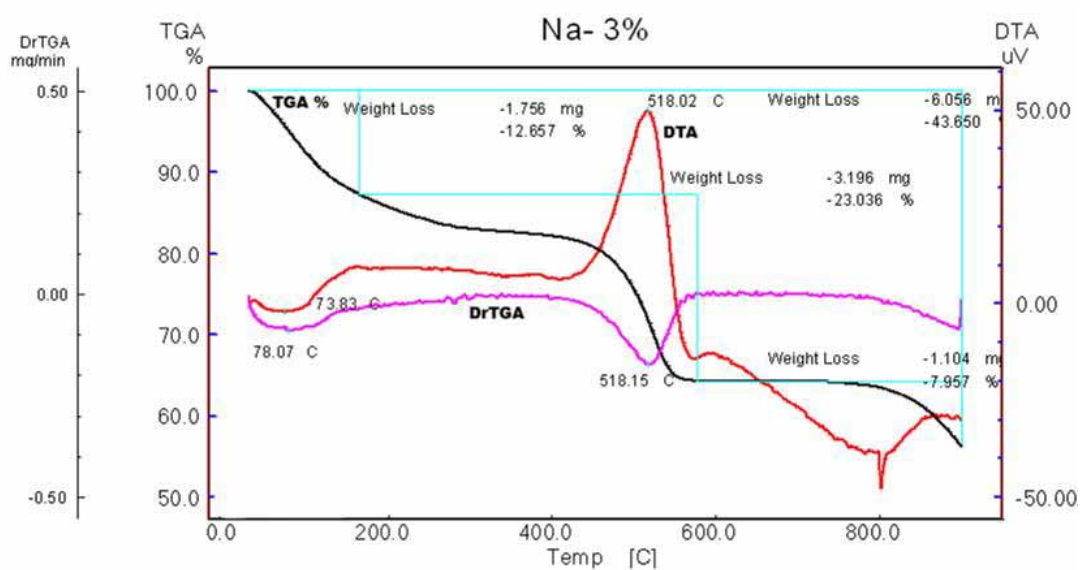
Figure 4.5-7 Thermal analyses of sol-gel titania with CNT and 3% Na (NaCl source)
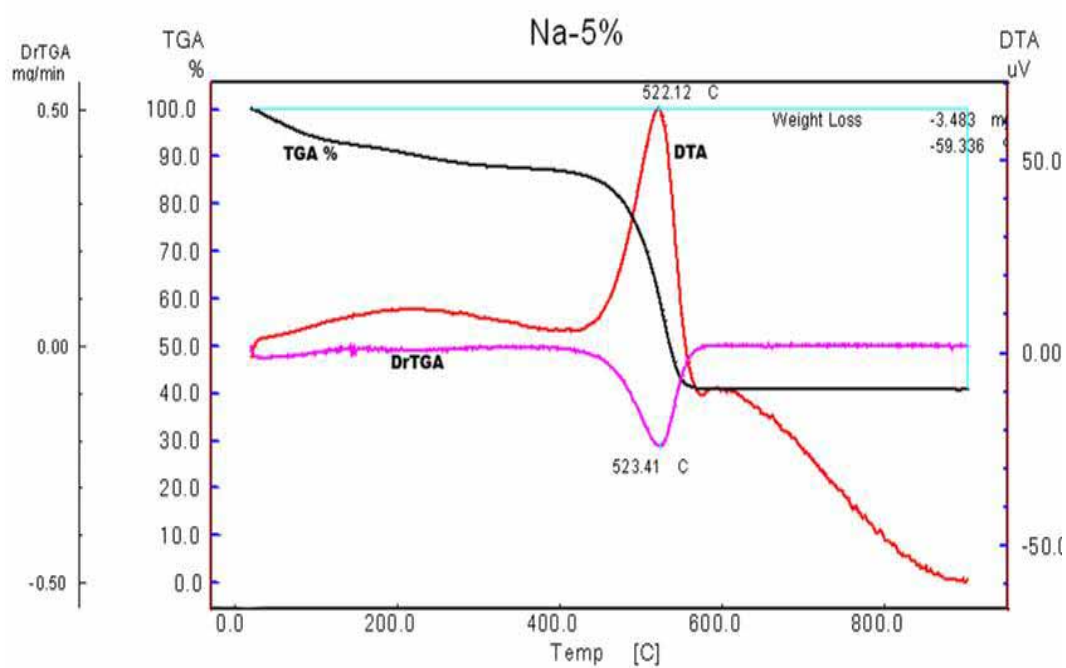
Figure 4.5-8 Thermal analyses of sol-gel titania with CNT and 5% Na (NaCl source)
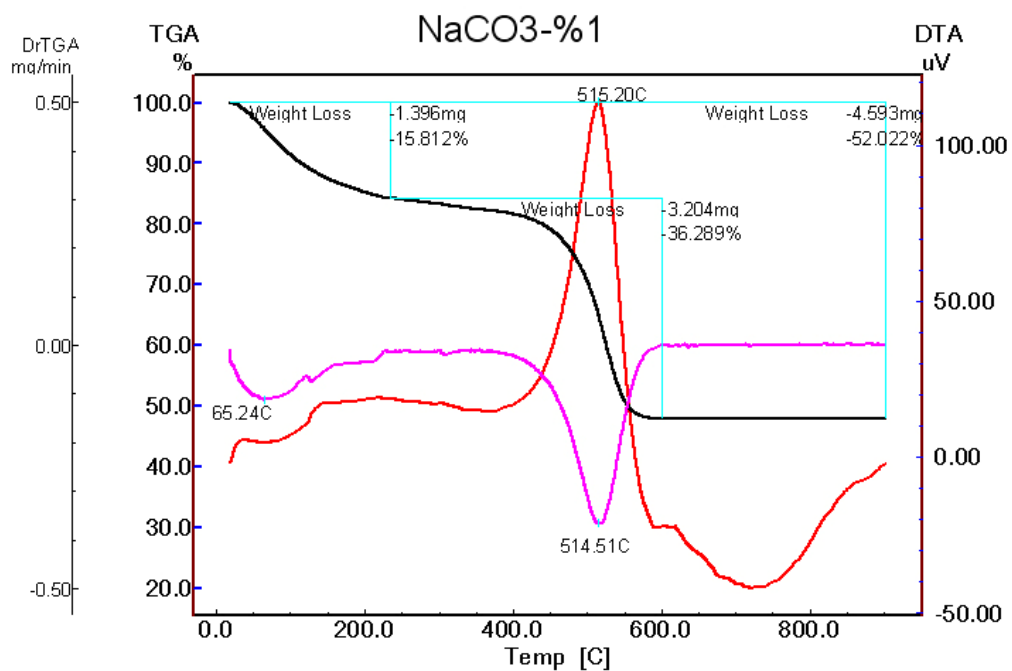
Figure 4.5-9 Thermal analyses of sol-gel titania with CNT and 1% Na (Na_2CO_3 source)
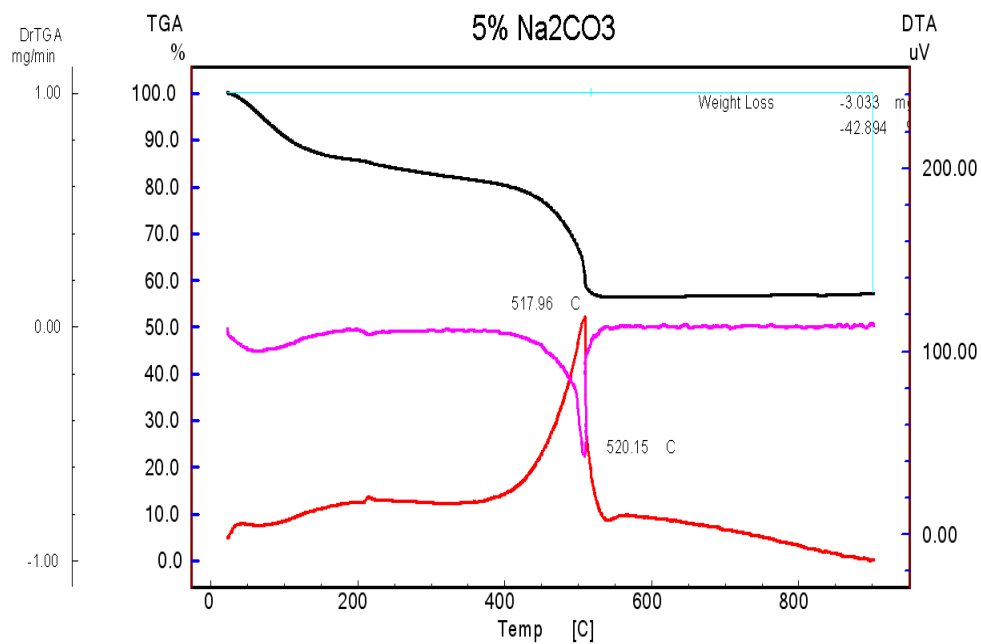
Figure 4.5-10 Thermal analyses of sol-gel titania with CNT and 5% Na (Na_2CO_3 source)

4.6. Surface area and Pore Size Distribution

Surface areas of CNT templated samples are tabulated at Table 4.6-1. Addition of CNT's obviously increased the surface area, but at first sight it is difficult to claim and explain the reason of the increase in surface area. The residual CNT's in the samples may contribute an enormous surface area and the effect of CNT use as template can not be determined directly from the surface area measurements. When TGA curves (Figure 4.5-6) and SEM images (Figure 4.4-5) of CNT-TiO_2-1%Na (NaCl source) is examined, if there are some CNT residual, CNT-TiO_2-1%Na should have the most. To check the CNT content of the samples, additional carbon analysis was performed with CHO elemental analyzer. According to the CHO analysis (Table 4.6-1), the sample contains 33.81% carbon after 2 hours of heat treatment at 400 ºC in absence of oxygen. When air is used in calcinations at the same temperature for 2 hours, the carbon content drops to 22.22 %. Increasing the calcinations temperature to 500 ºC, for 2 hours, causes the drop in the carbon amount to 10.02 % and finally at 570 ºC after 2 hours, the carbon residual was determined as 0.07 % only which can be stated that the CNT's was oxidized completely. Although the sintering reaction will compete with the CNT template on the surface, one can state that the surface area will be determined by templating effect on the samples which are calcined at 570 ºC under air flow. As it is seen from the Table 4.6-2 the addition of CNT's increases the surface area drastically. The effect of sintering and the effect of CNT templating can be clearly seen from the results.

Table 4.6-1 Carbon content of CNT-TiO_2-1%Na (NaCl Source) after heat treatment and calcinations

Sample CNT-TiO_2-1%Na (NaCl Source)	Heat treated with N_2 @ 400 °C	Calcined @ 400 °C	Calcined @ 500 °C	Calcined @ 570 °C
Carbon Percentage (%)	33.81	22.22	10.02	0.07

Table 4.6-2 Surface areas of CNT added titania samples

Sample	Heat treated with N_2 @ 400 °C (m^2/g)	Calcined with air @ 400 °C (m^2/g)	Calcined with air @ 500 °C (m^2/g)	Calcined with air @ 570 °C (m^2/g)
TiO_2	10	22	20	20
CNT-TiO_2	96	105	55	46
CNT-TiO_2-1%Na (NaCl Source)	153	162	84	58
CNT-TiO_2-3%Na (NaCl Source)	152	98	74	40
CNT-TiO_2-5%Na (NaCl Source)	138	123	52	44
CNT-TiO_2-1%Co	146	191	68	63
CNT-TiO_2-1%Fe	135	133	73	47
CNT-TiO_2-1%Na (Na_2CO_3 Source)	139	151	58	50
CNT-TiO_2-5%Na (Na_2CO_3 Source)	111	91	45	37

4.7. Photocatalytic Activity of CNT Samples

Titania synthesized with CNT's have been attracting great attention in literature. Some similar studies [212, 221, 222] were published without thermal treatment and calcination. These studies report that CNT's act as a photosensitizer and titania become active under visible light. Faria et al. prepared TiO_2-CNT catalysts and characterized them in a system where the volume where 0.8 L and TiO_2 content was 1 g/L. The system was irradiated with visible light and total phenol conversion was achieved in 6 hours. So the photocatalytic activity of these samples will be very informative on the further explanation of the effect of CNT presence on the TiO_2 sol-gel preparations. For this purpose, the photocatalytic activity was measured with the degradation reaction of 2 ppm methylene blue (MB) solution at 25 °C irradiated under 300 W/m^2 and known catalyst concentration (TiO_2 content in the system is 1 g TiO_2/liter). The MB concentration was determined by measuring the absorbance

of reaction mixture at 665 nm by UV-Vis spectrometer. All of the initial decomposition rate constants are tabulated at Table 4.7-1. The results of 2 ppm MB degradation with CNT-TiO$_2$ catalysts are presented in Figure 4.7-1. When the degradation curves presented in Figure 4.7-1 and initial decomposition rate constant are examined, it is clear that the best result was obtained from the sample heat treated at 400 ºC with N$_2$ (1.3 hr^{-1}). In addition to that, with increasing calcination temperature the activity decreases significantly form 1.3 to 0.6 hr^{-1} as surface area of the catalyst samples also decreases. While the
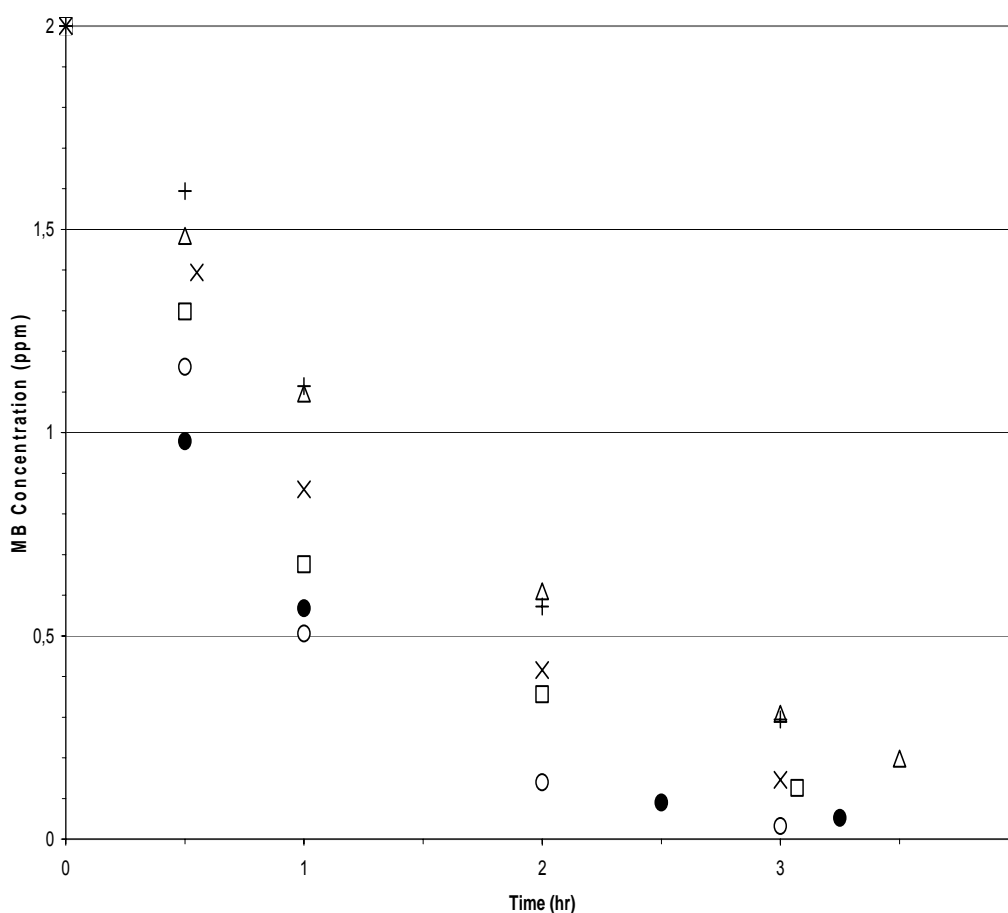
Figure 4.7-1 Photocatalytic Activity of CNT-TiO$_2$ group samples (0.1 L solution, 1 g TiO$_2$/L, 300 W/m^2 irradiation) (●, CNT-TiO$_2$ heat treated with N$_2$ @ 400 °C; O, CNT-TiO$_2$ calcined @ 400 °C; □, CNT-TiO$_2$ calcined @ 500 °C; △, CNT-TiO$_2$ calcined @ 570 °C; X, TiO$_2$ calcined @ 400 °C; +, TiO$_2$ calcined @ 570 °C)

initial decomposition rate constant of CNT-TiO$_2$, which is calcined at 400 °C, is 1.3 hr^{-1}, this constant drops to 0.8 hr^{-1} for TiO$_2$ when calcined at the same conditions. On the other hand, CNT-TiO$_2$ and TiO$_2$ calcined at 570 °C have the same initial decomposition rate constants (0.6 hr^{-1}). Elemental analyses proved that there can not be any CNT residues at that condition so this shows us that the presence of CNT's in the system enhances the photocatalytic activity.

Table 4.7-1 Initial decomposition rate constants of titania samples

Sample	Heat treated with N$_2$ @ 400 °C (hr^{-1})	Calcined with air @ 400 °C (hr^{-1})	Calcined with air @ 500 °C (hr^{-1})	Calcined with air @ 570 °C (hr^{-1})
TiO$_2$	-	0.8	-	0.6
CNT-TiO$_2$	1.3	1.3	1.0	0.6
CNT-TiO$_2$-1%Na (NaCl Source)	1.9	1.4	0.9	0.8
CNT-TiO$_2$-3%Na (NaCl Source)	0.9	0.8	0.5	0.5
CNT-TiO$_2$-5%Na (NaCl Source)	1.1	1.1	0.6	0.5
CNT-TiO$_2$-1%Co	1.1	1.0	0.6	0.5
CNT-TiO$_2$-1%Fe	1.2	0.8	0.5	0.6
CNT-TiO$_2$-1%Na (Na$_2$CO$_3$ Source)	0.9	0.8	0.7	0.7
CNT-TiO$_2$-5%Na (Na$_2$CO$_3$ Source)	1.9	1.5	1.2	1.1

The results of MB degradation with CNT-TiO$_2$-1%Na (NaCl Source) catalysts with similar conditions are presented in Figure 4.7-2. Like the previous results, the best result was obtained from the sample heat treated at 400 °C with N$_2$ (1.9 hr^{-1}). With that sample, in 3 hours, MB amount dropped to 0%.

With other samples, in 4 hours, MB amount dropped to about 5%. Similar to CNT-TiO$_2$ samples, by introducing air and with increasing temperature, initial inactivation rate constants dropped significantly form 1.9 to 0.8 hr^{-1}; parallel to the surface area decrease. When initial decomposition rate constants of CNT-TiO$_2$-1%Na (NaCl source) and CNT-TiO$_2$ are compared, Na added samples are more active than the undoped ones. Also at 570 °C condition, Na added samples activity (0.8 hr^{-1}) is better that TiO$_2$'s activity (0.6 hr^{-1}). When Figures 4-4.12 and 4-4.13 are examined, Na doped one has wider peak at 25.27 °, showing
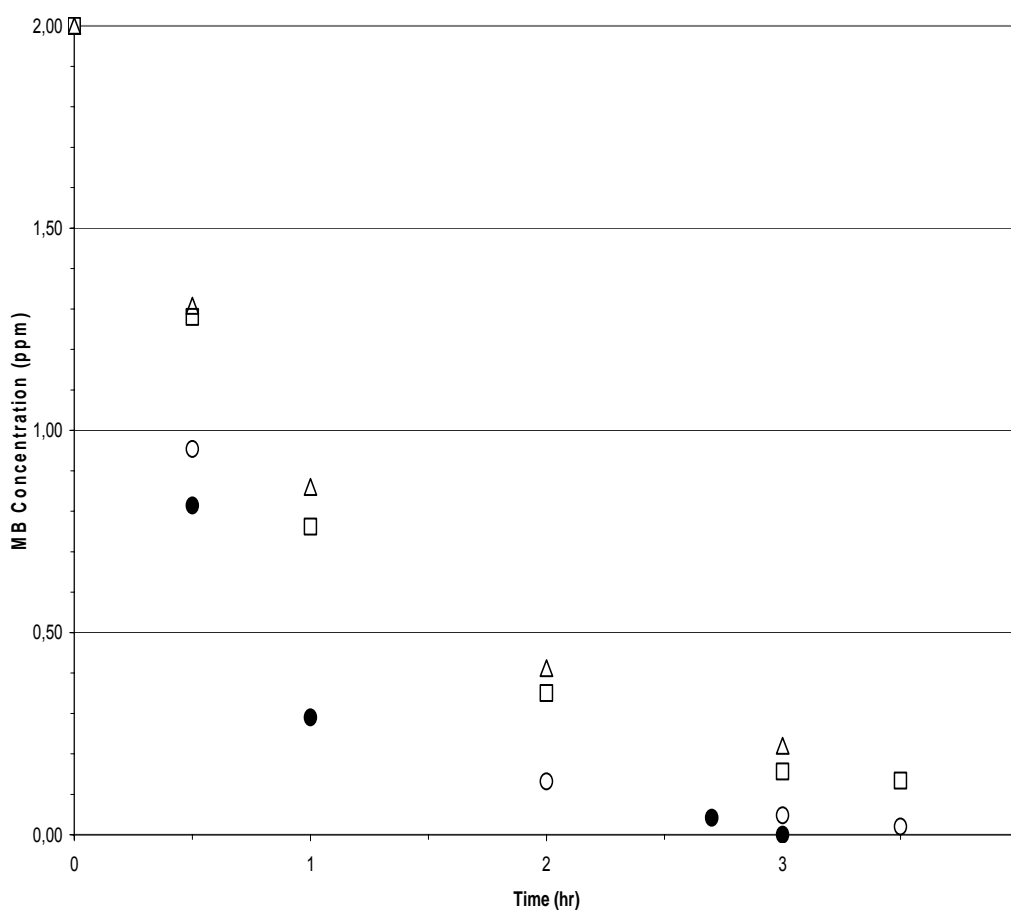
Figure 4.7-2 Photocatalytic Activity of CNT-TiO$_2$-1%Na (NaCl Source) group samples (0.1 L solution, 1 g TiO$_2$/L, 300 W/m^2 irradiation) (●, CNT-TiO$_2$-Na heat treated with N$_2$ @ 400 °C; O, CNT-TiO$_2$-Na calcined @ 400 °C; □, CNT-TiO$_2$-Na calcined @ 500 °C; △, CNT-TiO$_2$-Na calcined @570 °C)

that it has smaller crystallite size. This also may contribute to better photocatalytic activity. Thus, we can conclude that addition of 1% Na (NaCl source) increases the photocatalytic activity.

The results of MB degradation with CNT-TiO$_2$-3%Na and CNT-TiO$_2$-5%Na (NaCl Source) catalysts with similar conditions are presented in Figure 4.7-3 and Figure 4.7-4 respectively. For both of them, again the best results were obtained from the samples heat treated at 400 °C with N$_2$ (0.9 and 1.1 hr^{-1} respectively). Similar to previous samples, by introducing air and with increasing
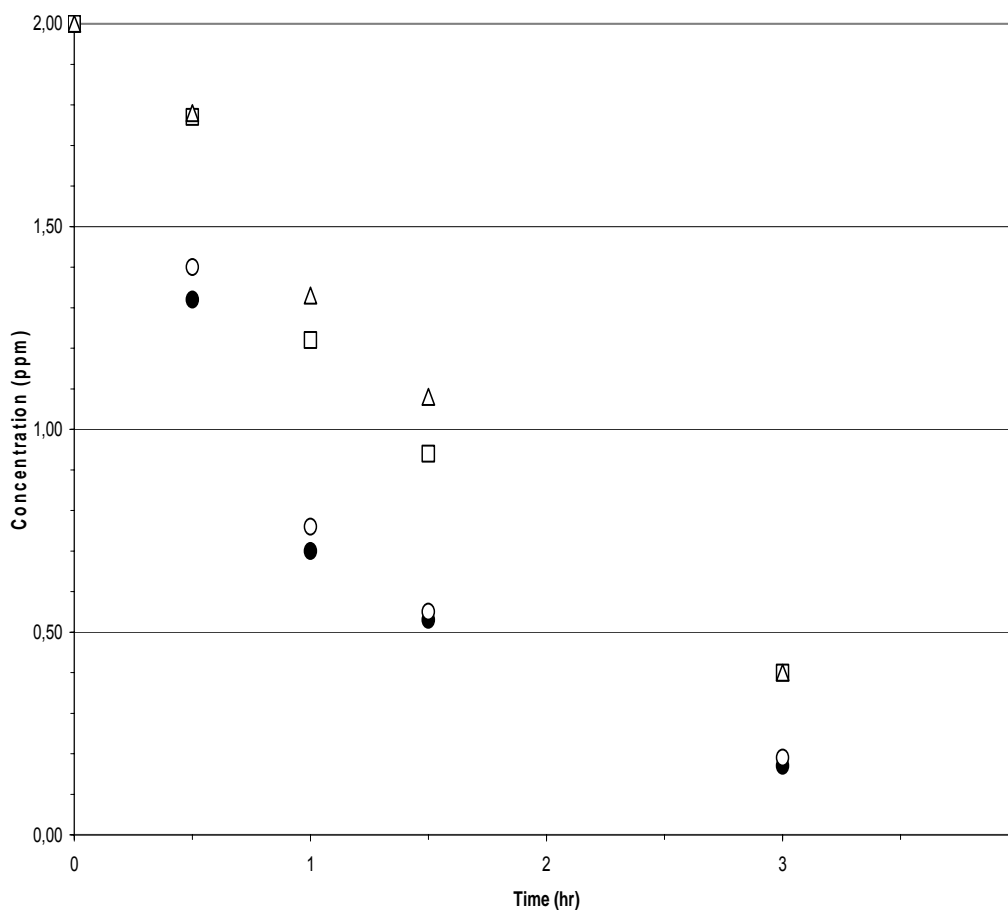
Figure 4.7-3 Photocatalytic Activity of CNT-TiO$_2$-3%Na (NaCl Source) group samples (0.1 L solution, 1 g TiO$_2$/L, 300 W/m^2 irradiation) (●, CNT-TiO$_2$-Na heat treated with N$_2$ @ 400 °C; O, CNT-TiO$_2$-Na calcined @ 400 °C; □, CNT-TiO$_2$-Na calcined @ 500 °C; △, CNT-TiO$_2$-Na calcined @570 °C)

temperature, initial decomposition rate constants dropped considerably form 0.9 to 0.5 hr^{-1} for 3% Na and dropped from 1.1 to 0.5 hr^{-1} for 5% Na; parallel to the surface area decrease. In 4 hours, MB amount dropped to about 10%. When initial rates are compared, 5% Na and 3% Na added samples are less active than 1% Na added samples. The activity is even less than CNT-TiO_2's activity, close to the photocatalytic activity of TiO_2. When SEM images (Figure 4.4-5, 4.4-6 and 4.4-7) and TGA curves (Figures 4.5-6, 4.5-7 and 4.5-8) are examined 3% and 5% Na samples should have lesser amount of CNT's. From the comparison
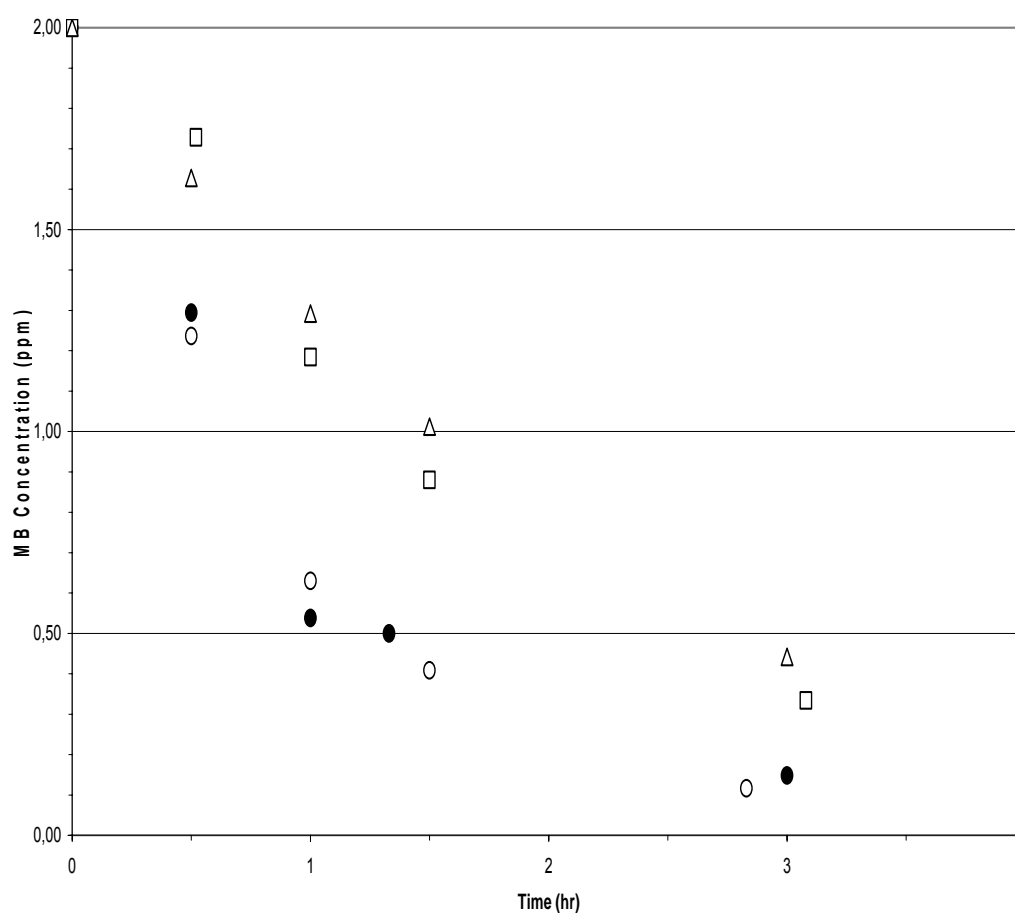
Figure 4.7-4 Photocatalytic Activity of CNT-TiO_2-5%Na (NaCl Source) group samples (0.1 L solution, 1 g TiO_2/L, 300 W/m^2 irradiation) (●, CNT-TiO_2-Na heat treated with N_2 @ 400 °C; O, CNT-TiO_2-Na calcined @ 400 °C; □, CNT-TiO_2-Na calcined @ 500 °C; △, CNT-TiO_2-Na calcined @570 °C)

between CNT-TiO$_2$ and TiO$_2$, we have seen that CNT enhances the photocatalytic activity. So this may be one reason for smaller initial decomposition rate constant. In addition to that, from Figures 4.4-14 and 4.4-15, we observed that there is NaCl peak at about 32 °. Chloride in the system probably poisons the active sites on TiO$_2$, which also explains the lower activity of 3% and 5% Na added samples that TiO$_2$ calcined at 570 °C.

MB degradation results with CNT-TiO$_2$-1%Fe are presented in Figure 4.7-5. Analogous to the previous results the best result was obtained from the
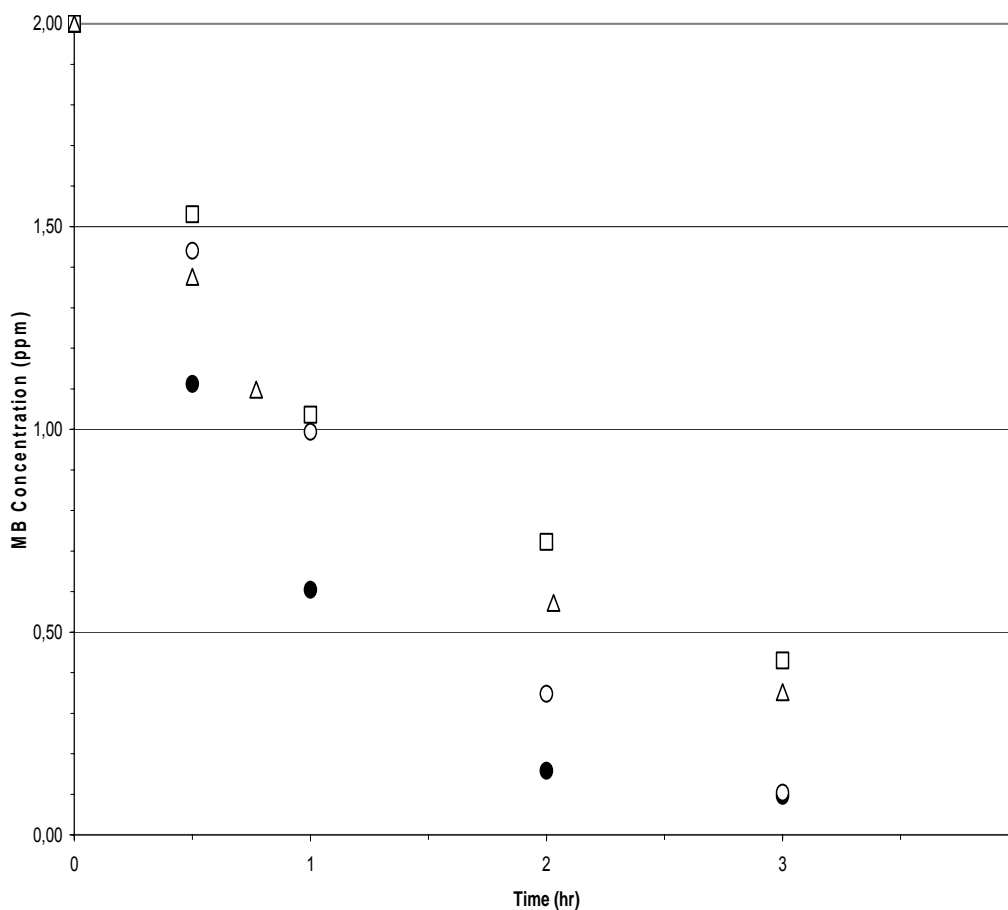
Figure 4.7-5 Photocatalytic Activity of CNT-TiO$_2$-1%Fe group samples (0.1 L solution, 1 g TiO$_2$/L, 300 W/m^2 irradiation) (●, CNT-TiO$_2$-Fe heat treated with N$_2$ @ 400 °C; O, CNT-TiO$_2$-Fe calcined @ 400 °C; □, CNT-TiO$_2$-Fe calcined @ 500 °C; △, CNT-TiO$_2$-Fe calcined @570 °C)

sample heat treated at 400 ºC with N_2 (1.2 hr^{-1}). Similar to previous samples, by introducing air and with increasing temperature, initial decomposition rate constants dropped considerably form 1.2 to 0.6 hr^{-1}; parallel to the surface area decrease. In 4 hours, MB amount dropped to about 10%. When initial rates are compared, 1% Fe added samples are less active than 1% Na added samples and CNT-TiO_2 samples without any doping, but they have almost the same activity with TiO_2 and 3% Na (NaCl source) added catalysts. When TGA curve of CNT-TiO_2-1%Fe (Figure 4.5-4) is examined, it should have more CNT residues than CNT-TiO_2, thus have a better activity. However the activity is not better. So Fe in the system should be decreasing the activity. Fe is probably interacts with CNT not TiO_2, because the initial decomposition rate constant of CNT-TiO_2-1%Fe and TiO_2 calcined at 570 °C are same. We can conclude that the interaction of Fe with CNT prevents the positive contribution CNT to photocatalytic activity.

MB degradation results with CNT-TiO_2-1%Co are presented in Figure 4.7-6. As the previous ones, the best result was obtained from the sample heat treated at 400 ºC with N_2 (1.1 hr^{-1}). Again similar to previous samples, by introducing air and with increasing temperature, initial decomposition rate constants dropped significantly form 1.1 to 0.5 hr^{-1}; parallel to the surface area decrease. In 4 hours, MB amount dropped to about 10%. When initial rates are compared, 1% Co added samples activity is close to 1% Fe added samples activity. Again the lower activity can be described with interaction of Co with CNT's.

The results of MB degradation with CNT-TiO_2-1%Na and CNT-TiO_2-5%Na (Na_2CO_3 source) catalysts are presented in Figure 4.7-7 and Figure 4.7-8 respectively. For both of them, again the best results were obtained from the samples heat treated at 400 ºC with N_2 (0.9 and 1.9 hr^{-1} respectively). Similar to previous samples, by introducing air and with increasing temperature, initial decomposition rate constants dropped form 0.9 to 0.7 hr^{-1} for 1% Na and dropped from 1.9 to 1.1 hr^{-1} for 5% Na; parallel to the surface area decrease. In 4 hours, MB amount dropped to about 5%. When initial rates are compared, 1% Na (Na_2CO_3 source) added samples activities are close 1% Co added samples and 5% Na (Na_2CO_3 source) added samples have the best activity. When the samples calcined at 570 °C are examined, like the 1% Na (NaCl source), we can see the positive contribution of Na to the photocatalytic activity. Also at that temperature, we observe that with Na_2CO_3 source photocatalytic activity is better. This situation may prove the poisoning effect of chloride.
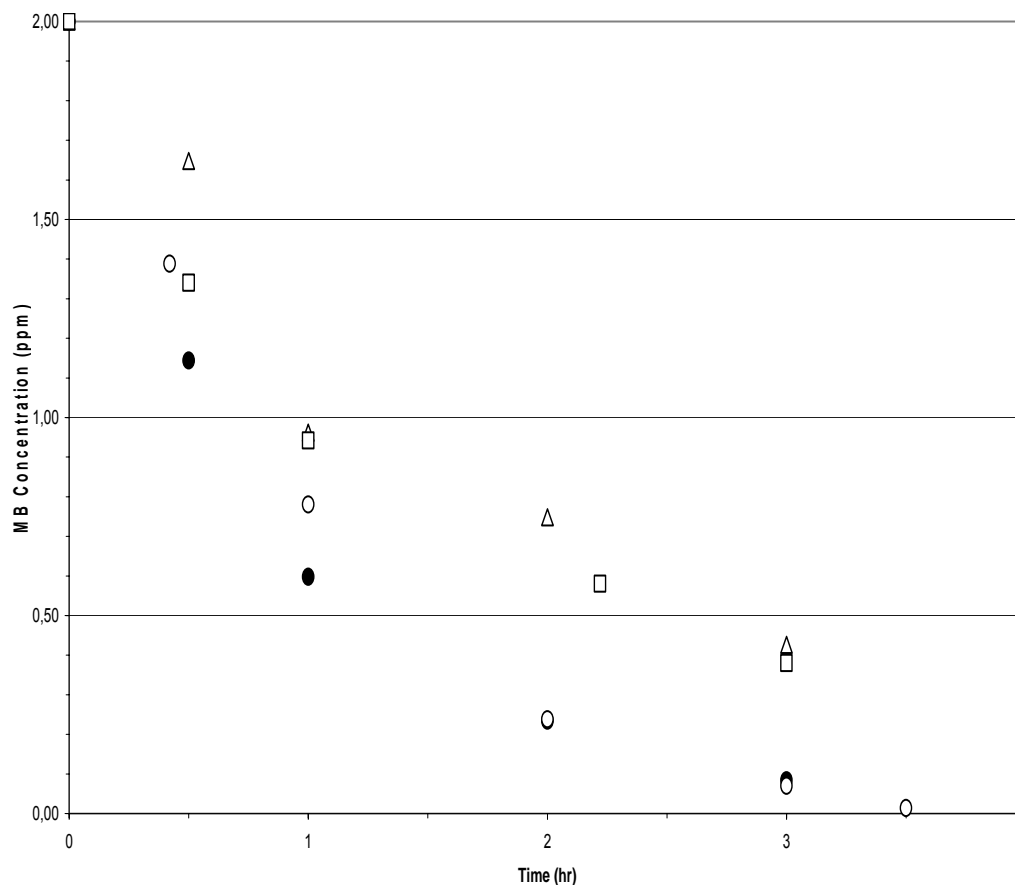
Figure 4.7-6 Photocatalytic Activity of CNT-TiO$_2$-1%Co group samples (0.1 L solution, 1 g TiO$_2$/L, 300 W/m^2 irradiation) ($\bullet$, CNT-TiO$_2$-Co heat treated with N$_2$ @ 400 °C; O, CNT-TiO$_2$-Co calcined @ 400 °C; $\square$, CNT-TiO$_2$-Co calcined @ 500 °C; $\triangle$, CNT-TiO$_2$-Co calcined @570 °C)

All the activities of the samples seem to be parallel with the surface areas. The more the surface area is, the more the activity recorded. But, as mentioned above, there may be some other parameters. CNT content is higher in the samples calcined at lower temperatures. In literature it is stated that CNT's increases the photocatalytic activity of titania particles. This effect comes from the point defects on CNT's [237]. Zheng et al. [240], made some research on the effect of transition metals on CNT's and they have found some results shown in Figure 4.7-9. When Ti atom interacts with these defects a new defect forms.
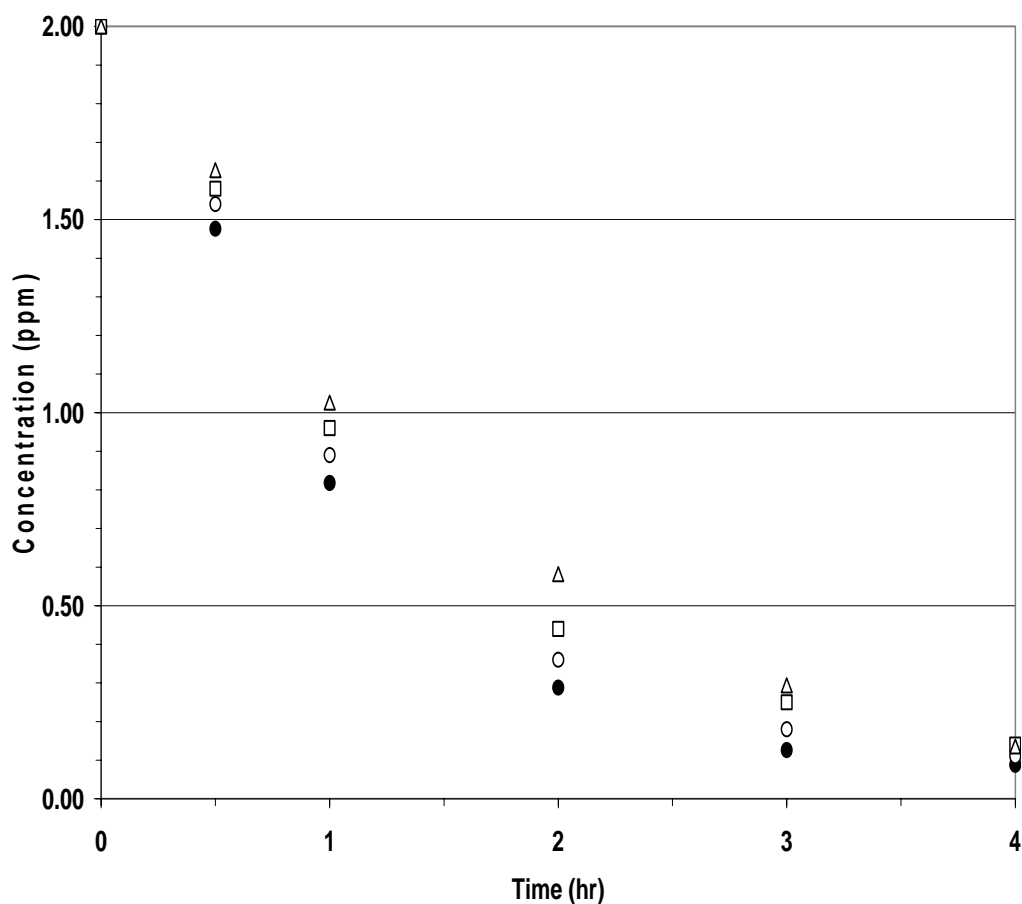
Figure 4.7-7 Photocatalytic Activity of CNT-TiO$_2$-1%Na (Na$_2$CO$_3$ source) group samples (0.1 L solution, 1 g TiO$_2$/L, 300 W/m^2 irradiation) ($\bullet$, CNT-TiO$_2$-1%Na heat treated with N$_2$ @ 400 °C; O, CNT-TiO$_2$-1%Na calcined @ 400 °C; □, CNT-TiO$_2$-1%Na calcined @ 500 °C; $\triangle$, CNT-TiO$_2$-1%Na calcined @570 °C)

This means that CNT-TiO$_2$ sample should be more active than TiO$_2$ sample. Which in our case, it is true. This also explains why CNT oxidation temperature drops when TiO$_2$ is added to the system. The other result they observed was when Co or Fe atom interacts with defective CNT's, defects vanish. From this we can conclude that CNT-TiO$_2$-Fe or CNT-TiO$_2$-Co samples should be less active than CNT-TiO$_2$. Again, in our case, it is true. As before, it also explains the higher oxidation temperature of Co and Fe doped catalysts. So from the results, we may speculate that Na atoms interact with CNT's like Ti atoms do, and

94
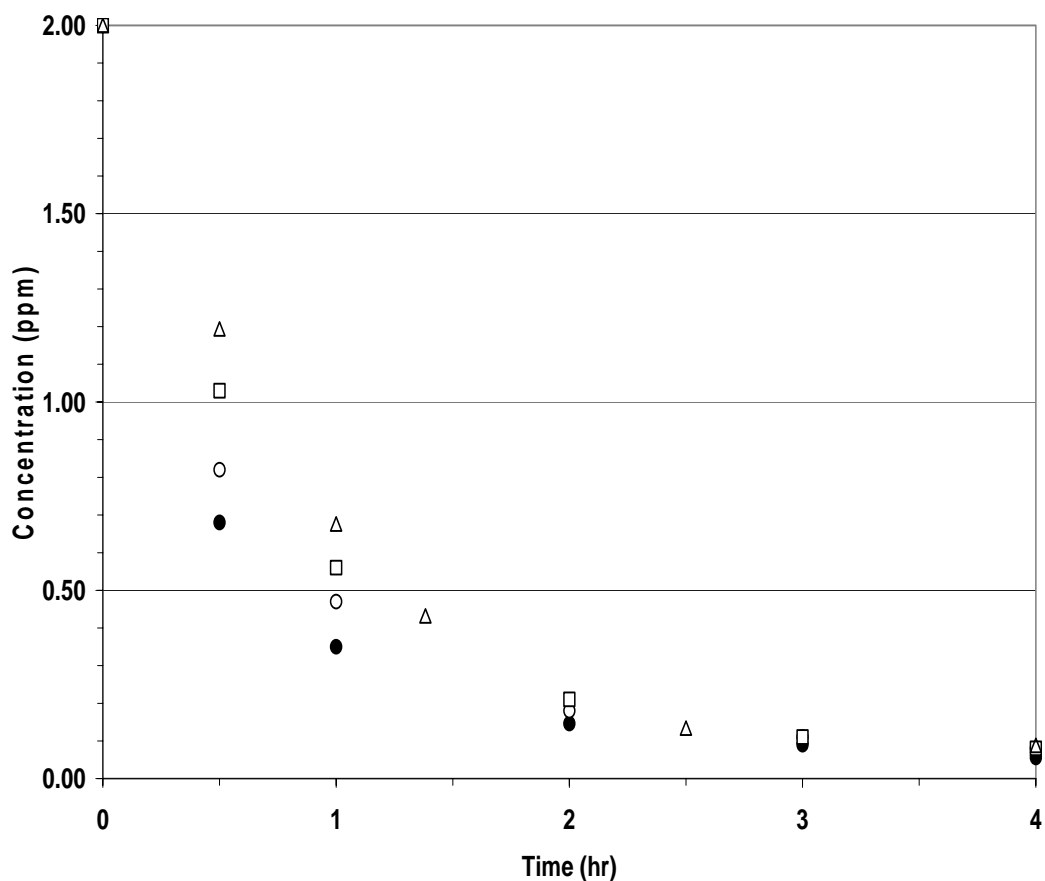
Figure 4.7-8 Photocatalytic Activity of CNT-TiO$_2$-5%Na (Na$_2$CO$_3$ source) group samples (0.1 L solution, 1 g TiO$_2$/L, 300 W/m^2 irradiation) ($\bullet$, CNT-TiO$_2$-5%Na heat treated with N$_2$ @ 400 °C; O, CNT-TiO$_2$-5%Na calcined @ 400 °C; $\square$, CNT-TiO$_2$-5%Na calcined @ 500 °C; $\triangle$, CNT-TiO$_2$-5%Na calcined @570 °C)

improve photocatalytic activity. This suggestion may be true but from the photocatalytic activity experiments we also observed that Na interacts with Ti and improves the activity.
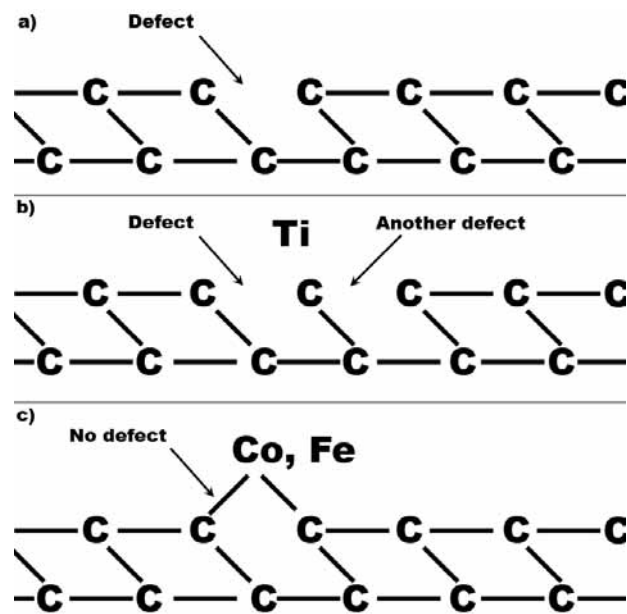
Figure 4.7-9 Interaction of defective CNT (a) with Ti (b) and Co or Fe (c) atoms

CHAPTER 5

CONCLUSIONS

The aim of this study was to synthesize nanostructured titania with better photocatalytic activity. This goal was achieved in two main parts. In the first part, titania was synthesized with sol-gel method and modified with hydrothermal and post-hydrothermal treatments. For comparison, the same hydrothermal treatment procedures were also applied to commercial anatase samples. In this part, the effect of hydrothermal treatment time on the structure and photocatalytic activity was investigated. The synthesized samples were characterized by SEM, XRD, BET and photocatalytic antimicrobial activity against *E. Coli*. The following observations have been made:

- Commercial anatase and sol-gel synthesized titania, after hydrothermal treatment with 10 N NaOH, transformed to significantly different structures. Commercial samples, after the treatment, resemble nanotube bundles. In addition to that, increase in hydrothermal treatment time, shortens the size of bundles. Conversely hydrothermally treated sol-gel anatase has nano-sized lamellar structure and increase in hydrothermal treatment time thickens the structure.

- The hydrothermally treated samples under alkaline conditions were further treated under neutral conditions. After post treatment with distilled water, Com24 was converted into small dispersed particles. When the post treatment time was increased, crystal growth was observed with an octagon like shape. On the other hand, the Com48, after post treatment, transformed into curvy and spiked nano particles. Similarly with increasing time, crystal growth was observed. SG samples after post treatment showed a drastic change in particle

morphology. Particles have a very distinct octagonal shape and like commercial counterpart, crystal growth was observed with increasing post treatment time. The crystal growth under neutral conditions is attributed as the thermal stabilization on nanostructured crystallites as a result of Ostwald ripening process.

- These observations were also verified by the XRD results. When XRD peaks of hydrothermally treated samples were carefully examined, it was seen that anatase structure converted into trititanate proportional with treatment time. After the post treatment, the nanotube (or nanoplates) structure was diminished considerably and the anatase peaks became more intense, indicating the destruction of trititanate structure and the formation of anatase phase as a result of crystal growth which was also observed in SEM analysis. This might be further explained by the similar structures of the building blocks of anatase and trititanate both having TiO_6 octahedron building blocks attached to each other by protons. By post hydrothermal treatment, trititanate particles dehydrate and anatase nanoparticles form.

- From the BET analysis, samples showed Type-IV isotherms with type H3 hysteresis loops indicating the presence of mesoporous structure. For commercial samples, the first and second hydrothermal treatments increased the surface area. While on the other hand, surface areas of sol-gel samples did not increased that much after those treatments. Also the analyses showed that post treatment with distilled water results with surface restructuring; nanotubes and nanoplates form ditetragonal (bipyramidal) structures which causes the porosity to decrease.

- For photocatalytic antimicrobial characterization: all commercial, anatase samples and their hydrothermally treated counterparts exhibit antimicrobial activity and complete inactivation of *E.coli* was obtained. Also it was observed that hydrothermal treatment under alkaline conditions enhanced the antimicrobial activity when compared with untreated commercial anatase. Following hydrothermal post treatment with distilled water, no significant effect was observed on the initial microbial inactivation rate. However, samples demonstrated limited antimicrobial activity. For sol-gel samples: limited antimicrobial activity was observed. Although the

98

initial inactivation rate of Sol–Gel synthesized TiO_2 was nearly the same with commercial anatase, a complete inactivation could not be assessed, which might be attributed to its lower specific surface area in comparison with commercial anatase. However, the alkali treatment enhanced the activity and complete inactivation was achieved. The effect of post treatment with distilled water on the antimicrobial activity was similar with the commercial counterpart; after a certain time, samples show a limited activity. This behavior was attributed to the concentration of oxidative species which directly influence the microbial inactivation rate. During the post treatment with distilled water, samples are dehydrated and lose their oxidative surface species, thus the samples become less photoactive. To regenerate lost oxidative species, post treated samples were exposed into UV irradiation in aqueous medium for some time. After that treatment, the highest inactivation rate was observed and shortest complete inactivation time was obtained.

- As a conclusion for the first part: both the commercial and sol–gel derivative with their mesoporous structure possess improved photocatalytic antimicrobial activities than untreated samples. Further hydrothermal treatment of these samples with distilled water yields almost pure anatase phase with improved crystallinity and active (101) faces in expense of limited antimicrobial activity. The limited activity of the hydrothermally synthesized samples can be enhanced by regenerating active sites on (101) face with treatment process under UV irradiation in the presence of water which results in the most active catalysts.

In the second part, titanium dioxide was synthesized with sol-gel method and during synthesis, multi-walled carbon nanotubes were added. The reason for adding carbon nanotubes was to use them as templates to achieve higher surface area after their removal on calcination stage. For that the effect of calcination temperatures was investigated. Also the effect heat treatment under N_2 atmosphere was investigated. Additionally, the catalytic effect of sodium, iron and cobalt on the oxidation temperature of carbon nanotubes were also examined. During this section, synthesized photocatalysts were characterized by SEM, AFM, XRD, BET, TGA-DTA and photocatalytic activity against methylene blue. The following observations have been made:

- From the analyses we observed that, all samples which are heat treated, have a heterogeneous structure of TiO_2 and CNT's. The CNT content start to decrease with increasing calcination temperature and we can not observe CNT's at 570 °C. Only samples with 1% Na doping (NaCl source) have some fibrous structure at that level. Disappearance of CNT's reveals a porous titania structure, but with increasing temperature, porous titania structure collapses as a result of sintering.

- XRD analysis of undoped, Na, Co, and Fe doped CNT-TiO_2 samples were examined and it was seen that all samples have anatase structure. Also increase in calcination temperature, increased the crystallinity. Similarly, calcined samples are more crystalline when compared with heat treated samples. When peak widths are examined, Na doped samples (with Na_2CO_3 source) have the widest peaks, suggesting that they have the smallest crystallite size.

- TGA-DTA curves showed that, when titania is synthesized with CNT's, the oxidation temperature of CNT's drops about 130 °C indicating the strong interaction of CNT structure with titanium dioxide. Except for 1% Na doped (with NaCl source) sample, doping with Na, Fe and Co drops this temperature further. This result indicates that the CNT decomposition temperature is significantly lowered by the chemical environment of the sol-gel recipe. This effect might be explained by the contribution of these metals to catalyze the CNT oxidation.

- After BET analyses we have observed that addition of CNT's increases the surface area drastically. The elemental analyses proved that, the CNT template is successfully removed and the high surface area is contributed by titania structure. However the effect of sintering limits the calcination temperature for further crystallinity.

- When the effect of calcination temperature and presence of oxygen was investigated, samples heat treated at 400 °C with N_2 had the best activity. In addition to that, it was seen that with increasing calcination temperature, initial rates are decreasing as surface area is also decreasing. This decrease was also explained by the decrease in the CNT content since, in literature, CNT's are reported to enhance photocatalytic activity of titania. CNT mixed titania's activity was

better than pure titania, showing that CNT improves to the activity. This situation was explained by the CNT's ability to transfer exited electrons of titania to CNT bundle, thus delaying charge recombination. Also titanium can create defects on CNT's which enhances this process. When doping was considered, the best activity was obtained from Na doped samples. On the other hand, Fe and Co doped samples had the worst activity. Decreased activity after doping was explained by the disappearance of defects on CNT's.

- As a conclusion for the second part: The synergy of TiO_2 and CNT's enhanced the photocatalytic activity. So keeping the calcination or heat treatment temperature as low as possible will result in more active catalysts. Additionally, doping the sample with Na increased the photocatalytic activity. However we recommend that more experiments should made on Na to understand the mechanism of this enhancement. Changing the Na source and content will probably clarify this condition.

REFERENCES

[1]   Diebold, U., "The surface science of titanium dioxide", Surface Science Reports, 2003, 48, 53.

[2]   Kronos International, 1996.

[3]   L.G. Phillips, D.M. Barbano, "The influence of fat substitutes based on protein and titanium dioxide on the sensory properties of lowfat milks", Journal of Dairy Science, 80 (1997) 2726.

[4]   J. Hewitt, "Formulating water-resistant TiO_2 sunscreens", Cosmetics & Toiletries 114 (1999) 59.

[5]   J. Lausmaa, M. Ask, U. Rolander, B. Kasemo, Mater. Res. Soc. Symp. Proc. 110 (1988) 647.

[6]   P.K. Dutta, A. Ginwalla, B. Hogg, B.R. Patton, B. Chwieroth, Z. Liang, P. Gouma, M. Mills, S. Akbar, "Interaction of carbon monoxide with anatase surfaces at high temperatures : optimization of a carbon monoxide sensor", Journal of Physical Chemistry 103 (1999) 4412.

[7]   Y. Xu, K. Yao, X. Zhou, Q. Cao, "Platinum-titania oxygen sensors and their sensing mechanisms", Sensors and Actuators B: Chemical 14 (1993) 492.

[8]   A. Fujishima, K. Honda, "Electrochemical Photolysis of Water at a Semiconductor Electrode", Nature 238 (1972) 37.

[9]   V.E. Henrich, G. Dresselhaus, H.J. Zeiger, "Observation of Two-Dimensional Phases Associated with Defect States on the Surface of TiO_2", Physical Review Letters 36 (1976) 1335.

[10]   W.J. Lo, Y.W. Chung, G.A. Somorjai, "Electron spectroscopy studies of the chemisorption of O_2, H_2 and H_2O on the TiO_2(100) surfaces with varied stoichiometry: Evidence for the photogeneration of Ti^{+3} and for its importance in chemisorption",Surface Science 71 (1978) 199.

[11]   H.O. Finklea. Semiconductor Electrodes, Elsevier, Amsterdam, 1988.

[12]   B. O'Regan, M. Gratzel, "A low-cost, high-efficiency solar cell based on dye-sensitized colloidal TiO_2 films",Nature 353 (1991) 737.

[13]   C.N. Satterfield, Heterogeneous Catalysis in Industrial Practice, 2nd ed., McGraw-Hill, New York, 1991.

[14]   J. Biener, J. Wang, R.J. Madix, "Direct observation of the growth of vanadium on $TiO_2(110)$-(1×2)", Surface Science 442 (1999) 47.

[15]   Q. Guo, S. Lee, D.W. Goodman, "Vanadium oxides thin films grown on rutile $TiO_2(110)$-(1×1) and (1×2) surfaces", Surface Science 437 (1999) 38.

[16]   M. Sambi, G. Sangiovanni, G. Granozzi, F. Parmigiani, "Early stages of epitaxial growth of vanadium oxide at the $TiO_2(110)$ surface studied by photoelectron diffraction", Physical Review B 54 (1996) 13464.

[17]   Z. Zhang, V.E. Henrich, " Electronic interactions in the vanadium/$TiO_2(110)$ and vanadia/$TiO_2(110)$ model catalyst systems", Surface Science 277 (1992) 263

[18]   Ando, M., Kobayashi, T., Haruta, M., "Combined effects of small gold particles on the optical gas sensing by transition metal oxide films", Catalysis Today, 1997, 36, 135.

[19]   Z. Huang, P. Maness, D. Blake, E. Wolfrum, "Bactericidal mode of titanium dioxide photocatalysis", Journal of Photochemistry and Photobiology A: Chemistry, 130, 163 (2000)

[20]   A. Mills, H.R. Davies, D. Worsley, "Water purification by semiconductor photocatalysis", Chemical Society Reviews 22 (1993) 417.

[21]   Erkan A., Bakir U., Karakas G., "Photocatalytic microbial inactivation over Pd doped SnO_2 and TiO_2 thin films", Journal of Photochemistry and Photobiology A: Chemistry, 184, 313 (2006)

[22]   Erdural B.K., Yurum A., Bakir U., Karakas G., "Hydrothermal synthesis of nanostructured TiO_2 particles and characterization of their photocatalytic antimicrobial activity", Journal of Nanoscience and Nanotechnology, 8 878 (2008)

[23] Y. Paz, Z. Luo, L. Rabenberg, A. Heller, "Photooxidative self-cleaning transparent titanium dioxide films on glass", Journal of Material Research Society 10 (1995) 2842.

[25] Gu X.-N., Ye M., Wu X.-L., Wei L., Hu Y., Hou X.-G., Liu X.-G., Liu A.-D., "Deposition of silver on titania films by electron beam irradiation", Nuclear Instruments and Methods in Physics Research B, 2006, 247, 279.

[26] Choudhary, T. V., Goodman, D. W., "Catalytically active gold: The role of cluster morphology", Applied Catalysis A: General, 2005, 291, 32.

[27] Idakiev, V., Yuan, Z. Y., Tabakova, T., Su, B. L., "Titanium oxide nanotubes as supports of nano-sized gold catalysts for low temperature water-gas shift reaction", Applied Catalysis A: General, 2005, 281, 149.

[28] Kasuga T., Hiramatsu M., Hoson A., Sekino T., Niihara K., "Formation of Titanium Oxide Nanotube", Langmuir 14, 3160 (1998)

[29] Kasuga T., Hiramatsu M., Hoson A., Sekino T., Niihara K., "Titania Nanotubes Prepared by Chemical Processing", Advanced Materials 11, 1307 (1999)

[30] Du G. H., Chen Q., Che R. C., Yuan Z. Y., Peng L. M., "Preparation and structure analysis of titanium oxide nanotubes", Applied Physics Letters 79, 3702 (2001)

[31] Chen, Q., Zhou, W., Du, G., Peng, L.-M., "Trititanate Nanotubes Made via a Single Alkali Treatment", Advanced Materials, 2002, 14, 1208.

[32] Yoshida, R., Suzuki, Y., Yoshikawa, S., "Effects of synthetic conditions and heat-treatment on the structure of partially ion-exchanged titanate nanotubes", Materials Chemistry and Physics, 2005, 91, 409.

[33] Yu J., Yu H., Cheng B., Zhao X., Zhang Q., "Preparation and photocatalytic activity of mesoporous anatase TiO_2 nanofibers by a hydrothermal method", Journal of Photochemistry and Photobiology A: Chemistry, 182, 121 (2006)

[34] P.V. Kamat, "Photoinduced transformations in semiconductor–metal nanocomposite assemblies", Pure Applied Chemistry 74 (9), 1693 (2002)

[35] Iijima, S., "Helical microtubules of graphitic carbon", Nature, 1991, 354, 56.

[36] Iijima, S, Ichihashi, T., "Single-shell carbon nanotubes of 1-nm diameter", Nature, 1993, 363, 603.

[37] Hamada, N., Sawada, S, Oshiyama, A., "New one-dimensional conductors: Graphitic microtubules", Physical Review Letters, 1992, 68, 1579.

[38] Lau, K. T., Lu, M., Hui, D., "Coiled carbon nanotubes: Synthesis and their potential applications in advanced composite structures", Composites: Part B, 2006, 37, 437.

[39] Du, G. H., Chen, Q., Che, R. C., Yuan, Z. Y., Peng, L. M., "Preparation and structure analysis of titanium oxide nanotubes", Applied Physics Letters, 2001, V 79, N 22, 3702.

[40] Kasuga, T., Hiramatsu, M., Hoson, A., Sekino, T., Niihara, K., "Formation of Titanium Oxide Nanotube", Langmuir, 1998, 14, 3160.

[41] Watanabe M., "The investigation of sodium titanates by the hydrothermal reactions of TiO_2 with NaOH", Journal of Solid State Chemistry 36, 91 (1981)

[42] Tomiha M., Masaki N., Uchida S., Sato T., "Hydrothermal synthesis of alkali titanates from nano size titania powder", Journal of Materials Science 37, 2341 (2002)

[43] Tsai C.-C., Teng H., "Structural Features of Nanotubes Synthesized from NaOH Treatment on TiO_2 with Different Post-Treatments", Chemistry of Materials 18, 367 (2006)

[44] Zhang D., Qi L., "Synthesis of mesoporous titania networks consisting of anatase nanowires by templating of bacterial cellulose membranes", Chemical Communications 21, 2735 (2005)

[45] Yu J., Yu H., Cheng B., Trapalis C., "Effects of calcination temperature on the microstructures and photocatalytic activity of titanate nanotubes", Journal of Molecular Catalysis A: Chemical 249, 135 (2006)

[46] G. Sberveglieri, L.E. Depero, M. Ferroni, V. Guidi, G. Martinelli, P. Nelli,C. Perego, L. Sangaletti, "A novel method for the preparation of nanosized tio$_2$ thin films", Advanced Materials 8 (1996) 334–337.

[47] Okudera H., Yokogawa Y., "Formation of TiO_2 thin films by hydrolysis of Ti–tetraethoxide in ethanol: kinetics, surface morphology, constituent phases and their formation mechanism", Thin Solid Films 401, 124 (2001)

[48] Karthikeyan A., Almeida R. M., "Crystallization of SiO_2–TiO_2 glassy films studied by atomic force microscopy", Journal of Non-Crystalline Solids 274, 169 (2000)

[49] Kemmitt T., Al-Salim N. I., Waterland M., Kennedy V. J., Markwitz A., "Photocatalytic titania coatings", Current Applied Physics 4, 189 (2004)

[50] Ho W., Yu J. C., Yu J., "Photocatalytic TiO_2/Glass Nanoflake Array Films", Langmuir 21, 3486 (2005)

[51] Meilert K. T., Laub D., Kiwi J., "Photocatalytic self-cleaning of modified cotton textiles by TiO_2 clusters attached by chemical spacers", Journal of Molecular Catalysis A: Chemistry 237, 101 (2005)

[52] Habibi M. H., Esfahani M. N., Egerton T. A., "Photochemical Characterization and Photocatalytic Properties of a Nanostructure Composite TiO2 Film", International Journal of Photoenergy 2007, id13653 (2007)

[53] Yuranova T., Rincon A. G., Pulgarin C., Laub D., Xantopoulos N., Mathieu H.-J., Kiwi J., "Performance and characterization of Ag–cotton and Ag/TiO_2 loaded textiles during the abatement of *E. coli*", Journal of Photochemistry & Photobiology A: Chemistry 181, 363 (2006)

[54] Guan K.-S., Yin Y.-S., "Effect of rare earth addition on super-hydrophilic property of TiO_2/SiO_2 composite film", Materials Chemistry & Physics 92, 10 (2005)

[55] Jung K. Y., Park S. B., "Photoactivity of SiO_2/TiO_2 and ZrO_2/TiO_2 mixed oxides prepared by sol–gel method", Materials Letters 58, 2897 (2004)

[56] Cernigoj U., Stangar U. L., Trebse P., Krasovec U. O., Gross S., "Photocatalytically active TiO_2 thin films produced by surfactant-assisted sol–gel processing", Thin Solid Films 495, 327 (2006)

[57] Arai Y., Tanaka K., Khlaifat A. L., "Photocatalysis of SiO_2-loaded TiO_2", Journal of Molecular Catalysis A: Chemical 243, 85 (2006)

[58] Mrowiec-Bialon J., Jarzebski A. B., Kholdeeva O. A., Trukhan N. N., Zaikovski V. I., Kriventsov V. V., Olejniczak Z., "Properties of the sol–gel TiO_2–SiO_2 oxidation catalysts prepared using ethyl silicate 40 as a silica precursor", Applied Catalysis A: General 273, 47 (2004)

[59] Tanaka T., Teramure K., Yamamoto T., Takenaka S., Yoshida S., Takuzo F., "TiO_2/SiO_2 photocatalysts at low levels of loading: preparation, structure and photocatalysis", Journal of Photochemistry & Photobiology A: Chemistry 148, 277 (2002)

[60] Aguado J., van Grieken R., Lopez-Munoz M.-J., Marugan J., "A comprehensive study of the synthesis, characterization and activity of TiO_2 and mixed TiO_2/SiO_2 photocatalysts", Applied Catalysis. A: General 312, 202 (2006)

[61] Nakamura M., Kobayashi M., Kuzuya N., Komatsu T., Mochizuka T., "Hydrophilic property of SiO_2/TiO_2 double layer films", Thin Solid Films 502, 121 (2006)

[62] United States Geological Survey. 2006.

[63] Lin H., Huang C. P., Li W., Ni C., Ismat S. S., Tseng Y.-H., "Size dependency of nanocrystalline TiO_2 on its optical property and photocatalytic reactivity exemplified by 2-chlorophenol", Applied Catalysis B: Environmental 68, 1 (2004)

[64] A. Mills, S. L. Hunte, "An overview of semiconductor photocatalysis", Journal of Photochemistry and Photobiology A: Chemistry, 108:1–35, 1997.

[65] AB Sherrill, JW Medlin, JG Chen, MA Barteau, "NEXAFS investigations of cyclooctatetraene on TiO_2(0 0 1) ", Surface Science, 492(3):203 – 213, 2001.

[66] VS Lusvardi, MA Barteau, JG Chen, J Eng, B Fruhberger, A Teplyakov. "An NEXAFS investigation of the reduction and reoxidation of TiO_2(001)", Surface Science, 397(1-3):237 – 250, 1998.

[67] MA Henderson, WS Epling, CL Perkins, CHF Peden, U Diebold, "Interaction of Molecular Oxygen with the Vacuum-Annealed TiO_2(110) Surface: Molecular and Dissociative Channels", Journal of Physical Chemistry B, 103(25):5328 – 5337, 1999.

[68] Henderson M. A., "The interaction of water with solid surfaces: fundamental aspects revisited", Surface Science Reports 46, 1 (2002)

[69] AB Sherrill, VS Lusvardi, J Eng, JGG Chen, MA Barteau, "NEXAFS investigation of benzaldehyde reductive coupling to form stilbene on reduced surfaces of TiO_2(0 0 1) ", Catalysis Today, 63(1):43 – 51, 2000.

[70] AB Sherrill, MA Barteau, JGG Chen, Abstracts of Papers of The American Chemical Society, 219:U532 – U532, 2000.

[71] MA Henderson, "Acetone and Water on TiO_2(110): H/D Exchange", Langmuir, 21(8):3451 – 3458, 2005.

[72] MA Henderson, "Acetone Chemistry on Oxidized and Reduced TiO2(110)", Journal of Physical Chemistry B, 108(49):18932 – 18941, 2004.

[73] M Calatayud, A Markovits, M Menetrey, B Mguig, C Minot, "Adsorption on perfect and reduced surfaces of metal oxides", Catalysis Today, 85(2-4):125 – 143, 2003.

[74] U Diebold, "Structure and properties of TiO_2 surfaces: a brief review", Applied Physics A-Materials Science and Processing, 76(5):681 – 687, 2003.

[75] MA Henderson, J Szanyi, CHF Peden, "Conversion of N_2O to N_2 on TiO_2(1 1 0)", Catalysis Today, 85(2-4):251 – 266, 2003.

[76] M Bowker, P Stone, R Bennett, N Perkins, "Formic acid adsorption and decomposition on TiO_2(1 1 0) and on Pd/TiO_2(1 1 0) model catalysts", Surface Science, 511(1-3):435 – 448, 2002.

[77] U Diebold, M Li, O Dulub, ELD Hebenstreit, W. Hebenstreit, "The Relationship between Bulk and Surface Properties of Rutile TiO2(110)", Surface Review and Letters, 7(5-6):613 – 617, 2000.

[78] M Li, W Hebenstreit, U Diebold, MA Henderson, DR Jennison, " Oxygen-induced restructuring of rutile TiO2(110) : formation mechanism, atomic models, and inýuence on surface chemistry", Faraday Discussions, (114):245 – 258, 1999.

[79] VS Lusvardi, KG Pierce, MA Barteau, "Steady-State Catalytıc C-C Bond Formatıon on Reduced TiO2 Surfaces", Journal of Vacuum Science and Technology A-Vacuum Surfaces and Films, 15(3):1586 – 1591, 1997.

[80] KG Pierce, MA Barteau, "Cyclotrimerization of sterically hindered alkynes in ultrahigh vacuum: TPD of *tert*-butylacetylene on the reduced TiO_2(001) surface", Surface Science, 326(3):L473 – L476, 1995.

[81] KG Pierce, MA Barteau, "Ketone Coupling on Reduced TiO2 (001) Surfaces: Evidence of Pinacol Formation", Journal of Organic Chemistry, 60(8):2405 – 2410, 1995.

[82] Y Yamaguchi, H Onishi, Y Iwasawa, "Catalytic Decomposition Reaction of Formic Acid on an Ar+-bombarded TiO2(110) Surface: Steady-State Kinetics and Microscopic Structure", Journal of the Chemical Society-Faraday Transactions, 91(11):1663 – 1668, 1995.

[83] H Idriss, MA Barteau, "Characterization of TiO_2 surfaces active for novel organic syntheses", Catalysis Letters, 26(1-2):123 – 139, 1994.

[84] H Idriss, MA Barteau, "Reductive Coupling of Cyclic Ketones on Reduced TiO2(001) single and Polycrystalline TiO2", Studies In Surface Science And Catalysis, 78:463 – 470, 1993.

[85] H Idriss, M Libby, MA Barteau, "Carbon-Carbon bond formation on metal oxides: from single crystal toward catalysis", Catalysis Letters, 15(1-2):13 – 21, 1992.

[86] T Sahm, L Madler, A Gurlo, N Barsan, SE Pratsinis, U Weimar, "Flame spray synthesis of tin dioxide nanoparticles for gas sensing", Sensors and Actuators B-Chemical, 98(2-3):148 – 153, 2004.

[87] JR Mccormick, JR Kitchin, MA Barteau, JG Chen, "A four-point probe correlation of oxygen sensitivity to changes in surface resistivity of TiO_2(0 0 1) and Pd-modified TiO_2(0 0 1)", Surface Science, 545(1-2):L741 – L746, 2003.

[88] S. Semancik, R. E. Cavicchi, "The use of surface and thin film science in the development of advanced gas sensors", Applied Surface Science 70-71, 337–346, 1993.

[89] Jiri Janata, Principles of Chemical Sensors, Plenum Pres, 1989.

[90] W. Gopel, "Solid-state chemical sensors: Atomistic models and research trends", Sensors and Actuators 16, 167–193, 1989.

[91] Rober J. Huber, Jiri Janata, editor, Solid State Chemical Sensors, Academic Press, 1985.

[92] Bragg L., Claringbull G. F., Taylor W. H., Crystal Structures of Minerals, Vol. IV, G. Bell and Sons, London, 1965.

[93]   Jade Database.

[94]   Tonejc M., Djerdj I., Tonejc A, "Evidence from HRTEM image processing, XRD and EDS on nanocrystalline iron-doped titanium oxide powders", Materials Science and Engineering: B, 85, 55 (2001)

[95]   Yang P., Lu C., Hua N., Du Y., "Titanium dioxide nanoparticles co-doped with Fe^{3+} and Eu^{3+} ions for photocatalysis", Materials Letters, 57, 794 (2002)

[96]   Sivakumar S., Sibu C. P., Mukundan P., Pillai P. K., Warrier K. G. K., "Nanoporous titania–alumina mixed oxides—an alkoxide free sol–gel synthesis", Materials Letters, 58, 2664 (2004)

[97]   Su C., Hong B. Y., Tseng C. M., "Sol–gel preparation and photocatalysis of titanium dioxide", Catalysis Today, 96, 119 (2004)

[98]   Wu M., L,n G., Chen D., Wang G., He D., Feng S., Xu R., "Sol-hydrothermal synthesis and hydrothermally structural evolution of nanocrystal titanium dioxide", Chemistry of Materials, 14, 1974 (2002)

[99]   Zhang Q., "Effects of calcination on the photocatalytic properties of nanosized TiO_2 powders prepared by $TiCl_4$ hydrolysis", Applied Catalysis B: Environmental, 26, 207 (2000)

[100]   Shi Y., Zhang X., Li H., "Liquid phase deposition templates synthesis of nanostructures of anatase titania", Materials Science and Enginnering A, 333, 239 (2002)

[101]   Ois N. F., Ginzberg B., "Parameters Involved in the Sol-Gel Transition of Titania in Reverse Micelles", Journal of Sol-Gel Science and Technology, 13, 341 (1998)

[102]   Li B., Wang X., Yan M., Li L., "Preparation and characterization of nano-TiO_2 powder", Material Chemistry and Physics, 78, 184 (2003)

[103]   Sugimoto T., Zhou X. P., Muramatsu A., "Synthesis of Uniform Anatase TiO_2 Nanoparticles by Gel–Sol Method: 1. Solution Chemistry of $Ti(OH)_n^{(4-n)+}$ Complexes", Journal of Colloid and Interface Science, 252, 339 (2002)

[104]   Sugimoto T., Zhou X. P., "Synthesis of Uniform Anatase TiO_2 Nanoparticles by the Gel–Sol Method: 2. Adsorption of OH^- Ions to $Ti(OH)_4$ Gel and TiO_2 Particles", Journal of Colloid and Interface Science, 252, 347 (2002)

[105] Sugimoto T., Zhou X. P., " Synthesis of uniform anatase TiO_2 nanoparticles by gel–sol method: 3. Formation process and size control", Journal of Colloid and Interface Science, 259, 43 (2003)

[106] Sugimoto T., Zhou X. P., Muramatsu A., "Synthesis of uniform anatase TiO_2 nanoparticles by gel–sol method: 4. Shape control", Journal of Colloid and Interface Science, 259, 53 (2003)

[107] Miao L., Tanemura S., Toh S., Kaneko K., Tanemura M., "Heating-sol–gel template process for the growth of TiO_2 nanorods with rutile and anatase structure", Applied Surface Science, 238, 175 (2004)

[108] Uekawa N., Kajiwara J., Kakegawa K., Sasaki Y., "Low Temperature Synthesis and Characterization of Porous Anatase TiO_2 Nanoparticles", Journal of Colloid and Interface Science, 250, 285 (2002)

[109] Al-Salim N. Y., Abagshaw S., Bittar A., Kemmett T., McQuilla A. J., Mills A. M., "Characterisation and activity of sol–gel-prepared TiO_2 photocatalysts modified with Ca, Sr or Ba ion additives", Journal of Materials Chemsitry, 10, 2358 (2000)

[110] Li Y., White T. J., Lim S. H., "Low-temperature synthesis and microstructural control of titania nano-particles", Journal of Solid State Chemistry, 177, 1372 (2004)

[111] Kim C.-S., Moon B. K., Park J.-H., Chung S.-T., Son S.-M., "Synthesis of nanocrystalline TiO_2 in toluene by a solvothermal route", Journal of Crystal Growth, 254, 405 (2003)

[112] Zhang Y. X., Li G. H., Zhang, "Hydrothermal synthesis and photoluminescence of TiO_2 nanowires", Chemical Physics Letters, 365, 300 (2002)

[113] Kolen'ko Y. V., Burukhin A. A., Churagulov B. R., Oleynikov N. N., "Synthesis of nanocrystalline TiO_2 powders from aqueous $TiOSO_4$ solutions under hydrothermal conditions", Materials Letters, 57, 1124 (2003)

[114] Kominami H., Kato J.-I., Murakami S.-Y., "Solvothermal syntheses of semiconductor photocatalysts of ultra-high activities", Catalysis Today, 84, 181 (2003)

[115] Chen, Q., Du, G.H., Zhang, S., Peng, L.-M., "The structure of trititanate nanotubes", Acta Crystallographica Section B, 2002, 58, 587.

[116] Fujishima A., Rao T. N., Tryk D. A., "Titanium dioxide photocatalysis", Journal of Photochemistry and Photobiology C: Photochemistry Reviews, 1, 1 (2000)

[117] Cushing B. L., Kolesnichenko V. L., O'Connor C. J., "Recent advances in the liquid-phase syntheses of inorganic nanoparticles", Chemical Reviews, 104, 3893 (2004)

[118] Tromp R. M., Hannon J. B., "Thermodynamics Of Nucleation And Growth", Surface Review and Letters, 9, 1565 (2002)

[119] Chu R., Yan J., Lian S., Wang Y., Yan F., Chen D., "Shape-controlled synthesis of nanocrystalline titania at low temperature", Solid State Communication, 130, 789 (2004)

[120] Borse P. H., Kankate L. S., Dassenoy F., Vogel W., Urban J., Kulkarni S. K., "Synthesis and investigations of rutile phase nanoparticles of TiO2", Journal of Materials Science, 13, 553 (2002)

[121] Eriksson S., Nylen U., Rojas S., Boutonnet M., "Preparation of catalysts from microemulsions and their applications in heterogeneous catalysis", Applied Catalysis A: General, 265, 207 (2004)

[122] Nakaso K., Fujimoto T., Seto T., Shimada M., Okuyama K., Lunden M. M., "Size Distribution Change of Titania Nano-Particle Agglomerates Generated by Gas Phase Reaction, Agglomeration, and Sintering ", Aerosol Science and Technology, 35, 929 (2001)

[123] Nakaso K., Okuyama K., Shimada M., Pratsinis S. E., "Effect of reaction temperature on CVD-made TiO_2 primary particle diameter", Chemical Engineering Science, 58, 3327 (2003)

[124] Kim C. S., Okuyama K., Nakaso K., Shimada M., "Direct measurement of nucleation and growth modes in titania nanoparticles generation by a CVD method", Journal of Chemical Engineering of Japan, 37, 1379 (2004)

[125] Adachi M., Okuyama K., Fujimoto T., "Film Formation by a New Chemical Vapor Deposition Process Using Ionization of Tetraethylorthosilicate", Japanese Journal of Applied Physics, 34, 1148 (1995)

[126] Van de Krol R., Goossens A., Schoonman J., "Mott-Schottky analysis of nanometer-scale thin-film anatase TiO_2", Journal of Electrochemical Society, 144, 1723 (1997)

[127] Swihart M. T., "Vapor-phase synthesis of nanoparticles", Current Opinion in Colloid and Interface Science, 8, 127 (2003)

[128] Jun Y., Yung Y., Cheon J., "Architectural Control of Magnetic Semiconductor Nanocrystals", Journal of the American Chemical Society, 124, 615 (2002)

[129] Peng A., Peng X. G., "Formation of High-Quality CdTe, CdSe, and CdS Nanocrystals Using CdO as Precursor", Journal of the American Chemical Society, 123, 183 (2001)

[130] Penn R. L., Banfiled J. F., "Oriented attachment and growth, twinning, polytypism, and formation of metastable phases: insights from nanocrystalline TiO_2", American Mineralogist, 83, 1077 (1998)

[131] Dimitrijevic N. M., Rabatic B. M., Rajh T., "Assembly and Charge Transfer in Hybrid TiO_2 Architectures Using Biotin−Avidin as a Connector", Journal of the American Chemical Society, 127, 1344 (2005)

[132] Saponjic Z. V., Tiede D. M., Barnard A. S., "Shaping Nanometer-Scale Architecture Through Surface Chemistry", Advanced Materials 17, 965 (2005)

[133] Chemseddine A., Moritz T., "Nanostructuring Titania: Control over Nanocrystal Structure, Size, Shape, and Organization", European Journal of Inorganic Chemistry, 2, 235 (1999)

[134] Joo J., Kwon S. G., Yu T. Y., Cho M., Lee J., Yoon J., Hyeon T., "Large-scale synthesis of TiO2 nanorods via nonhydrolytic sol-gel ester elimination reaction and their application to photocatalytic inactivation of E. coli", Journal of Physical Chemistry B, 109, 15297 (2005)

[135] Jun Y. W., Casula M. F., Sim J. H., "Surfactant-Assisted Elimination of a High Energy Facet as a Means of Controlling the Shapes of TiO_2 Nanocrystals", Journal of the American Chemical Society, 125, 15981 (2003)

[136] Tian Z. R., Voigt J. A., Liu J., McKenzie B., Xu H. F., "Large Oriented Arrays and Continuous Films of TiO_2-Based Nanotubes", Journal of the American Chemical Society, 125, 12384 (2003)

[137] Hoffmann A. J., Carraway E. R., "Photocatalytic production of H_2O_2 and organic peroxides on quantum-sized semiconductor colloids", Environmental Science and Technology, 28, 776 (1994)

113

[138] Manna L., Scher E. C., Alivisatos A. P., "Shape control of colloidal semiconductor nanocrystals", Journal of Cluster Science, 13, 521 (2002)

[139] Mills A., Morris S., Davies R., "Shape control of colloidal semiconductor nanocrystals", Journal of Photochemistry and Photobiology A: Chemistry, 70, 183 (1993)

[140] Zhu Y. C., Ding C. X., "Oriented growth of nano-TiO_2 whiskers", Nanostructured Materials, 11, 427 (1999)

[141] Li X. H., Liu W. M., L, H. L., "Template synthesis of well-aligned titanium dioxide nanotubes", Applied Physics A: *Materials Science & Processing*, 80, 317 (2005)

[142] Lee J. H., Leu I. C., Hsu M. C., Chung Y.-W., "Fabrication of Aligned TiO_2 One-Dimensional Nanostructured Arrays Using a One-Step Templating Solution Approach", Journal of Physical Chemsitry B: Letters, 109, 13056 (2005)

[143] Wang Y. Q., Hu G. Q., Duan X. F., "Microstructure and formation mechanism of titanium dioxide nanotubes", Chemical Physics Letters, 365, 427 (2002)

[144] Wei M., Konishi Y., Zhou H., "Formation of nanotubes TiO_2 from layered titanate particles by a soft chemical process", Solid State Communications, 133, 493 (2005)

[145] Aminian M. K., Taghavinia N., Iraji-zad A., Mahdavi S. M., "Highly porous TiO_2 nanofibres with a fractal structure", Nanotechnology, 17, 520 (2006)

[146] Zhu H. Y., Lan Y., Gao X. P., Ringer S. P., Zheng Z. F., "Phase Transition between Nanostructures of Titanate and Titanium Dioxides via Simple Wet-Chemical Reactions", Journal of the American Chemical Society, 127, 6730 (2005)

[147] Yin S., Li R., He Q., Sato T., "Low temperature synthesis of nanosize rutile titania crystal in liquid media", Materials Chemistry and Physics, 75, 76 (2002)

[148] Beydoun D., Amal R., Low G., McEvoy S., "Role of Nanoparticles in Photocatalysis", Journal of Nanoparticle Research, 1, 439 (1999)

[149] Burda C., Chen X., Narayanan R., "Chemistry and Properties of Nanocrystals of Different Shapes", Chemistry Reviews, 105, 1025 (2005)

[150] Murray C. B., Kagan C. R., Bawendi M. G., "Synthesis and Characterization of Monodisperse Nanocrystals and Close Packed Nanocrystal Assemblies", Annual Review of Material Science, 30, 545 (2000)

[151] Wang R., Hashimoto K., Fujishima A., Chikuni, M., Kojima E., Kitamura A., Shimohigoshi M., Watanabe T., "Light-induced amphiphilic surfaces", Nature, 388, 431 (1997)

[152] Wang R., Hashimoto K., Fujishima A., Chikuni, M., Kojima E., Kitamura A., Shimohigoshi M., Watanabe T., "Photogeneration of Highly Amphiphilic TiO_2 Surfaces", Advanced Materials, 10, 135 (1998)

[153] Xu X., Zhang J., Song G., "Effect of complexation on the zeta potential of titanium dioxide dispersion", Journal of Dispersion Science and Technology, 24, 527 (2003)

[154] Miyauchi M., Ikezawa A., Hashimoto K., "Zeta Potential and Photocatalytic Activity of Nitrogen Doped TiO2 Thin Films", Physical Chemistry Chemical Physics, 6, 865 (2004)

[155] Molino F., Barthez J. M., Marignan J., "Influence of surfactants on the structure of titanium oxide gels: Experiments and simulations", Physical Review E, 53, 921 (1996)

[156] Sato T., Kohnosu S., "Effect of polyvinylpyrrolidone on the physical properties of titanium dioxide suspensions", Colloids and Surfaces A: Physicochemical and Engineering Aspects, 88, 197 (1994)

[157] Mandzy N., Grulke E., Druffel T., "Breakage of TiO_2 agglomerates in electrostatically stabilized aqueous dispersions", Powder Technology, 160, 121 (2005)

[158] Gumy D., Morais C., Bowen P., "Catalytic activity of commercial of TiO_2 powders for the abatement of the bacteria (*E. coli*) under solar simulated light: Influence of the isoelectric point", Applied Catalysis B: Environmental, 63, 76 (2006)

[159] Palarcik J., Jandera J., Svoboda L., CHISA 2004-16th International Congress of Chemical and Process Engineeriing, 2004, 8133

[160] Lebrette S., Pagnoux C., "Stability of aqueous TiO_2 suspensions: influence of ethanol", Journal of Colloid and Interface Science, 280, 400 (2004)

[161] Tryk D. A., Fujishima A., Honda K., "Recent topics in photoelectrochemistry: achievements and future prospects", Electrochimica Acta, 45, 2363 (2000)

[162] Carp O., Huisman C. L., Reller A., "Photoinduced reactivity of titanium dioxide", Progress in Solid State Chemistry, 32 (1-2), pages 33-177 (2004)

[163] Hoffmann M. R., Martin S. T., Choi W., Bahnemann D. W., "Environmental Applications of Semiconductor Photocatalysis", Chemical Reviews, 95, 69 (1995)

[164] Fox M. A., Dulay M. T., "Heterogeneous photocatalysis", Chemical Review, 93, 341 (1993)

[165] Mao Y., Schoneich C., Asmus K. D., "Identification of organic acids and other intermediates in oxidative degradation of chlorinated ethanes on titania surfaces en route to mineralization: a combined photocatalytic and radiation chemical study", Journal of Physical Chemistry, 95, 80 (1991)

[166] Stanford U., Gray K. A., Kamat P. V., "An in situ diffuse reflectance FTIR investigation of photocatalytic degradation of 4-chlorophenol on a TiO_2 powder surface", Chemical Physics Letters, 205-1, pages 55-61 (1993)

[167] Vorontsov A. V., Kurkin E. N., Savinon E. N., "Study of TiO_2 Deactivation during Gaseous Acetone Photocatalytic Oxidation", Journal of Catalysis, 186, 318 (1999)

[168] Kim S. B., Hong S. C., "Kinetic study for photocatalytic degradation of volatile organic compounds in air using thin film TiO_2 photocatalyst", Applied Catalysis B: Environmental, 35-4, pages 305-315 (2002)

[169] Li Y., Li X., Li J., Yin J., "Photocatalytic degradation of methyl orange by TiO_2-coated activated carbon and kinetic study", Water Research, 40, 1119 (2006)

[170] Serrano B., de Lasa H., "Photocatalytic Degradation of Water Organic Pollutants. Kinetic Modeling and Energy Efficiency", Industrial and Engineering Chemistry Research, 36 (11), pages 4705-4711 (1997)

[171] Priya M. H., Madras G., "Kinetics of Photocatalytic Degradation of Chlorophenol, Nitrophenol, and Their Mixtures", Industrial and Engineering Chemistry Research, 45, 482 (2006)

[172] Priya M. H., Madras G., "Kinetics of photocatalytic degradation of phenols with multiple substituent groups", Journal of Photochemistry and Photobiology A: Chemistry, 179, 256 (2006)

[173] Herrmann J.-M., "Heterogeneous photocatalysis: fundamentals and applications to the removal of various types of aqueous pollutants", Catalysis Today, 53, 115 (1999)

[174] Chen D., Ray A. K., "Photocatalytic kinetics of phenol and its derivatives over UV irradiated TiO_2", Applied Catalysis B: Environmental, 23, 143 (1999)

[175] Braun A. M., Oliveros E., "How to evaluate photochemical methods for water treatment", Water Science and Technology, 35-4, pages 17-23 (1997)

[176] Ohno T., Masaki Y., Hirayama S., Matsumura M., "TiO_2-Photocatalyzed Epoxidation of 1-Decene by H_2O_2 under Visible Light", Journal of Catalysis, 204, 163 (2001)

[177] Meada H., Miyamoto H. Mizuno K., "Synthesis of 3,3,6,6-Tetraaryl-1,2-Dioxanes via TiO_2-catalyzed Photooxygenation of 1,1-Diarylethenes in the Presence of $Mg(ClO_4)_2$", Chemistry Letters, 33-4, pages 462-463 (2004)

[178] Mohamed O. S., El-Aal A., Gaber M., Abdel-Wahab A. A., "Photocatalytic oxidation of selected aryl alcohols in acetonitrile", Journal of Photochemistry and Photobiology A: Chemistry, 148, 205 (2002)

[179] Wang R., Hashimoto K., Fujishima A., Chikuni M., Kojima E., Kitamura A., "Photogeneration of Highly Amphiphilic TiO_2 Surfaces ", Advanced Materials, 10, 135 (1998)

[180] Chatterjee D., Dasgupta S., Journal of Photochemistry and Photobiology C: Photochemistry Review, 6, 186 (2005)

[181] Shchukin D. G., Sviridov D. V., "Photocatalytic processes in spatially confined micro- and nanoreactors", Journal of Photochemistry and Photobiology C: Photochemistry Review, 7-1, pages 23-39 (2006)

[182] Shephard G. S., Stockenstrom S., de Villiers D., Engelbrecht W. J., Sydenham E. W., Wessels G. F. S., "Degradation of microcystin toxins in a falling film photocatalytic reactor with immobilized titanium dioxide catalyst", Water Research, 36, 140 (2002)

[183] Sonawane R. S., Hegde S. G., Dongare M. K., "Preparation of titanium(IV) oxide thin film photocatalyst by sol–gel dip coating", Materials Chemistry and Physics, 77, 744 (2002)

[184] Sunada K., Watanabe T., Hashimoto K., "Studies on photokilling of bacteria on TiO_2 thin film", Journal of Photochemistry and Photobiology A: Chemistry, 156, 227 (2003)

[185] Shioya Y., Ikeue K., Ogawa M., Anpo M., "Synthesis of transparent Ti-containing mesoporous silica thin film materials and their unique photocatalytic activity for the reduction of CO_2 with H_2O", Applied Catalysis A: General, 254, 251 (2003)

[186] Manna L., Scher E., Alivisatos A. P., "Synthesis of Soluble and Processable Rod-, Arrow-, Teardrop-, and Tetrapod-Shaped CdSe Nanocrystals", Journal of the American Chemical Society, 122, 12700 (2000)

[187] Milliron D. J., Hughes S. M., Cui Y., Manna L., Li J., Wang L.-W., Alivisatos A. P., "Colloidal nanocrystal heterostructures with linear and branched topology", Nature, 430, 190 (2004)

[188] Mills A., Elliott N., Parkin I. P., O'Neill S. A., Clark R. J., "Novel TiO_2 CVD films for semiconductor photocatalysis", Journal of Photochemistry and Photobiology A: Chemistry, 151(1-3), pages 171-179 (2002)

[189] Mills A., Wang J., "Simultaneous monitoring of the destruction of stearic acid and generation of carbon dioxide by self-cleaning semiconductor photocatalytic films", Journal of Photochemistry and Photobiology A: Chemistry, 182, 181 (2006)

[190] Arana J., Rendon E. T, Rodriguez J. M. D., "High concentrated phenol and 1,2-propylene glycol water solutions treatment by photocatalysis: Catalyst recovery and re-use", Applied Catalysis B: Environmental, 30, 1 (2001)

[191] Scotti R., D'Arienzo M., Testino A., Morazzoni F., "Photocatalytic mineralization of phenol catalyzed by pure and mixed phase hydrothermal titanium dioxide", Applied Catalysis B: Environmental, article in press (2008)

[192] Tasai S., Cheng S., "Effect of TiO_2 crystalline structure in photocatalytic degradation of phenolic contaminants", Catalysis Today, 33, 227 (1997)

[193] Parra S., Olivero J., Pacheco L., Pulgarin C., "Structural properties and photoreactivity relationships of substituted phenols in TiO_2 suspensions", Applied Catalysis B: Environment, 43, 293 (2003)

[194] Mills A., Wang J., "Photobleaching of methylene blue sensitised by TiO_2: an ambiguous system?", Journal of Photochemistry and Photobiology A: Chemistry, 127, 123 (1999)

[195] Neppolian B., Choi H. C., Sakthivel S., "Solar/UV-induced photocatalytic degradation of three commercial textile dyes", Journal of Hazardous Materials B, 89, 303 (2002)

[196] Auguliaro V., Baiocchi C., Prevot A. B., "Azo-dyes photocatalytic degradation in aqueous suspension of TiO_2 under solar irradiation", Chemosphere, 49, 1223 (2002)

[197] Vohra M. S., Davis A. P., "TiO_2-Assisted photocatalysis of lead–EDTA", Water Research, 34, 952 (2000)

[198] Zhang R., Gao L., "Photodegradation of surfactants on the nanosized TiO_2 prepared by hydrolysis of the alkoxide titanium", Chemosphere, 54, 405 (2004)

[199] Bems B., Jentoft F. C., Schlogl R., "Photoinduced decomposition of nitrate in drinking water in the presence of titania and humic acids", Applied Catalysis B: Environmental, 20, 155 (1999)

[200] Kataoka S., Lee E., Tejedor M. I., Anderson M. A., "Photocatalytic degradation of hydrogen sulfide and in situ FT-IR analysis of reaction products on surface of TiO_2", Applied Catalysis B: Environmental, 61, 159 (2005)

[201] Furuzono T., Iwasaki M., Yasuda S., Korematsu A., Yoshioka T., Ito S., "Photoreactivity and cell adhesiveness of amino-group-modified titanium dioxide nano-particles on silicone substrate coated by covalent linkage ", Journal of Materials Science Letters, 22, 1737 (2003)

[202] Stevenson M., Bullock K., Lin W. Y., Rajeshwar K., "Sonolytic enhancement of the bactericidal activity of irradiated titanium dioxide suspensions in water", Research on Chemical Intermediates, 23, 311 (1997)

[203] Nakajima A., Koizumi S. I., Watanabe T., Hashimoto K., "Effect of repeated photo-illumination on the wettability conversion of titanium dioxide", Journal of Photochemistry and Photobiology A: Chemistry, 146, 129 (2001)

[204] Yu J. G., Zhao X. J., "Effect of surface microstructure on the super-hydrophilic property of the sol-gel derived porous TiO2 thin films", Journal of Materials Science Letters, 20 (7), pages 671-673 (2001)

[205] Nakajima A., Fujishima A., Hashimoto K., Watanabe T., "Preparation of Transparent Superhydrophobic Boehmite and Silica Films by Sublimation of Aluminum Acetylacetonate", Advanced Materials, 11, 1365 (1999)

[206] Abe R. Sayama K., Domen K., "A new type of water splitting system composed of two different TiO_2 photocatalysts (anatase, rutile) and a IO_3^-/I^- shuttle redox mediator", Chemical Physics Letters, 344, 339 (2001)

[207] Khalil L. B., Rophael M. W., Mourad W. E., "The removal of the toxic Hg(II) salts from water by photocatalysis", Applied Catalysis B: Environmental, 36, 125 (2002)

[208] Mills A., Lee S.-K., Lepre A., "Photodecomposition of ozone sensitised by a film of titanium dioxide on glass", Journal of Photochemistry and Photobiology A: Chemistry, 155, 199 (2003)

[209] M Lan Y., Gao X., Zhu H., Zheng Z., Yan T., Wu F., Ringer S. P., Song D., "Titanate Nanotubes and Nanorods Prepared from Rutile Powder", Advanced Functional Materials 15, 1310 (2005)

[210] Endo M., Takeuchi K., Tajiri T., Park K. C., Wang F., Kim Y.-A., Hayashi T., Terrones M., Dresselhaus M. S., "Sodium chloride-catalyzed oxidation of multi-wall carbon nanotubes for environmental benefit", Journal of Physical Chemistry B 110, 12017 (2006)

[211] Serp P., Corrias M., Kalck P., "Carbon nanotubes and nanofibers in catalysis", Applied Catalysis A 253, 337 (2003)

[212] Wang W., Serp P., Kalck P., Silva C. G., Faria J. L., "Preparation and characterization of nanostructured $MWCNT-TiO_2$ composite materials for photocatalytic water treatment applications", Materials Research Bulletin 43, 958 (2008)

[213] Li X. H., Niu J. L., Zhang H. L., Li H. L., Liu Z. F., "Labeling the defects of single-walled carbon nanotubes using titanium dioxide nanoparticles", Journal of Physical Chemistry B 107 (11   ), pages 2453-2458 (2003)

[214] Lo A. Y. H., Schurko R. W. , Vettraino M., Skadtchenko B. O., Trudeau M., Antonelli D. M., "olid-State ^{23}Na and ^{7}Li NMR Investigations of Sodium- and Lithium-Reduced Mesoporous Titanium Oxides", Inorganic Chemistry 45, 1828 (2006)

[215] Zhang M., Jin Z., Zhang J., Guo X., Yang J., Li W., Wang X., Zhang Z., "Effect of annealing temperature on morphology, structure and photocatalytic behavior of nanotubed $H_2Ti_2O_4(OH)_2$", Journal of Molecular Catalysis A: Chemical 217, 203 (2004)

[216] Rincón A, Rincón G., Pulgarin C., "Use of coaxial photocatalytic reactor (CAPHORE) in the TiO_2 photo-assisted treatment of mixed *E. coli* and *Bacillus* sp. and bacterial community present in wastewater", Catalysis Today 101, 331 (2005)

[217] Penn R. L., Banfield J. F., "Morphology development and crystal growth in nanocrystalline aggregates under hydrothermal conditions: insights from titania", Geochemica et Cocmochimica Acta 63 (10), pages 1549-1557 (1999)

[218] Cho C. H., Han M. H., Kim D. H., Kim D. K., "Morphology evolution of anatase TiO_2 nanocrystals under a hydrothermal condition (pH = 9.5) and their ultra-high photo-catalytic activity", Materials Chemistry & Physics 92, 104 (2005)

[219] Lachheb H., Puzenat E., Houas A., Ksibi M., Elaloui E., Guillard C., Herrmann J.-M., "Photocatalytic degradation of various types of dyes (Alizarin S, Crocein Orange G, Methyl Red, Congo Red, Methylene Blue) in water by UV-irradiated titania", Applied Catalysis B: Environmental 39, 75 (2002)

[220] 27. Yu J., Su Y., Cheng B., Zhou M., "Effects of pH on the microstructures and photocatalytic activity of mesoporous nanocrystalline titania powders prepared via hydrothermal method", Journal of Molecular Catalysis A: Chemical 258 (1-2), pages 104-112 (2006)

[221] Wang W., Serp P., Kalck P., Faria J. L., "Visible light photodegradation of phenol on MWNT-TiO_2 composite catalysts prepared by a modified sol–gel method", Journal of Molecular Catalysis A: Chemical 235, 194 (2005)

[222] Wang W., Serp P., Kalck P., Faria J. L., "Photocatalytic degradation of phenol on MWNT and titania composite catalysts prepared by a modified sol–gel method", Applied Catalysis B: Environmental 56, 305 (2005)

[223] Brinker C. J., Scherer G. W., "Sol-Gel Science: The Physics and Chemistry of Sol-Gel Processing", Academic Press, 1990.

[224] Fua Y., Jina Z., Nia Y., Dub H., Wang T., "Microstructure, optical and optoelectrical properties of mesoporous nc-TiO2 films by hydrolysis-limited sol–gel process with different inhibitors", Thin Solid Films 57 (119), 6534 (2009)

[225] Nandiyantoa A. B. D., Iskandara F., Okuya K., "Macroporous anatase titania particle: Aerosol self-assembly fabrication with photocatalytic performance", Chemical Engineering Journal, article in press

[226] N. Alexakia, T. Stergiopoulosa, A.G. Kontosa, D.S. Tsouklerisa, A.P. Katsoulidisb, P.J. Pomonisb, D.J. LeClerec, P. Skeldonc, G.E. Thompsonc, P. Falaras, "Mesoporous titania nanocrystals prepared using hexadecylamine surfactant template:Crystallization progress monitoring, morphological characterization and application in dye-sensitized solar cells", Microporous and Mesoporous Materials, article in press

[227] Dongliang H., Xiangju M., Yanchun T., Lin Z., Fengshou X., "Synthesis of Carbon-Doped TiO_2 Using Porous Resin and Its Excellent Photocatalytic Properties", Chinese Journal Of Catalysis, (2009) 30 (2), 83.

[228] Jitianu A., Cacciaguerra T., Benoit S., Delpeux S., Be´guin F., Bonnamy S., "Synthesis and characterization of carbon nanotubes-TiO2 nanocomposites", Carbon 42, (2004), 1147

[229] Kar P., Raja K. S., Misra M., Agasanapur B. N., "Formation and stability of anatase phase of phosphate incorporated and carbon doped titania nanotubes", Materials Research Bulletin 44, (2009) 398.

[230] Gao B., Chen G. Z., Puma G. L., "Carbon nanotubes/titanium dioxide (CNTs/TiO_2) nanocomposites prepared by conventional and novel surfactant wrapping sol–gel methods exhibiting enhanced photocatalytic activity", Applied Catalysis B: Environmental 89, (2009), 503.

[231] Zhu J., Xiea J., Lüa X., Jianga D., "Synthesis and characterization of superhydrophobic silica and silica/titania aerogels by sol–gel method at ambient pressure", Colloids and Surfaces A: Physicochem. Eng. Aspects 342, (2009), 97.

[232] K. Guan, "Relationship between photocatalytic activity, hydrophilicity and self-cleaning effect of TiO_2/SiO_2 films", Surf. Coat. Technol. 191, (2005), 155.

[233] Mo J., Zhang Y., Xu Q., Yang R., "Effect of TiO_2/adsorbent hybrid photocatalysts for toluene decomposition in gas phase", Journal of Hazardous Materials 168, (2009), 276.

[234] Bennania J., Dillert R., Gesing T. M., Bahnemanna D., "Physical properties, stability, and photocatalytic activity of transparent TiO2/SiO2 films", Separation and Purification Technology 67, (2009), 173.

[235] Cho J., Schaab S., Roether J. A., Boccaccini A. R., "Nanostructured carbon nanotube/TiO2 composite coatings using electrophoretic deposition (EPD)", J Nanopart Res 10, (2008), 99.

[236] Yao Y., Li G., Ciston S., Lueptow R. M., Gray K. A., "Photoreactive TiO2/Carbon Nanotube Composites: Synthesis and Reactivity", Environ. Sci. Technol. 42, (2008), 4952.

[237] Vargas M., Rincon M. E., Ramos E., "Formation and Characterization of TiO2∕CNT Nanomaterials Dried under Supergravity Conditions", Journal of Nanomaterials V. 2009, Article ID 879016.

[238] Lee S.-W., Sigmund W. M., "Formation of anatase TiO_2 nanoparticles on carbon nanotubes", Chemical communications 6, (2003), 780.

[239] N. Wetchakun, S. Phanichphant, "Effect of temperature on the degree of anatase–rutile transformation in titanium dioxide nanoparticles synthesized by the modified sol–gel method", Current Applied Physics, Volume 8, Issues 3-4, (2008), 343.

[240] H.L. Zhuang, G.P. Zheng , A.K. Soh, "Interactions between transition metals and defective carbon nanotubes", Computational Materials Science, Volume 43, Issue 4, (2008), 823.

[241] C.S. Turchi, D.F. Ollis, "Photocatalytic degradation of organic water contaminants: mechanisms involving hydroxyl radical attack", Journal of Catalysis, 122(1), (1990), 178.

[242] A.V. Emeline, V. Ryabchuk, N. Serpone, "Factors affecting the efficiency of a photocatalyzed process in aqueous metal-oxide dispersions - prospect of distinguishing between two kinetic models", Journal of Photochemistyry and Photobiology: A Chemistry, 133(1–2), (2000) 89.

[243] A. Mills, J. Wang, D. F. Ollis, "Kinetics of Liquid Phase Semiconductor Photoassisted Reactions: Supporting Observations for a Pseudo-Steady-State Model", Journal of Physical Chemistry B, 110, (2006), 14386.

APPENDIX A

XRD RESOURCES

Table A-1 XRD data for Rutile

d (Å)	Intensity (%)	hkl
3.217	100	110
2.487	50	101
2.297	8	200
2.188	25	111
2.054	10	210
1.6874	60	211
1.6237	20	220
1.4797	10	002
1.4528	10	310
1.4243	2	221
1.3598	20	301
1.3465	12	112
1.3041	2	311
1.2441	4	202
1.2006	2	212
1.1702	6	321
1.1483	4	400
1.1143	2	410
1.0936	8	222
1.0827	4	330
1.0425	6	411
1.0364	6	312
1.0271	4	420
0.9703	2	421
0.9644	2	?03
0.9438	2	113
0.9072	4	402
0.9009	4	510
0.8892	8	213
0.8774	8	431
0.8738	8	332
0.8437	6	422
0,.8292	8	303
0.8196	12	521
0.8120	2	440
0.7877	2	530
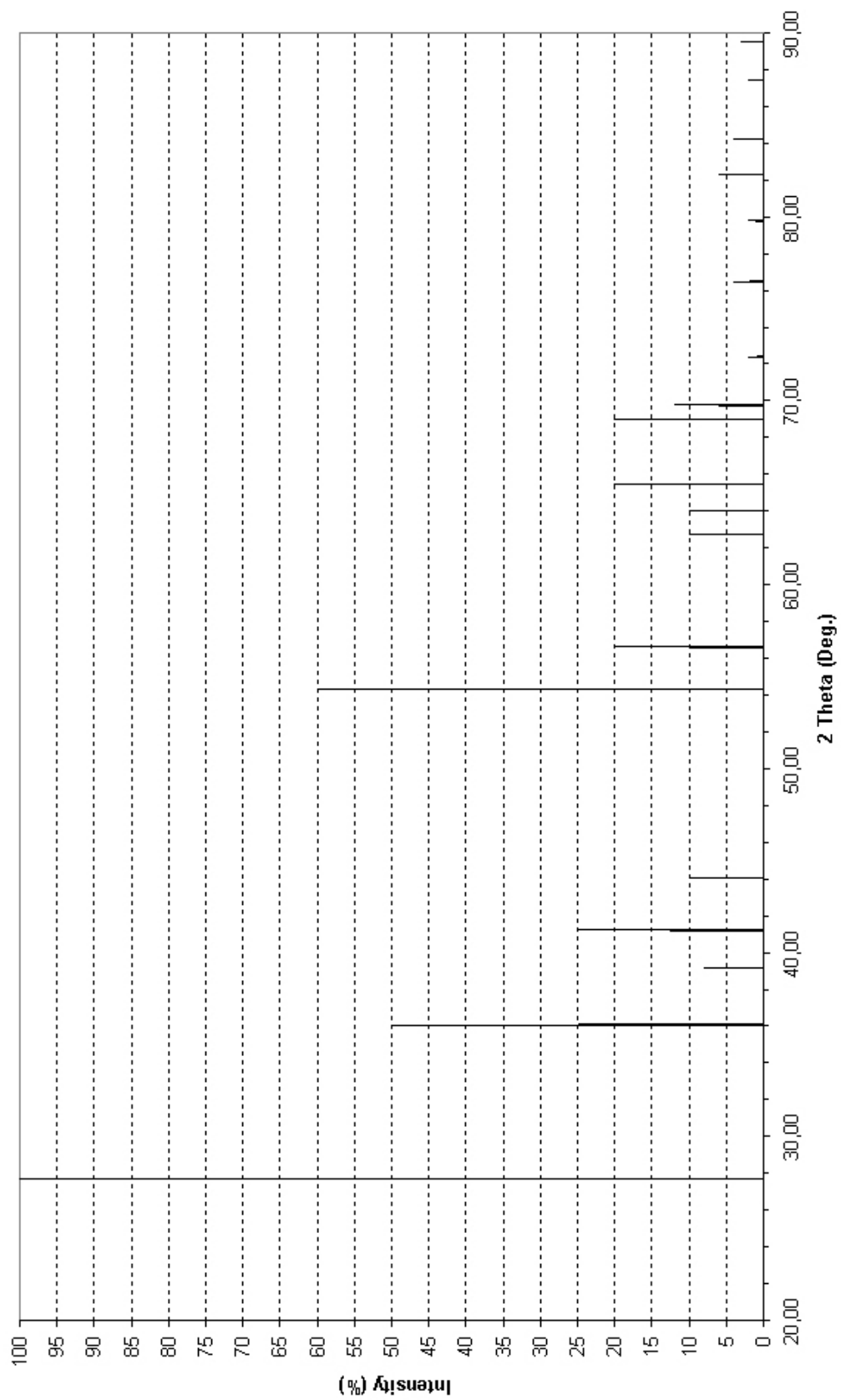
Figure A-1 XRD graph of pure Rutile with copper source

125

Table A-2 XRD data for Anatase

d (Å)	Intensity (%)	hkl
3.52	100	101
2.431	10	103
2.378	20	004
2.332	10	112
1.892	35	200
1.6999	20	105
1,6665	20	211
1.493	4	213
1.4808	14	204
1.3641	6	116
1.3378	6	220
1.2795	<2	107
1.2649	10	215
1.2509	4	301
1.1894	<2	008
1.1725	2	303
1.1664	6	224
1.1608	4	312
1.06	2	217
1.0517	4	305
1.0436	4	321
1.0182	2	109
1.007	2	208
0.9967	2	323
0.9555	4	316
0.9464	4	400
0.9246	<2	307
0.9192	2	325
0.9138	2	411
0.8966	4	219
0.889	2	228
0.8819	<2	413
0.8793	2	404
0.8464	2	420
0.8308	<2	327
0.8268	4	415
0.8102	2	309
0.7974	4	424
0.7928	2	00$\underline{12}$
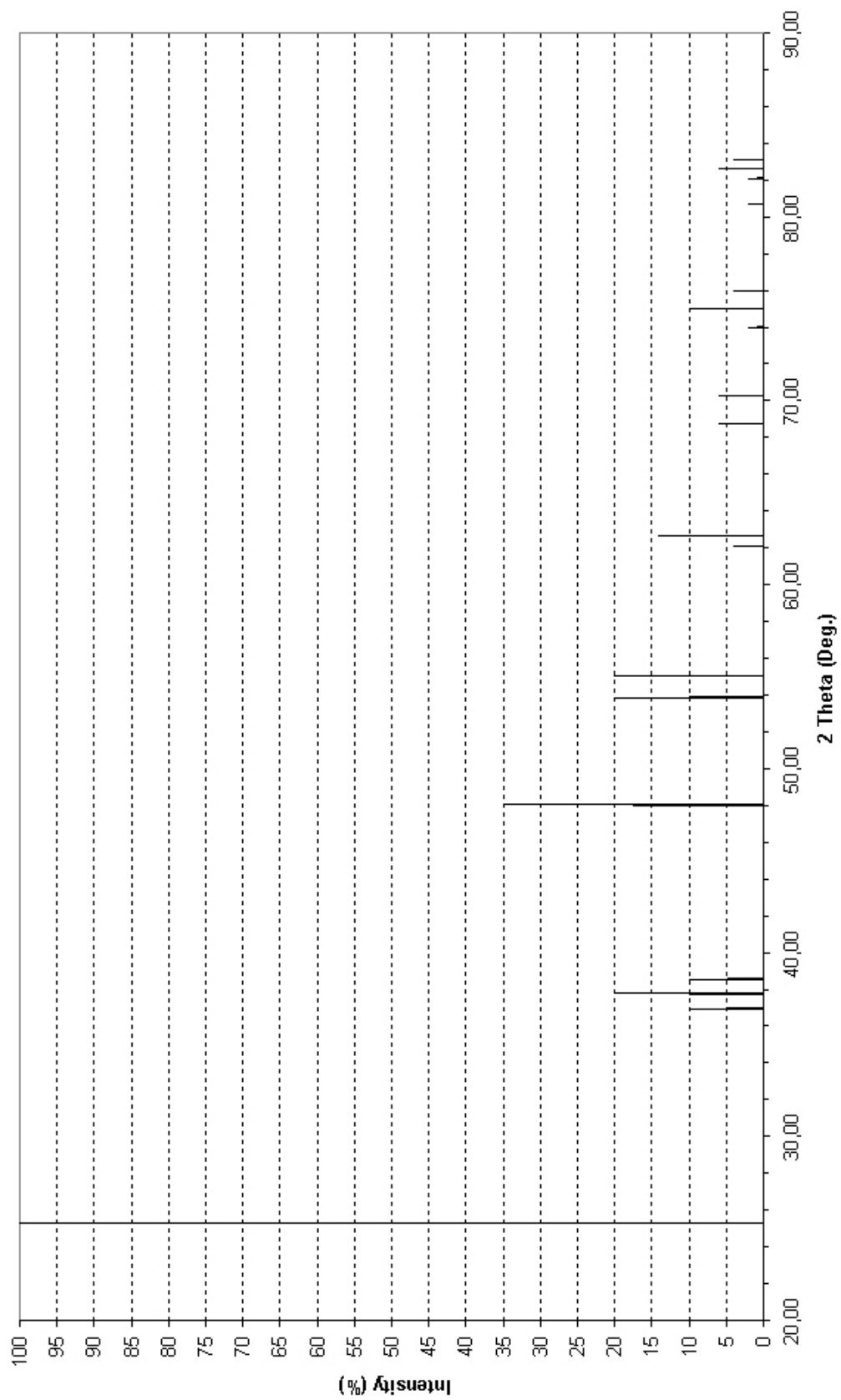
Figure A-2 XRD graph of pure Anatase with copper source

Table A-3 XRD data for Brookite

d (Å)	Intensity (%)	hkl
3.512	100	120
3.465	80	111
2.900	90	121
2.729	4	200
2.476	25	012
2.409	18	201
2.370	6	131
2.344	4	220
2.332	4	211
2.296	5	040
2.254	8	112
2.244	18	022
2.133	16	221
1.9685	16	032
1.8934	30	231
1.8514	18	132
1.8332	3	212
1.7568	3	240
1.6908	20	320
1.6617	30	241
1.6486	5	151
1.6098	13	113
1.5968	2	232
1.5408	7	123
1.4942	10	052
1.4729	4	160
1.4656	9	312
1.4609	12	251
1.4515	12	203
1.4415	6	133
1.4336	10	213
1.4167	9	161
1.364	5	400
1.3358	8	332
1.3186	3	401
1.3116	2	233
1.2852	2	004
1.2381	10	024
1.2107	2	431
1.2074	1	124
1.1552	4	333
1.1480	2	080
1.1432	2	441
1.1217	4	044
1.0399	3	521, 423
1.0366	2	281
1.0237	4	324
0.9873	2	125
0.9829	4	372, 254
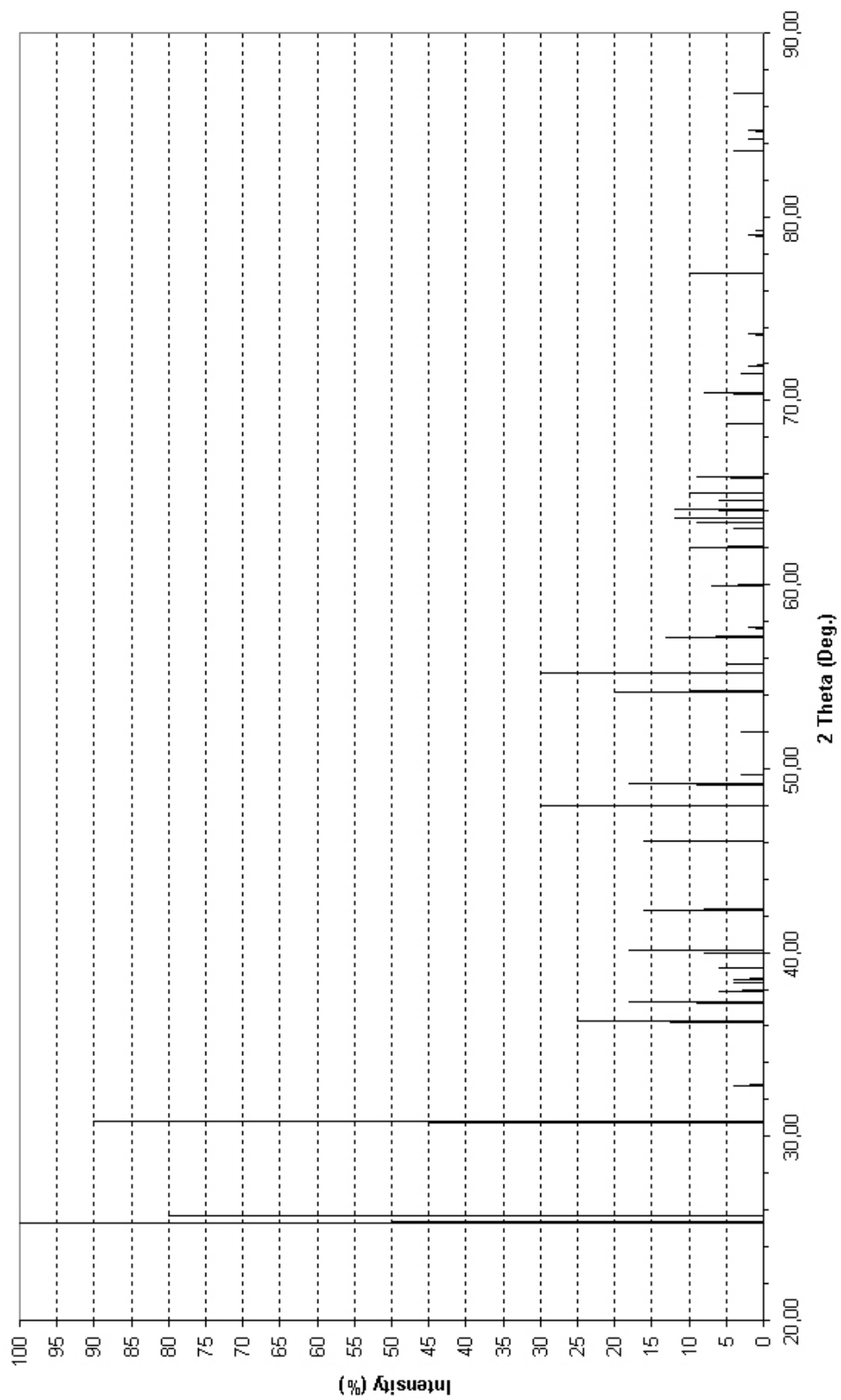
Figure A-3 XRD graph of pure Brookite with copper source

129

APPENDIX B

PHP CODE FOR XRD DATA'S NOISE REDUCTION FOR PEAK ANALYSIS

The following PHP code, smoothes the XRD data by averaging pre-defined amount of data.

```
<?
header("Expires: Mon, 5 Jul 1980 05:00:00 GMT");
header("Cache-Control: no-cache, must-revalidate");
header("Pragma: no-cache");
ini_set("memory_limit","32M");

$count_theta=0;
$count_inten=0;
$step_theta=0;
$step_inten=0;
$theta=0;
$inten=0;
$char_theta="";
$char_inten="";

$okunmus=file("raw_xrd.txt");
$kadar=count($okunmus);

for($i=0;$i<$kadar;$i++)
{
$icerik=$okunmus[$i];
$uzun=strlen($icerik);

for($j=0;$j<$uzun;$j++)
{
if($icerik[$j]=="\t")
```

```php
        {
         $a=$j+1;
         $j=$uzun;
         $count_theta++;
         $theta_array[$count_theta]=$char_theta;
         $char_theta="";
         $theta=$theta+$theta_array[$count_theta];
         $step_theta++;
        }
        else
        {
         $char_theta=$char_theta.$icerik[$j];
        }
}

for($j=$a;$j<$uzun;$j++)
{
        $char_inten=$char_inten.$icerik[$j];
}

$count_inten++;
$inten_array[$count_inten]=$char_inten;
$char_inten="";
$inten=$inten+$inten_array[$count_inten];
$step_inten++;

if($step_theta==10)
{
 $ave=$theta/10;
 echo $ave."-";
 $theta=0;
 $step_theta=0;
 $hede=fopen("reduced.txt","a+");
 fwrite($hede,$ave."\t");
}

if($step_inten==10)
{
 $ave=$inten/10;
 echo $ave."<br>";
```

```php
  $inten=0;
  $step_inten=0;
  $hede=fopen("reduced.txt","a+");
  fwrite($hede,$ave."\n");
}
}
?>
```

APPENDIX C

SAMPLE CALCULATIONS

C.1 Calculation of Crystallite Size

The crystallite size was calculated by using the Scherrer Method. The crystallite size for a specific peak pr reflection can be calculated by the equation below <C.1-1>:

$$t = \frac{K\lambda}{B\cos\theta_B}$$ <C.1-1>

where, K is Scherrer constant, λ is the wavelength of radiation ($\lambda_{Cu,K\alpha}$ = 0.154 nm) and B is the integral breadth of peak (in radians 2θ) located at angle θ_B. The crystallite size of anatase, synthesized with sol-gel method, was calculated from the (101) plane (2Θ=25.27°).

For TiO_2 synthesized with sol-gel method,

$$B = 0.42° = 0.42° * \frac{2\Pi}{360°} = 0,0073 rad$$

$$t = \frac{0,9 * 0,154}{0.0073 * \cos(25.27/2)} = 19,5 nm$$

For TiO_2 synthesized with CNT and calcined at 570 °C,

$$B = 0.57° = 0.57° * \frac{2\Pi}{360°} = 0,0100 rad$$

$$t = \frac{0,9 * 0,154}{0.0100 * \cos(25.27/2)} = 14.1 nm$$

For TiO$_2$ synthesized with CNT and calcined at 500 °C,

$$B = 0.95° = 0.95° * \frac{2\Pi}{360°} = 0,0166 rad$$

$$t = \frac{0,9 * 0,154}{0.0166 * \cos(25.27/2)} = 8.6 nm$$

For TiO$_2$ synthesized with CNT and calcined at 400 °C,

$$B = 1.14° = 1.14° * \frac{2\Pi}{360°} = 0,0200 rad$$

$$t = \frac{0,9 * 0,154}{0.0200 * \cos(25.27/2)} = 7.1 nm$$

For TiO$_2$ synthesized with CNT and heat treated at 400 °C with N$_2$,

$$B = 1.56° = 1.56° * \frac{2\Pi}{360°} = 0,0272 rad$$

$$t = \frac{0,9 * 0,154}{0.0272 * \cos(25.27/2)} = 5.2 nm$$

APPENDIX D

LIGHT SPECTRUM OF THE UV SIMULATOR
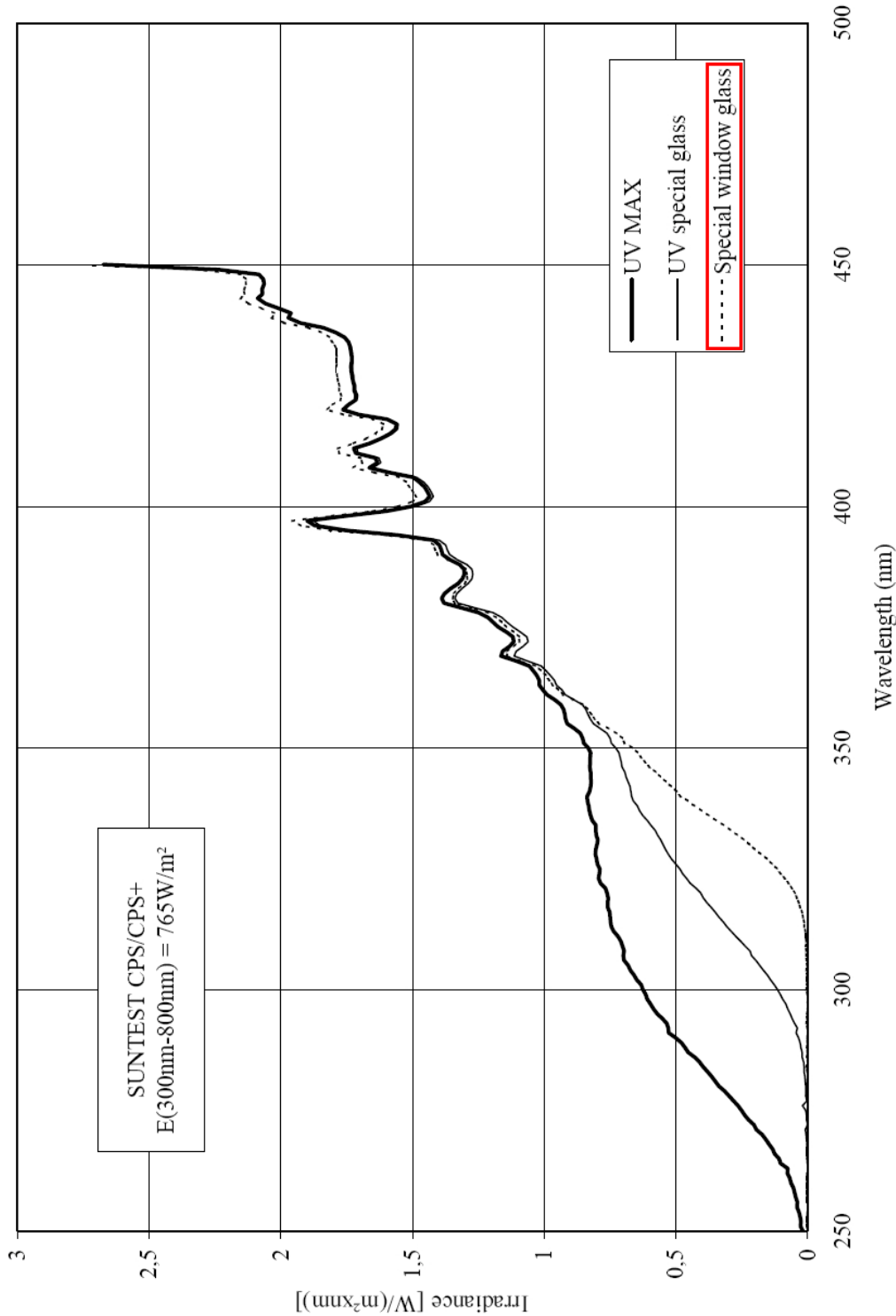
Figure D-1 Light spectrum of the UV simulator

APPENDIX E

UV ABSORBANCE DATA OF CNT SERIES SAMPLES

Table E-1 UV absorbance data of TiO_2 calcined @ 600 ºC

MB, TiO_2 (1 g TiO_2/L) calcined @ 600 ºC, PP beaker, Quartz cap, UV absorbance @ 665 nm			
Time (hr)	Absorbance	Multiplier	Concentration (ppm)
Blank	0,0001	0,000	0,00
0	0,4017	1,000	2,00
0,5	0,3204	0,797	1,59
1	0,2241	0,557	1,11
2	0,1150	0,286	0,57
3	0,0595	0,147	0,29
4	0,0266	0,066	0,13

Table E-2 UV absorbance data of TiO_2 calcined @ 400 ºC

MB, TiO_2 (1 g TiO_2/L) calcined @ 400 ºC, PP beaker, Quartz cap, UV absorbance @ 665 nm			
Time (hr)	Absorbance	Multiplier	Concentration (ppm)
Blank	0,0003	0,000	0,00
0	0,2716	1,000	2,00
0,55	0,1895	0,697	1,39
1	0,1172	0,430	0,86
2	0,0568	0,208	0,42
3	0,0202	0,073	0,15
4	0,0115	0,041	0,08

Table E-3 UV absorbance data of CNT-TiO$_2$ heat treated with N$_2$ @ 400 ºC

MB, CNT-TiO$_2$ (1 g TiO$_2$/L) heat treated with N$_2$ @ 400 ºC, PP beaker, Quartz cap, UV absorbance @ 665 nm			
Time (hr)	Absorbance	Multiplier	Concentration (ppm)
Blank	-0,0001	0,000	0,00
0	0,2211	1,000	2,00
0,5	0,1082	0,490	0,98
1	0,0628	0,284	0,57
2,5	0,0099	0,045	0,09
3,25	0,0057	0,026	0,05
4	0,0046	0,021	0,04

Table E-4 UV absorbance data of CNT-TiO$_2$ calcined @ 400 ºC

MB, CNT-TiO$_2$ (1 g TiO$_2$/L) calcined @ 400 ºC, PP beaker, Quartz cap, UV absorbance @ 665 nm			
Time (hr)	Absorbance	Multiplier	Concentration (ppm)
Blank	-0,0006	0,000	0,00
0	0,2668	1,000	2,00
0,5	0,1548	0,581	1,16
1	0,0671	0,253	0,51
2	0,0183	0,070	0,14
3	0,0037	0,016	0,03

Table E-5 UV absorbance data of CNT-TiO$_2$ calcined @ 500 ºC

MB, CNT-TiO$_2$ (1 g TiO$_2$/L) calcined @ 500 ºC, PP beaker, Quartz cap, UV absorbance @ 665 nm			
Time (hr)	Absorbance	Multiplier	Concentration (ppm)
Blank	-0,0001	0,000	0,00
0	0,2829	1,000	2,00
0,5	0,1837	0,649	1,30
1	0,0957	0,338	0,68
2	0,0504	0,178	0,36
3,07	0,0179	0,063	0,13
4	0,0092	0,032	0,06

Table E-6 UV absorbance data of CNT-TiO$_2$ calcined @ 570 ºC

MB, CNT-TiO$_2$ (1 g TiO$_2$/L) calcined @ 570 ºC, PP beaker, Quartz cap, UV absorbance @ 665 nm			
Time (hr)	Absorbance	Multiplier	Concentration (ppm)
Blank	0,0001	0,000	0,00
0	0,2583	1,000	2,00
0,5	0,1919	0,742	1,48
1	0,1416	0,548	1,10
2	0,0789	0,305	0,61
3	0,0400	0,154	0,31
3,5	0,0258	0,099	0,20

Table E-7 UV absorbance data of CNT-TiO$_2$-1%Na (NaCl Source) heat treated with N$_2$ @ 400 ºC

MB, CNT-TiO$_2$-1%Na (1 g TiO$_2$/L) heat treated with N$_2$ @ 400 ºC, PP beaker, Quartz cap, UV absorbance @ 665 nm			
Time (hr)	Absorbance	Multiplier	Concentration (ppm)
Blank	-0,0009	0,000	0,00
0	0,2997	1,000	2,00
0,5	0,1220	0,407	0,81
1	0,0435	0,145	0,29
2,7	0,0640	0,021	0,04
3	-0,0040	0,000	0,00

Table E-8 UV absorbance data of CNT-TiO$_2$-1%Na (NaCl source) calcined @ 400 ºC

MB, CNT-TiO$_2$-1%Na (1 g TiO$_2$/L) calcined @ 400 ºC, PP beaker, Quartz cap, UV absorbance @ 665 nm			
Time (hr)	Absorbance	Multiplier	Concentration (ppm)
Blank	-0,0003	0,000	0,00
0	0,2897	1,000	2,00
0,5	0,1383	0,477	0,95
2	0,0191	0,066	0,13
3	0,0068	0,024	0,05
3,5	0,0028	0,010	0,02

Table E-9 UV absorbance data of CNT-TiO$_2$-1%Na (NaCl source) calcined @ 500 ºC

Time (hr)	Absorbance	Multiplier	Concentration (ppm)
MB, CNT-TiO$_2$-1%Na (1 g TiO$_2$/L) calcined @ 500 ºC, PP beaker, Quartz cap, UV absorbance @ 665 nm			
Blank	0,0000	0,000	0,00
0	0,2721	1,000	2,00
0,5	0,1742	0,640	1,28
1	0,1039	0,381	0,76
2	0,0478	0,175	0,35
3	0,0212	0,078	0,16
3,5	0,0183	0,067	0,13

Table E-10 UV absorbance data of CNT-TiO$_2$-1%Na (NaCl source) calcined @ 570 ºC

Time (hr)	Absorbance	Multiplier	Concentration (ppm)
MB, CNT-TiO$_2$-1%Na (1 g TiO$_2$/L) calcined @ 570 ºC, PP beaker, Quartz cap, UV absorbance @ 665 nm			
Blank	-0,0003	0,000	0,00
0	0,2555	1,000	2,00
0,5	0,1671	0,654	1,31
1	0,1098	0,430	0,86
2	0,0525	0,206	0,41
3	0,0278	0,110	0,22
4	0,0168	0,066	0,13

Table E-11 UV absorbance of CNT-TiO$_2$-1%Fe heat treated with N$_2$ @ 400 ºC

Time (hr)	Absorbance	Multiplier	Concentration (ppm)
MB, CNT-TiO$_2$-1%Fe (1 g TiO$_2$/L) heat treated with N$_2$ @ 400 ºC, PP beaker, Quartz cap, UV absorbance @ 665 nm			
Blank	-0,0009	0,000	0,00
0	0,3860	1,000	2,00
0,5	0,2143	0,556	1,11
1	0,1162	0,302	0,60
2	0,0297	0,079	0,16
3	0,0179	0,048	0,10
4	0,0161	0,044	0,09

Table E-12 UV absorbance data of CNT-TiO$_2$-1%Fe calcined @ 400 ºC

MB, CNT-TiO$_2$-1%Fe (1 g TiO$_2$/L) calcined @ 400 ºC, PP beaker, Quartz cap, UV absorbance @ 665 nm			
Time (hr)	Absorbance	Multiplier	Concentration (ppm)
Blank	0,0002	0,000	0,00
0	0,2904	1,000	2,00
0,5	0,2092	0,720	1,44
1	0,1447	0,497	0,99
2	0,0507	0,174	0,35
3	0,0153	0,052	0,10
4	0,0066	0,022	0,04

Table E-13 UV absorbance data of CNT-TiO$_2$-1%Fe calcined @ 500 ºC

MB, CNT-TiO$_2$-1%Fe (1 g TiO$_2$/L) calcined @ 500 ºC, PP beaker, Quartz cap, UV absorbance @ 665 nm			
Time (hr)	Absorbance	Multiplier	Concentration (ppm)
Blank	-0,0001	0,000	0,00
0	0,2982	1,000	2,00
0,5	0,2283	0,765	1,53
1	0,1546	0,518	1,04
2	0,1076	0,361	0,72
3	0,0641	0,215	0,43
4	0,0471	0,153	0,31

Table E-14 UV absorbance data of CNT-TiO$_2$-1%Fe calcined @ 570 ºC

MB, CNT-TiO$_2$-1%Fe (1 g TiO$_2$/L) calcined @ 570 ºC, PP beaker, Quartz cap, UV absorbance @ 665 nm			
Time (hr)	Absorbance	Multiplier	Concentration (ppm)
Blank	0,0002	0,000	0,00
0	0,3122	1,000	2,00
0,5	0,2151	0,688	1,38
0,77	0,1717	0,549	1,10
2,03	0,0894	0,286	0,57
3	0,0551	0,176	0,35
4	0,0337	0,107	0,21

Table E-15 UV absorbance of CNT-TiO$_2$-1%Co heat treated with N$_2$ @ 400 ºC

MB, CNT-TiO$_2$-1%Co (1 g TiO$_2$/L) heat treated with N$_2$ @ 400 ºC, PP beaker, Quartz cap, UV absorbance @ 665 nm			
Time (hr)	Absorbance	Multiplier	Concentration (ppm)
Blank	-0,0004	0,000	0,00
0	0,2439	1,000	2,00
0,5	0,1394	0,572	1,14
1	0,0727	0,299	0,60
2	0,0283	0,117	0,23
3	0,0099	0,042	0,08
4	0,0083	0,035	0,07

Table E-16 UV absorbance data of CNT-TiO$_2$-1%Co calcined @ 400 ºC

MB, CNT-TiO$_2$-1%Co (1 g TiO$_2$/L) calcined @ 400 ºC, PP beaker, Quartz cap, UV absorbance @ 665 nm			
Time (hr)	Absorbance	Multiplier	Concentration (ppm)
Blank	0,0002	0,000	0,00
0	0,2227	1,000	2,00
0,42	0,1546	0,694	1,39
1	0,0870	0,390	0,78
2	0,0266	0,119	0,24
3	0,0080	0,035	0,07
3.5	0,0017	0,007	0,01

Table E-17 UV absorbance data of CNT-TiO$_2$-1%Co calcined @ 500 ºC

MB, CNT-TiO$_2$-1%Co (1 g TiO$_2$/L) calcined @ 500 ºC, PP beaker, Quartz cap, UV absorbance @ 665 nm			
Time (hr)	Absorbance	Multiplier	Concentration (ppm)
Blank	-0,0001	0,000	0,00
0	0,3247	1,000	2,00
0,5	0,2178	0,670	1,34
1	0,1532	0,471	0,94
2.22	0,0941	0,290	0,58
3	0,0619	0,190	0,38
4	0,0369	0,113	0,23

Table E-18 UV absorbance data of CNT-TiO$_2$-1%Co calcined @ 570 ºC

MB, CNT-TiO$_2$-1%Co (1 g TiO$_2$/L) calcined @ 570 ºC, PP beaker, Quartz cap, UV absorbance @ 665 nm			
Time (hr)	Absorbance	Multiplier	Concentration (ppm)
Blank	-0,0002	0,000	0,00
0	0,2492	1,000	2,00
0,5	0,2054	0,824	1,65
1	0,1199	0,481	0,96
2	0,0931	0,374	0,75
3	0,0531	0,213	0,43
4	0,0371	0,149	0,30

Table E-19 UV absorbance of CNT-TiO$_2$-5%Na (NaCl source) heat treated with N$_2$ @400ºC

MB, CNT-TiO$_2$-5%Na (1 g TiO$_2$/L) heat treated with N$_2$ @ 400 ºC, PP beaker, Quartz cap, UV absorbance @ 665 nm			
Time (hr)	Absorbance	Multiplier	Concentration (ppm)
Blank	-0,0003	0,000	0,00
0	0,3560	1,000	2,00
0,5	0,2304	0,647	1,29
1	0,0956	0,269	0,54
1,33	0,0889	0,250	0,50
3	0,0261	0,074	0,15
4	0,0180	0,051	0,10

Table E-20 UV absorbance data of CNT-TiO$_2$-5%Na (NaCl source) calcined @ 400 ºC

MB, CNT-TiO$_2$-5%Na (1 g TiO$_2$/L) calcined @ 400 ºC, PP beaker, Quartz cap, UV absorbance @ 665 nm			
Time (hr)	Absorbance	Multiplier	Concentration (ppm)
Blank	0,0003	0,000	0,00
0	0,3728	1,000	2,00
0,5	0,2308	0,618	1,24
1	0,1177	0,315	0,63
1,5	0,0766	0,204	0,41
2,83	0,0222	0,058	0,12
4	0,0077	0,020	0,04

Table E-21 UV absorbance data of CNT-TiO$_2$-5%Na (NaCl source) calcined @ 500 ºC

Time (hr)	Absorbance	Multiplier	Concentration (ppm)
MB, CNT-TiO$_2$-5%Na (1 g TiO$_2$/L) calcined @ 500 ºC, PP beaker, Quartz cap, UV absorbance @ 665 nm			
Blank	-0,0001	0,000	0,00
0	0,3594	1,000	2,00
0,52	0,3108	0,864	1,73
1	0,2128	0,592	1,18
1.5	0,1582	0,440	0,88
3,08	0,0601	0,167	0,33
4	0,0446	0,124	0,25

Table E-22 UV absorbance data of CNT-TiO$_2$-5%Na (NaCl source) calcined @ 570 ºC

Time (hr)	Absorbance	Multiplier	Concentration (ppm)
MB, CNT-TiO$_2$-5%Na (1 g TiO$_2$/L) calcined @ 570 ºC, PP beaker, Quartz cap, UV absorbance @ 665 nm			
Blank	-0,0006	0,000	0,00
0	0,3582	1,000	2,00
0,5	0,2916	0,814	1,63
1	0,2310	0,646	1,29
1.5	0,1809	0,506	1,01
3	0,0788	0,221	0,44
4	0,0446	0,159	0,32

Table E-23 UV absorbance of CNT-TiO$_2$-3%Na (NaCl source) heat treated with N$_2$ @400ºC

Time (hr)	Absorbance	Multiplier	Concentration (ppm)
MB, CNT-TiO$_2$-3%Na (1 g TiO$_2$/L) heat treated with N$_2$ @ 400 ºC, PP beaker, Quartz cap, UV absorbance @ 665 nm			
Blank	-0,0003	0,000	0,00
0	0,3311	1,000	2,00
0,5	0,2185	0,660	1,32
1	0,1159	0,350	0,70
1,5	0,0877	0,265	0,53
3	0,0281	0,085	0,17
4	0,0169	0,051	0,10

Table E-24 UV absorbance data of CNT-TiO$_2$-3%Na (NaCl Source) calcined @ 400 ºC

MB, CNT-TiO$_2$-3%Na (1 g TiO$_2$/L) calcined @ 400 ºC, PP beaker, Quartz cap, UV absorbance @ 665 nm			
Time (hr)	Absorbance	Multiplier	Concentration (ppm)
Blank	-0,0005	0,000	0,00
0	0,3374	1,000	2,00
0,5	0,2365	0,701	1,40
1	0,1282	0,380	0,76
1,5	0,0924	0,274	0,55
3	0,0321	0,095	0,19
4	0,0152	0,045	0,09

Table E-25 UV absorbance data of CNT-TiO$_2$-3%Na (NaCl source) calcined @ 500 ºC

MB, CNT-TiO$_2$-3%Na (1 g TiO$_2$/L) calcined @ 500 ºC, PP beaker, Quartz cap, UV absorbance @ 665 nm			
Time (hr)	Absorbance	Multiplier	Concentration (ppm)
Blank	0,0004	0,000	0,00
0	0,3410	1,000	2,00
0,5	0,3018	0,885	1,77
1	0,2087	0,612	1,22
1.5	0,1599	0,469	0,94
3	0,0692	0,203	0,40
4	0,0460	0,135	0,27

Table E-26 UV absorbance data of CNT-TiO$_2$-3%Na (NaCl source) calcined @ 570 ºC

MB, CNT-TiO$_2$-3%Na (1 g TiO$_2$/L) calcined @ 570 ºC, PP beaker, Quartz cap, UV absorbance @ 665 nm			
Time (hr)	Absorbance	Multiplier	Concentration (ppm)
Blank	0,0006	0,000	0,00
0	0,3229	1,000	2,00
0,5	0,2867	0,888	1,78
1	0,2147	0,665	1,33
1.5	0,1753	0,543	1,08
3	0,0655	0,203	0,40
4	0,0500	0,155	0,31

Table E-27 UV absorbance of CNT-TiO$_2$-1%Na (Na$_2$CO$_3$ source) heat treated with N$_2$ @ 400 ºC

MB, CNT-TiO$_2$-1%Na (1 g TiO$_2$/L) heat treated with N$_2$ @ 400 ºC, PP beaker, Quartz cap, UV absorbance @ 665 nm			
Time (hr)	Absorbance	Multiplier	Concentration (ppm)
Blank	0,0001	0,000	0,00
0	0,3693	1,000	2,00
0,5	0,2727	0,738	1,48
1	0,1514	0,409	0,82
2	0,0533	0,144	0,29
3	0,0236	0,063	0,13
4	0,0163	0,044	0,09

Table E-28 UV absorbance data of CNT-TiO$_2$-1%Na (Na$_2$CO$_3$ source) calcined @ 400 ºC

MB, CNT-TiO$_2$-1%Na (1 g TiO$_2$/L) calcined @ 400 ºC, PP beaker, Quartz cap, UV absorbance @ 665 nm			
Time (hr)	Absorbance	Multiplier	Concentration (ppm)
Blank	0,0003	0,000	0,00
0	0,3637	1,000	2,00
0,5	0,2867	0,770	1,54
1	0,2824	0,445	0,89
2	0,1632	0,180	0,36
3	0,0330	0,090	0,18
4	0,0202	0,055	0,11

Table E-29 UV absorbance data of CNT-TiO$_2$-1%Na (Na$_2$CO$_3$ source) calcined @ 500 ºC

MB, CNT-TiO$_2$-1%Na (1 g TiO$_2$/L) calcined @ 500 ºC, PP beaker, Quartz cap, UV absorbance @ 665 nm			
Time (hr)	Absorbance	Multiplier	Concentration (ppm)
Blank	0,0004	0,000	0,00
0	0,3651	1,000	2,00
0,5	0,2884	0,790	1,58
1	0,1752	0,480	0,96
2	0,0803	0,220	0,44
3	0,0456	0,125	0,25
4	0,0256	0,070	0,14

Table E-30 UV absorbance data of CNT-TiO$_2$-1%Na (Na$_2$CO$_3$ source) calcined @ 570 ºC

MB, CNT-TiO$_2$-1%Na (1 g TiO$_2$/L) calcined @ 570 ºC, PP beaker, Quartz cap, UV absorbance @ 665 nm			
Time (hr)	Absorbance	Multiplier	Concentration (ppm)
Blank	-0,0020	0,000	0,00
0	0,3566	1,000	2,00
0,5	0,2902	0,814	1,63
1	0,1831	0,513	1,03
2	0,1039	0,291	0,58
3	0,0523	0,147	0,29
4	0,0241	0,068	0,14

Table E-31 UV absorbance of CNT-TiO$_2$-5%Na (Na$_2$CO$_3$ source) heat treated with N$_2$ @ 400 ºC

MB, CNT-TiO$_2$-5%Na (1 g TiO$_2$/L) heat treated with N$_2$ @ 400 ºC, PP beaker, Quartz cap, UV absorbance @ 665 nm			
Time (hr)	Absorbance	Multiplier	Concentration (ppm)
Blank	0,0001	0,000	0,00
0	0,2828	1,000	2,00
0,5	0,0965	0,340	0,68
1	0,0499	0,175	0,35
2	0,0208	0,073	0,15
3	0,0131	0,045	0,09
4	0,0082	0,028	0,06

Table E-32 UV absorbance data of CNT-TiO$_2$-5%Na (Na$_2$CO$_3$ source) calcined @ 400 ºC

MB, CNT-TiO$_2$-5%Na (1 g TiO$_2$/L) calcined @ 400 ºC, PP beaker, Quartz cap, UV absorbance @ 665 nm			
Time (hr)	Absorbance	Multiplier	Concentration (ppm)
Blank	-0,0001	0,000	0,00
0	0,3073	1,000	2,00
0,5	0,1260	0,410	0,82
1	0,0722	0,235	0,47
2	0,0277	0,090	0,18
3	0,0169	0,055	0,11
4	0,0123	0,040	0,08

Table E-33 UV absorbance data of CNT-TiO$_2$-5%Na (Na$_2$CO$_3$ source) calcined @ 500 ºC

MB, CNT-TiO$_2$-5%Na (1 g TiO$_2$/L) calcined @ 500 ºC, PP beaker, Quartz cap, UV absorbance @ 665 nm			
Time (hr)	Absorbance	Multiplier	Concentration (ppm)
Blank	0,0002	0,000	0,00
0	0,2919	1,000	2,00
0,5	0,1503	0,515	1,03
1	0,0817	0,280	0,56
2	0,0306	0,105	0,21
3	0,0161	0,055	0,11
4	0,0117	0,040	0,08

Table E-34 UV absorbance data of CNT-TiO$_2$-5%Na (Na$_2$CO$_3$ source) calcined @ 570 ºC

MB, CNT-TiO$_2$-5%Na (1 g TiO$_2$/L) calcined @ 570 ºC, PP beaker, Quartz cap, UV absorbance @ 665 nm			
Time (hr)	Absorbance	Multiplier	Concentration (ppm)
Blank	-0,0004	0,000	0,00
0	0,3109	1,000	2,00
0,5	0,1855	0,597	1,19
1	0,1051	0,338	0,68
1.38	0,0670	0,216	0,43
2.5	0,0207	0,067	0,13
4	0,0134	0,044	0,09

CURRICULUM VITAE

PERSONAL INFORMATION

Surname, Name: Yürüm, Alp
Nationality: Turkish (TC)
Date and Place of Birth: 15 April 1979, Ankara
Martial Status: Single
Phone: +90 312 210 43 55
Fax: +90 312 210 26 00
E-mail: alp.yurum@gmail.com

EDUCATION

Degree	Institution	Year of Graduation
MS	METU Chemical Engineering	2003
BS	METU Chemical Engineering	2000
High School	Arı Fen High School, Ankara	1996

WORK EXPERIENCE

Year	Place	Enrollment
2007 – 2008	METU Chemical Engineering	Research Assistant
2000 – 2007	METU Chemical Engineering	Teaching Assistant
1998 July	Tepe – Knauf	Intern Engineering Student

FOREIGN LANGUAGES

Advanced English, Intermediate Japanese

HONORS AND AWARDS

Graduated as an honor student form Chemical Engineering Department

PUBLICATIONS

1. Research Articles

1. Erdural Beril K., Yürüm Alp, Bakır Ufuk; Karakaş Gürkan, "Hydrothermal Synthesis of Nanostructured TiO_2 Particles and Characterization of Their Photocatalytic Antimicrobial Activity", Journal of Nanoscience and Nanotechnology, Volume 8, Number 2, February 2008 , pp. 878-886(9).

2. Book Chapters

1. Erdural Beril, Yürüm Alp, Karakaş Gürkan, Bakır Ufuk, "Antimicrobial Properties of Titanium Nanoparticles", Vaseashta, Ashok K., Mihailescu, Ion N. (Eds.), Functionalized Nanoscale Materials, Devices and Systems, Springer, 2008.

3. International Conference Publications

1. Yürüm Alp, Erdural Beril, Karakaş Gürkan, Bakır Ufuk, "Synthesis and Characterization of Nano-structured Titania for Photocatalytic Applications", EUROPACAT VIII, Finland (2007).

2. Yürüm Alp, Erdural Beril, Karakaş Gürkan, Bakır Ufuk, "Effect Of Hydrothermal Treatment Conditions On The Photocatalytic Antimicrobial Activity Of Nanostructured Titania Particles", Nanotech Northern Europe – NTNE 2007, Finland (2007).

3. Bakır Ufuk, Karakaş Gürkan, Erkan Arcan, Yürüm Alp, Erdural Beril, "Semiconductor Metal Oxide Thin Films as Photocatalysts", European Technology Platform for Sustainable Chemistry, 6th Stakeholder and brokerage event – SusChem, Germany (2007).

4. Yürüm Alp, Erdural Beril, Karakaş Gürkan, Bakır Ufuk, "Preparation, Characterization and Antimicrobial Properties of Titanium Nanoparticles", International Workshop on Nanostructured Materials – NANOMAT 2006, Turkey (2006).

5. Mirkelamoğlu Burcu, Yürüm Alp, Karakaş Gürkan, "Activity of Potassium and Palladium Promoted Tin Oxide in CO Oxidation", 4th Chemical Engineering Conference for Collaborative Research in Eastern Mediterranean Countries – EMCC4, Israel (2006).

4. National Conference Publications

1. Erdural Beril, Yürüm Alp, Bakır Ufuk , Karakaş Gürkan, "Tio$_2$ Parçacıkların Fotokatalitik Özellikleri Üzerine Hidrotermal İşlemlerin Etkisi", Ulusal Kimya Mühendisliği Kongresi – UKMK-8 (2008).

2. Bayram Bilal, Yürüm Alp, Karakaş Gürkan, "Effects of Synthesis Parameters on the Photocatalytic Activity of Titania–Silica Mixed Oxides Prepared with co-Hydrolyzation Method", National Catalysis Conference – NCC-2 (2008).

3. Yürüm Alp, Erdural Beril, Karakaş Gürkan, Bakır Ufuk, "Synthesis and Characterization of Mesoporous Titania for Photocatalytic Antibacterial Surfaces", National Catalysis Conference – NCC-1 (2007).